To the Graduate Council:

I am submitting herewith a thesis written by Regina Natasha Holmes entitled "Development of Bioabsorbable Fiber-Reinforced Composites from Bicomponent Fibers of Polylactic Acid and its Copolymers " I have examined the final copy of this thesis for form and content and recommend that it be accepted in partial fulfillment of the requirements for the degree of Master of Science, with a major in Polymer Engineering.

Joseph E Spruiell, Major Professor

We have read this thesis
and recommend its acceptance:

Roberto S Benson

John F. Fellers

Accepted for the Council:

Associate Vice Chancellor
and Dean of the Graduate School

DEVELOPMENT OF BIOABSORBABLE FIBER-REINFORCED COMPOSITES FROM BICOMPONENT FIBERS OF POLYLACTIC ACID AND ITS COPOLYMERS

A Thesis

Presented for the

Master of Science

Degree

The University of Tennessee, Knoxville

Regina Natasha Holmes

December 2000

DEDICATION

This thesis is dedicated to my family and friends.

For breathing when

I did not want to take a

breath

For believing when

I could not

see

the light at the end of tunnel

For praying when I could not find words

For pushing when I refused to move

For reminding to keep my head when I was down

For patiently waiting until I was ready

And For knowing that

God

takes care of his children.

Thank You.

This moment is a reflection of all the

love and ***support***

you have given me.

Because of you, I have received many blessings.

ACKNOWLEDGEMENTS

Thanks to Dr. Joseph Spruiell for his support throughout this research. I am grateful to my committee members, Dr. Roberto Benson, and Dr. John Fellers for agreeing to serve in this capacity.

Support for this research was provided by BioAmide, Inc. Dr. Thomas Barrow's suggestions and contributions were envaluable.

Special thanks to Douglas Fielden and Gregory Jones for their expertise in the manufacture and maintenance of the equipment needed for this research. Without them, none of this would have been possible.

To the members of Dr. Spruiell's group, I am forever indebted. This has truly been a team effort. The assistance of my team members made the transition from school to work possible.

ABSTRACT

The feasibility of using core.sheath type bicomponent polylactide filaments to produce bioabsorbable continuous, fiber-reinforced composites was investigated The core component was poly(L-lactic acid) (PLLA) An adhesion study was used to determined that poly(L/DL-lactic acid) (PLDL) would be used as the sheath component. Bicomponent filaments with 1·2, 1 1, 2:1, 3:1, and 4:1 core:sheath ratios were produced by melting spinning and drawing processes. The 1·1 core:sheath filaments had the best mechanical properties with tensile strength and modulus values of approximately 300 MPa and 4000 MPa, respectively. The 1.1 PLLA PLDL filaments were consolidated into 2.0 mm composite rods using a pultusion die heated at 140 °C, 150 °C, 160 °C, 170 °C, and 175 °C. Maximum properties were achieved at a processing temperature of 150 °C. The tensile strength of the composite rods was 102 MPa, shear strength of 75 MPa, and bending strength of 117.9 MPa The properties of the bicomponent filaments were not transferred to the composite rods because consolidation of the filaments by heating resulting annealing behavior which reduced the strength of the core fibers. Other factors such as degradation, loss of amorphous orientation, and changes in fiber morphology also contributed to the loss of strength.

TABLE OF CONTENTS

CHAPTER			PAGE
1	**Introduction**		1
2	**Literature Survey**		5
	2.1	**Bioabsorbable Polymers**	5
		2.1.1 Poly(glycolic acid)	6
		2.1.2 Polydioxanone	7
		2.1.3 Poly(lactic acid)	8
	2.2	Bioabsorbable Composites	9
	2.3	Bioabsorbable Internal Fixation Devices	13
		2.3.1 Cellular Response of Pins and Screws	13
		2.3.2 Mechanical Properties of Internal Fixation Devices	14
	2.4	Fiber Extrusion	16
		2.4.1 Melt Spinning and Drawing	16
		2.4.2 Bicomponent Spinning	17
3	**Experimental Methods: Processing Techniques**		22
	3.1	Bicomponent Fiber Spinning	22
	3.2	Continuous Drawing	26
	3.3	Composite Rod Fabrication – Pultrusion Die	30
4	**Experimental Methods: Characterization Techniques**		32
	4.1	Materials	32
	4.2	Polymer Selection – Peel Test	32

CHAPTER PAGE

4.2.1 Sample Preparation 33

4.2.2 Testing 34

4.3 Draw Ratio Determination 36

4.4 Optical Microscopy 36

4.5 Optical Birefringence 36

4.5.1 Types of Birefringence 37

4.5.2 Methods 37

4.6 Dilute Solution Viscosity 38

4.6.1 Sample Preparation 39

4.6.2 Testing 39

4.7 Wide Angle X-Ray Diffraction 40

4.8 Static Tensile Testing 40

4.8.1 Fiber Sample Preparation and Testing 41

4.8.2 Composite Rod Sample Preparation and Testing 41

4.9 Static Shear Testing 41

4.10 Scanning Electron Microscopy 42

4.11 Differential Scanning Calorimetry 42

5 **Polymer Selection: Results and Discussion** 43

5.1 Peel Test – Sheath/Core Adhesion 43

5.2 Peel Test – Sheath Cohesion 52

6 **Preliminary Analysis: Results and Discussion** 54

CHAPTER PAGE

6.1 Rationale for Preliminary Test 54

6.2 Initial Bicomponent Spinning Experiments: Medical Grade Polylactides 54

6.2.1 Determination of Bicomponent Structure 54

6.2.2 Amorphous and Crystalline Orientation 56

6.2.3 Tensile Properties 59

6.3 Production of Composite Rods from Bicomponent Filaments 59

6.3.1 Mechanical Properties of Rods Prepared via Shrink Wrap Tubing 61

6.3.2 Composite Morphology 61

6.4 Bicomponent Spinning of Industrial-Grade Polylactides 65

6.5 Composite Rod Fabrication from Industrial-Grade Polylactides 68

6.6 Conclusions 78

7 **Analysis using Purac, Medical-Grade Polymers: Results and Discussion** 79

7.1 Analysis of Bicomponent Fibers 79

7.2 Degradation Due to Melt Spinning 79

7.3 Crystallinity and Molecular Orientation 80

7.3.1 Thermal Analysis – DSC 81

7.3.2 Crystalline Orientation – WAXD 81

7.3.3 Molecular Orientation – Birefringence 87

7.4 Mechanical Properties of 1:1 Core:Sheath Fibers 89

CHAPTER PAGE

7.5 SEM Analysis of Fracture Surfaces 93

8 **Final Analysis of Composite Rods** 96

8.1 Composite Rod Fabrication 96

8.2 Orientation of Composite Rods 96

8.3 Mechanical Properties of Composite Rods 98

8.4 Comparison of Fiber and Composite Properties 109

9 **Conclusions and Recommendations** 113

9.1 Conclusions 113

9.2 Recommendations 114

9.2.1 Processing Modifications 114

9.2.2 Additional Testing 116

REFERENCES 117

VITA 127

LIST OF TABLES

TABLE		PAGE
2.1.	Applications of bioabsorbable polymers.	6
2.2.	Initial mechanical properties of bioabsorbable polymeric rods manufactured by self-reinforcing (SR-) and injection-molding (IM-) techniques	15
2.3.	Literature Values for the bending strength of bioabsorbable pins.	16
3.1.	Bicomponent spinning conditions used at Randcastle Extruder Systems, Inc.	22
3.2.	Typical spinning conditions used with the spinning system at the University of Tennessee.	28
4.1.	Properties of polymers	33
4.2.	Polymers used in inherent viscosity measurements.	39
5.1.	Peel strength in N/mm for joints formed betrween PLLA and candidate sheath materials.	44
5.2.	Peel strength for PLDL-PLDL joints.	53
6.1.	The effects of core·sheath ratio on the mechanical properties of composite rods prepared via shrink wrap tubing.	62
7.1.	Thermal characteristics of polylactides before and after melt spinning.	80
7.2.	Effect of drawing on degree of crystallization as determined by DSC analysis.	86
8.1.	Flexural properties of composite rods made from 1·1 PLLA.70/30 PLDL filaments.	107
8.2.	Mechanical properties of 1:1 PLLA:70/30 PLDL rod and commercial control.	108
8.3.	Comparison of tensile properties of 1:1 PLLA:70/30 PLDL filaments before and after annealing.	109

LIST OF FIGURES

FIGURE		PAGE
2.1.	Poly(glycolic acid).	7
2.2.	Polydioxanone.	7
2.3.	Polylactic acid.	8
2.4.	Melt spinning and drawing techniques.	18
2.5.	Schematic illustration of Bicomponent Spinning setup.	19
2.6.	The three major types of fibers formed by co-extrusion of two polymers.	20
3.1.	Bicomponent spinning equipment. Bicomponent die block.	23
3.2.	Bicomponent spinning equipment Heating zones.	24
3.3.	Bicomponent spinning equipment. Metering zones.	25
3.4.	Bicomponent spinning system.	27
3.5.	Schematic of drawing system.	29
3.6.	Pultusion die system.	31
5.1.	Optical micrographs of PTMC peeled surfaces at 25X magnification.	45
5.2.	SEM micrographs of PTMC peeled surface at a magnification of 10X.	47
5.3.	Maximum peel strength for different polymer joints as a function of contact time.	48
5.4.	Peel strength as a function of temperature for different polymer joints.	50

FIGURE		PAGE
5.5	Optical micrographs of peeled surfaces of candidate sheath materials.	51
6.1.	Photo micrographs of bicomponent fiber cross-sections.	55
6.2.	Wide Angle X-Ray Diffraction patterns for bicomponent filaments.	57
6.3.	Overall orientation of as-spun PLLA PLDL filaments.	58
6.4.	Effect of drawing on the overall orientation of PLLA:PLDL filaments.	58
6.5.	Tensile strength of as-spun PLLA.PLDL filaments.	60
6.6.	Effect of drawing on the tensile strength of PLLA:PLDL filaments.	60
6.7.	SEM micrographs of fracture surfaces of composite rods tested under shear loads.	63
6.8.	SEM micrographs of fracture surfaces of composite rods tested under tensile loads.	64
6.9.	Maximum draw attained at various temperatures for PLA:PLDL filaments	67
6.10.	Overall orientation of PLA·PLDL filaments.	69
6.11.	Tensile strength of PLA PLDL filaments.	69
6.12.	Relationship between tensile strength and birefringence for PLA:PLDL filaments	70
6.13.	SEM micrographs of tensile fracture surfaces of PLA:PLDL filaments.	71
6.14.	Shear strength of PLA.PLDL composite rods.	72
6.15.	SEM micrographs of sheared surface of PLA:PLDL composite rod	74

FIGURE		PAGE
6.16.	Tensile strength of PLA:PLDL composite rods.	75
6.17.	Modulus and strain of PLA:PLDL composite rods.	75
6.18.	SEM micrographs of tensile fracture surfaces of PLA.PLDL composite rods.	76
6.19.	WAXD pattern of composite rod made from 1:1 PLA:PLDL filaments	77
7.1.	Maximum draw ratio attained at different drawing temperatures. ...	82
7.2.	DSC scan of 1:1 PLA:PLDL as-spun fiber.	83
7.3.	DSC scan of 1:1 PLA:PLDL drawn fiber.	84
7.4.	DSC scan of 1:1 PLA PLDL drawn fiber.	84
7.5.	DSC scan of 1 1 PLA:PLDL drawn fiber.	85
7.6.	DSC scan of 1:1 PLA:PLDL drawn fiber.	85
7.7.	WAXD patterns of 1 1 PLLA 70/30 PLDL bicomponent filaments.	86
7.8.	Effect of drawing on the overall orientation of filaments.	88
7.9.	Correlation between tensile strength and orientation of 1·1 PLLA:70/30 PLDL filaments.	90
7.10.	Effect of drawing on tensile strength of filaments.	91
7.11.	Modulus and elongation to break for drawn 1.1 PLLA:70/30 PLDL filaments.	91
7.12.	SEM micrographs of tensile fracture surfaces of 1:1 PLLA:70/30 PLDL filaments.	94
8.1.	WAXD patterns for composite rods.	97
8.2.	Stress versus strain for composite rods.	99

FIGURE		PAGE
8.3.	Effect of fabrication temperature on the tensile strength of the composite rods.	100
8.4.	Effect of fabrication temperature on the tensile modulus of the composite rods.	100
8.5.	SEM micrographs of tensile fracture surfaces of PLLA 70/30 PLDL composite rods.	101
8.6.	Effect of fabrication temperature on the shear strength of the composite rods.	105
8.7.	SEM micrographs of shear fracture surfaces of PLLA 70/30 composite rods.	106
8.8.	SEM micrographs of Bionx Smart Pin ™ fracture surfaces.	108
8.9.	WAXD patterns of 1 1 PLLA:70/30 PLDL filaments before and after annealing.	111

CHAPTER 1

Introduction

A new material with mechanical properties and performance characteristics that are superior to commercially available products is needed to improve the design of internal fixation devices. The use of many of the current internal fixation devices is limited because of their poor mechanical properties and their inability to maintain their strength long enough for healing to occur [1]. Therefore, these implants are only suitable for low load applications [1,2]. There is an increased interest in using bioabsorbable implants for internal fracture fixation. Currently research is underway to identify materials that successfully meet the design criteria for high performance, high strength fixation devices To date no fully bioabsorbable composites exist to develop such devices. The factors that limit the development of totally bioabsorbable composite fixation devices are two-fold: (1) a lack of understanding of the complex failure modes of theses types of systems; and (2) the inherent mechanical property limitations of the components of the composite systems [3].

The ideal material should be biocompatible, sufficiently elastic to permit healing, and absorbable to provide progressive transfer of stresses to the healing tissue [4]. Various biodegradable polymers are being used clinically in bone fixation surgery [5]. The advantages of these types of devices are:

1. They are less invasive because bioresorbable materials alleviate the need for additional operations to remove the fixation device upon healing [5].

2. With metallic devices, bone regrowth is restricted; and in some cases, bone resorption occurs [5,6]. However, with polymeric devices, bone regeneration occurs at the fixation site, leading to a gradual increase in bone strength.
3. The large difference in stiffness between bone and metals cause the bone to undergo prolonged stress shielding, creating a mechanically weaker bone structure. As a result the probability of refracture increases [4]. Biodegradable polymers effectively transfer stresses to the healing bone as the polymer is absorbed [3,7,8].

Examples of biodegradable polymers that have been used in clinical applications include poly(L-lactic acid) (PLLA), poly(glycolic acid) (PGA), and polydioxanone (PDS). Their primary biomedical applications include temporary fixation devices [3,9-11], drug delivery devices [12], and vascular prostheses [2] PGA and PDS have faster hydrolysis rates than PLLA causing their strength retention to be low *in vivo*. As a result, PLLA is preferred in applications where good mechanical performance and long resorption times are required [13-15].

Orientation of the polymer's molecular structure has been investigated in an effort to improve their mechanical properties. One method for enhancing polymer properties involves melt extrusion/spinning and drawing of fibers. Melt spinning is the process by which molten polymer is extruded through a die to produce filaments. If collected at low speeds, the filaments have low orientation and mechanical properties. Enhanced properties are achieved through the drawing process [16,17] Hot drawing can be used to

transform polymer chains into highly oriented fibrillar structures; and this process is generally used for objects with small cross-sections such as fibers [1]. Since the 1970's, researchers have used this technique to prepare highly oriented, nonresorbable polymeric materials with high strength and modulus. More recently, this method has been used to enhance the properties of bioabsorbable polymers [2]. PLLA fibers have been studied extensively leading to the production of PLLA and PDLLA fibers having a tensile strength of 0.28 GPa [2]. Further work in fiber spinning enabled the production of fibers with tensile strengths of 0.5 to 0.9 GPa and a modulus ranging from approximately 7-9 GPa [16,17].

BioAmide, Inc. is currently investigating the feasibility of developing a composite system from sheath/core bicomponent poly(lactic acid) fibers that will have substantially higher strength and higher performance than current bioabsorbable materials. In this system, the core fibers become the reinforcing agent for the sheath material that functions as the composite matrix. The structure development experienced in bicomponent spinning is expected to differ from the properties obtained in single component spinning due to the mutual interaction of the two components in the spinline. These interactions are influenced mainly by significant differences in their inherent properties (such as activation energy of elongation, viscosity, and solidification temperature [18].

The purpose of this research is to determine the technical feasibility of fabricating high strength, high performance, bioabsorbable fiber-reinforced composites from bicomponent PLLA fibers for use in high-load bearing orthopedic applications. The investigation involves three phases. First, the sheath material for use in spinning

bicomponent fibers of (PLLA) is selected, and the adhesive interaction between PLLA and the sheath material is investigated. Second, the choice of sheath polymer is confirmed through melt spinning and drawing sheath/core fibers to maximize the mechanical properties. Third, the fibers are thermally processed under tension to form fiber-reinforced composite rods. The optimal sheath/core ratio is determined by evaluating the mechanical properties of the rods through static tensile and shear testing. These results are then compared to the properties of a commercially available biodegradable pin (Bionx™ SR-PLLA pin).

CHAPTER 2

Literature Survey

2.1 Bioabsorbable Polymers

Generally, the biodegradable polymer undergoes degradation *in vivo* via hydrolytic and enzymatic mechanisms. The action of enzymes is influenced by the permeability of water in the polymer. Therefore factors such as crystallinity, chain branching, and decreased chain mobility will retard the degradation rate [19]. In addition, the following factors may affect biodegradation.

1. Molecular weight. Biodegradability decreases with increases in molecular weight. In a sample with broad molecular weight distribution, the rate of degradation decreases as the chains of lower molecular weight are consumed [20].
2. Accessibility to waterborne systems. The permeability of extracellular enzymes in the water will determine whether bulk or surface degradation will occur. Semicrystalline materials tend to limit the accessibility of water to the amorphous regions initially [21].
3. The glass transition temperature. Chain mobility is determined by the glass transition temperature. Above the glass transition temperature, diffusion is facilitated and chain cleavage can occur readily [19].
4 The presence of additives and impurities, along with environmental conditions affect biodegradation [19,20].

Polyesters, polyorthoesters, polyanhydrides and poly(amino acids) are examples of biomedical, resorbable polymers. Of these groups, more focus has been paid to aliphatic

polyesters derived from lactic and glycolic acid which are acids naturally occurring in the human body [20-22]. Because many of the bioabsorbable polymers are relatively brittle and rigid materials, incorporation of rubbery materials in the polymer chain has been investigated. Incorporation of carbonate linkages improves the polyester's mechanical and hydrolytic performance by creating a tougher material. Advantages to using these polymers in biomedical applications are: the degradation products are nontoxic; they exist as high molecular weight polymers with excellent mechanical properties; they are somewhat hydrophobic; and their properties can be modified and controlled by copolymerization to produce a material that is appropriate for a given application [21]. Some typical applications of bioabsorbable polymers are listed in **Table 2.1**.

2.1.1 Poly(glycolic acid)

Along with PLA, poly(glycolic acid) (PGA) is one the most commonly used synthetic bioabsorbable polymers. It is a highly crystalline aliphatic polyester with a high melting point and low solubility in organic solvents. It degrades faster than other aliphatic polyesters such as PLA because of its simple linear structure [20]. The

Table 2.1. Applications of bioabsorbable polymers [20,21].

Application	Shape	Example
Binding Materials	Suture, clip	PGA, PLA
Bone-setting materials	Plate, screw, rod, pin, splint	PLLA,
Artificial blood vessel	Fiber, porous material	PLLA
Artificial tendon and ligament	Fiber	PLLA, polyglactin
Synthetic skin	Fiber	PLA, polyurethane
Drug delivery system	Microcapsule, microsphere, hollow fiber	Polycaprolactone, glycolide/lactide polymers

structure of PGA is shown in **Figure 2.1.** PGA was used in the development of the first bioabsorbable sutures. It has been commercially available as sutures under the trade name Dexon since 1970 [20,22]. Also, Biofix® PGA pins are frequently used in internal bone fixation [11,21]. PGA's fiber strength and modulus is comparable to high-performance fibers such as aramide (Kevlar®) and ultra-high molecular weight polyethylene (Dynema®) [21].

2.1.2 Polydioxanone

Polydioxanone (PDS) is a colorless, crystalline polymer that also degrades by hydrolysis (see **Fig. 2.2**) [12] The primary use of this material was in the manufacture of bioabsorbable sutures. Breaking strength retention and delayed absorption made this material more appealing for a wider variety of surgical uses than other synthetic sutures [12] The inherent flexibility of this material enabled it to be fabricated into monofilament fibers and used for many suture sizes. These types of sutures became available in the United States in 1981 [20]. PDS has also been used successfully in other orthopedic and surgical applications, but it has not had the popularity of other biomaterials like PLA and PGA [22].

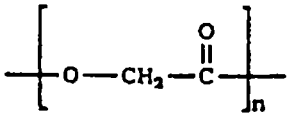


Figure 2.1. Poly(glycolic acid) [21].

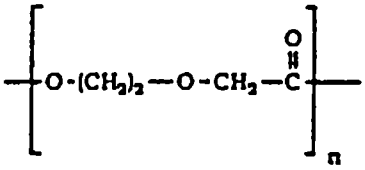


Figure 2.2. Polydioxanone [21].

2.1.3 Poly(lactic acid)

Poly(lactic acid) PLA, exits in four isomeric forms. These are L-lactide, D-lactide, and meso-lactide [20,21]. The fourth form is a mixture of the aforementioned isomers, often referred to as *d,l*-lactidePLLA. This type contains the same number of L-lactic acid and D-lactic acid ester groups. Poly(L-lactic acid) is considered an ideal implant material and is used most frequently because hydrolysis of this polymer leads to lactic acid which is found in the body. The general structure of PLA is shown in **Figure 2.3** PLLA implants are reported as the strongest bioabsorbable material used in bone fixation [23]. Slivka et al. [10] showed that PLLA is a good matrix material in bioabsorbable composite systems. Due to its semicrystalline nature, this polymer exhibits large strains and has the capability to absorb large amounts of energy. In addition, strength retention is high *in vivo* and *in vitro* [10]. It is a used in applications where high mechanical strength and toughness are required Some of its biomedical applications include temporary fixation devices [3,21,23], vascular prostheses [19,24], and drug delivery devices [25]

One concern with using PLLA is the possibility that absorption of the amorphous regions will result in large concentrations of debris that will retard hydrolysis and cause severe foreign body reactions. This is a problem that was encountered with injection-

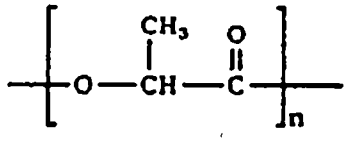


Figure 2.3. Poly(lactic acid) [21].

molded implants. Fiber-reinforced PLLA devices degrade and are absorbed in a shorter time with no evidence of complications in contrast to injection-molded devices [26]. In addition, loss of mechanical strength is delayed, with PLLA implants retaining their initial mechanical strength after 20 weeks *in vivo* [23].

2.2 Bioabsorbable Composites

In the early seventies, it was determined that bioabsorbable polymers like PGA and PLLA would require some type of reinforcing element to provide the strength and toughness necessary for clinical use in bone surgical applications [4] Thus partially absorbable composites were introduced Copolymers of methyl methacrylate and N-vinyl-pyrrolidone reinforced with polyamide fibers were used in over 1000 operations in Soviet medical centers [27] Other absorbable systems include rods of PGA/PLA copolymers reinforced with carbon fibers and poly(DL-lactide) plates reinforced with carbon and ceramic fibers [4]

Particulate and fibrous composites are the two main types of totally bioabsorbable polymeric composites that have been used experimentally and clinically in biomedical applications [4,28] Incorporation of particulate materials improves the fracture resistance in brittle polymer matrices by promoting and arresting crazing One example of this type of composite is PLLA reinforced with hydroxyapatite particles [5] The particles are effective in enhancing the stiffness of composites, but generally do not increase the strength [28]. In contrast, the incorporation of fibers helps to improve the strength properties of the material because fibers are much stronger than the bulk form of the same material [29] Examples of fibrous composites are absorbable polymers reinforced with ceramic fibers, self-reinforced PGA or PLA composites, and PLA matrix reinforced with PGA fibers [3]. Self-reinforced polyglycolide composites with fiber and matrix materials having the same chemical composition have been used for bone

fracture fixation [4,29] Dexon sutures are partially sintered at elevated temperature and pressure to form rods of various diameters. These rods had a bending modulus and bending strength of 15 GPa and 220 to 450 MPa, respectively [4].

The mechanical properties for fiber/matrix composites depend on the properties of the fiber and matrix individually, as well as the strength of the bond between them. Developing good adhesion between the matrix and the reinforcing element is always a concern when fabricating composites. If the interface is sufficiently strong, the stresses acting on the matrix can be transmitted to the fiber across the interface [31] As a result, the composite will have high static strength However, a composite having poor interfacial bonds has low tensile strength Poor adhesion is one of the major problems that limited the use of bioabsorbable composites because the weak bonds allow rapid diffusion of fluid to the interface leading to poor strength retention *in vivo* [4,32]. Adhesion between the fiber and matrix is attributed to four main mechanisms at the interface. They are wetting, interdiffusion, chemical bonding, and mechanical bonding [29,31].

The term wetting is usually used to describe the ability of a liquid to spread over the surface of a solid by displacing air and any contaminants that are on the surface. In this case, wetting can be used to describe how effectively a molten polymer wets the fiber surface. The idea of wetting is expressed mathematically as

$$\cos\theta = \frac{\gamma_{SV} - \gamma_{SL}}{\gamma_{LV}} \qquad \textbf{(2.1)}$$

where θ is the contact angle, γ is the surface energy or tension and the subscripts SV, SL, and LV are the solid/vapor, solid/liquid, and liquid/vapor interfaces, respectively. In most cases, partial wetting occurs where θ lies between 0° and 180°. Wetting will occur as long as the LV interfacial tension is less than some critical surface tension of the solid. In other words, the liquid surface tension must be less than the solid's critical surface tension [29,31,32].

Interdiffusion involves the penetration of polymer molecules on one surface into the molecular network of the other surface. Thus, the interfacial bond strength will rely on the number of entanglements and the amount of molecules involved. The interfacial strength of the interface also depends on the number and types of bonds present between the fiber and the matrix [29].

Lastly, mechanical bonding may occur by the mechanical interlocking of the two surfaces. The roughness of the fiber surface not only increases mechanical bonding, but it also facilitates chemical bonding by increasing the surface area available at the interface The shear strength of the interface is greatly influenced by the mechanical bond between the fiber and the matrix [32].

Other factors also affect the mechanical strength of composites. First, fiber bunching can cause resin poor regions. This issue becomes important when employing composites that undergo compressive loading because compressive strength is most affected by the matrix shear modulus. When fiber bunching occurs, the actual strength of the composite is lower than expected [28] Second, the presence of voids, depending on their size, can also lead to a reduction in compressive strength and interlaminar shear

strength [31]. Third, poor alignment can result in preferential fiber orientation that increases the probability of fiber buckling [28] Finally, fiber debonding may occur as a result of characteristic differences between the fiber and the matrix (such as differences in modulus or poisson's ratio) [28]. Continuous fiber-reinforced composites are candidates for totally bioabsorbable fixation devices. It is believed that these materials could provide higher strength and fatigue properties for use as plates and rods in load-bearing bones [10]

Failure of bioabsorbable composites is very complex Failure modes include fiber and/or matrix degradation, ply delamination, and fiber debonding [3]. Failure is often manifested by microvoids at the fiber-matrix interface. Slivka and Chu [3] found that the strain level, wicking, and type of reinforcing material play an important role in the failure of the composite *in vitro*. Moderate strains had a tremendous effect on the interface At 5 % strain, necking occurred and at strains above 10% fibers broke into fragments. "Wicking is a form of capillary action by which the degradation medium is drawn into the fiber-matrix interface and the degradation products are leached out [3] " Wicking serves to accelerate the degradation process.

Cracking, fiber breakage, and weld-line formation are other failure modes that composites undergo. Matrix cracking forms at right angles to the fiber-matrix interface. This type of shear cracking unloads the fiber and the stresses in the fiber are relaxed Weld lines, on the other hand, form between amorphous layers and results from fabrication techniques instead of the properties of the materials [3,28].

2.3 Bioabsorbable Internal Fixation Devices

2.3.1 Cellular Response of pins and screws

In healing, it is desirable that the rigidity of the fixation device depreciates with increasing strength of the healing bone. During the initial stages, a more rigid structure is needed to promote soft callus formation. The implant shields the tissue from any stresses due to loading As healing continues and bone or tissue growth ensues, the device degrades, becoming less rigid, to allow for increased motion and transfer of loads to the tissue [3,7,8]. Metallic implants do not transfer the load during the healing process Consequently, the tissue is not being used and tissue growth diminishes [3,22] The clinical success of absorbable implants is dependent on many factors including (but not limited to) biocompatibility, high initial strength, implant degradation rate, controlled strength retention, implant site, chemical structure, and fabrication/processing techniques [22,26]. Although polymeric devices show significant advantages over metallic devices, they also have their limitations. For example, resorbable polymers are not as strong as metallic devices. Also, they may cause adverse tissue responses. As the implants degrade, they form debris that can cause foreign-body reactions. In ideal situations, the debris is digested by giant cells and macrophages. However, if the reactions are not maintained at low levels, they could interfere with the healing process [29]. During the biodegradation process, some patients have local fluid accumulation (LFA) which is manifested by swelling, redness of the skin and pain. If not treated properly, it may lead to sinus formation [29]. This problem is often avoided by using colorless implants in highly vascularized sites where healing occurs rapidly [29].

In extensive animal studies, poly-α-hydroxy acids like PGA and PLLA have shown good biocompatibility. The use of SR-PGA rods and screws has been documented in thousands of operations with bone fracture healing comparable to that of metallic fixation devices [26]. Polydioxanone (PDS) and self-reinforced poly(glycolic acid) (PGA) bioabsorbable pins degrade quickly and do not have high strength retention [28]. Atkinson et al. also reported sinus formation, marked by intense swelling, and erythema occurred in 4 to 8% of patients with PDS rod implants [22]. Biofix® devices (PGA and PLA pins) are used routinely in clinical research in the USA, Australia, and Western Europe [26]. Severe complications with these devices were reported by Fridén and Rydhom in 1992; prompting an investigation into the use of these pins [11]. The surrounding tissue was unable to support the amount of debris produced by the rapidly degrading material. The adverse effects reported include swelling at the implantation site and sinus formation. In some instances, sterile abscess and effusions also occurred [11].

2.3.2 Mechanical Properties of Internal Fixation Devices

To ensure that bone fractures are fixed securely, metallic materials were used successfully because of their relatively high strength values. In an effort to further improve the healing response of bone, non-reinforced injection-molded biodegradable polymeric devices were employed [26]. PGA and PLLA implants only showed minimal mechanical strength when manufactured by nonreinforcing techniques (see **Table 2.2**). However, the mechanical properties (strength, modulus, toughness, etc) increased significantly when the polymer was oriented into structures such as microfibrils,

Table 2.2. Initial mechanical properties of bioabsorbable polymeric rods manufactured by self-reinforcing (SR-) and injection-molded (IM-) techniques [26].

Material	*Diameter (mm)*	*Deformation Mode*	*Bending Modulus (GPa)*	*Bending Strength (MPa)*	*Shear Strength (Mpa)*
SR-PGA	2.0	Free drawing	13	320	240
SR-PGA	3.2	Sintering	12	360	220
IM-PGA	2.0	—	7	218	95
SR-PLLA	1.3	Die drawing	10	300	220
SR-PLLA	3.2	Sintering	—	250	96
IM-PLLA	2.0	—	3	119	68

macrofibrils, or fibers by using free drawing, die drawing, shearing or rolling deformation techniques [26]. PLLA in fiber form has a higher strength, stiffness and strength retention than its molded form. Sintering or partial melting of polymer fibers under elevated pressures is another technique used to manufacture self-reinforced composites [26].

Solid-state extrusion of PLLA, poly(L/D-lactide) and poly(L/DL-lactide) produce highly oriented fibrillar structures with high strength and modulus. The values for flexural modulus and strength of experimental and commercial devices vary from 80 to 300 MPa and 3 to 13 GPa, respectively [33]. The study by Ferguson et al. showed that the mechanical properties of these polymers were affected by the draw ratio [33] The flexural strength and flexural modulus increased with draw ratio up to a draw ratio of 10. The maximum values for the flexural strength was 215 MPa and 13.7 GPa for the flexural modulus [33]. The bending strength for various types of bioabsorbable pins are listed in **Table 2.3.**

Table 2.3. Literature values for the bending strength of bioabsorbable pins [5,30].

Sample	*Manufacturing Process*	*Composition*	*Initial Bending Strength (Mpa)*
Polypin™	Injection molded	70:30 Poly(L-DL-lactide)	155-163
PDS pin	Die drawn	Poly(para-dioxanone)	53
SR-PGA pin	Sintered fibers	Polyglycolic acid	250
Die-drawn PLA pin	Die drawn	Poly(L-lactide)	240
Super-Fixsorb-MX®	Forging process	70:30 Poly(L-lactide) /Hydroxyapatite	270
Bionx SmartPin™	Sintered fibers	Poly(L-lactide)	200

2.4 Fiber Extrusion

There are a variety of techniques available for extrusion of fibers. The techniques commonly used are melt spinning and solution spinning [34]. These techniques have been used frequently for producing PLLA fibers [35]. In general, the highest tensile strengths have been realized with solution spinning. Tensile strength values of 1 to 2 GPa have been reported using this process which is at least twice as high as the 0.5 GPa value achieved through melt spinning [16,17,36]. Unfortunately, the use of toluene and chloroform as solvents prevents the use of the fibers produced through solution spinning in medical applications due to their toxicity [16,36].

2.4.1 Melt Spinning and Drawing

Melt spinning is a relatively simple process that requires lower energy consumption than other spinning techniques [37]. It is a process that uses high temperatures to melt the polymer and then the molten polymer is pumped through the die or spinneret. The spinneret can contain anywhere from one to any number of small holes.

If collected at low speeds, the fibers have low orientation and mechanical properties. Enhanced properties are achieved through the drawing process. Hot drawing can be used to transform polymer chains into highly oriented fibrillar structures. Since the 1970's, researchers have used this technique to prepare highly oriented, nonresorbable polymeric materials with high strength and modulus. More recently, this method has been used to enhance the properties of bioabsorbable polymers [17].

Two step stretching (TSS), spin draw take up (SDTU) and spin take up (STU) are examples of basic melt spinning and drawing techniques used commercially [38]. TSS is a process in which spinning and drawing are performed separately The fiber is spun and collected at low speeds ranging from 500 to 1500 m/min. Then in a separate step, the fibers are drawn and collected [38] In contrast, melt spinning and drawing are coupled into one continuous process in the SDTU technique Drawing occurs between the rollers of the godet at controlled temperatures. After passing over the final set of rollers, the fiber is wound onto a bobbin at moderate speeds ranging from 2000 to 5000 m/min [38]. The third process involves high speed spinning of fibers. STU is a one step process in which fibers are spun and wound onto a bobbin at speeds of 4000 to 6000 m/min [38]. **Figure 2.4** contains schematics of the three techniques.

2.4.2 Bicomponent Fiber Spinning

Since the 1960's, efforts have been made to blend polymers in an effort to modify the material properties. Bicomponent melt spinning which involves extruding two different materials through one spinneret hole, is a technology that has been used successfully to manufacture fibers having two or more components [39]. A simple

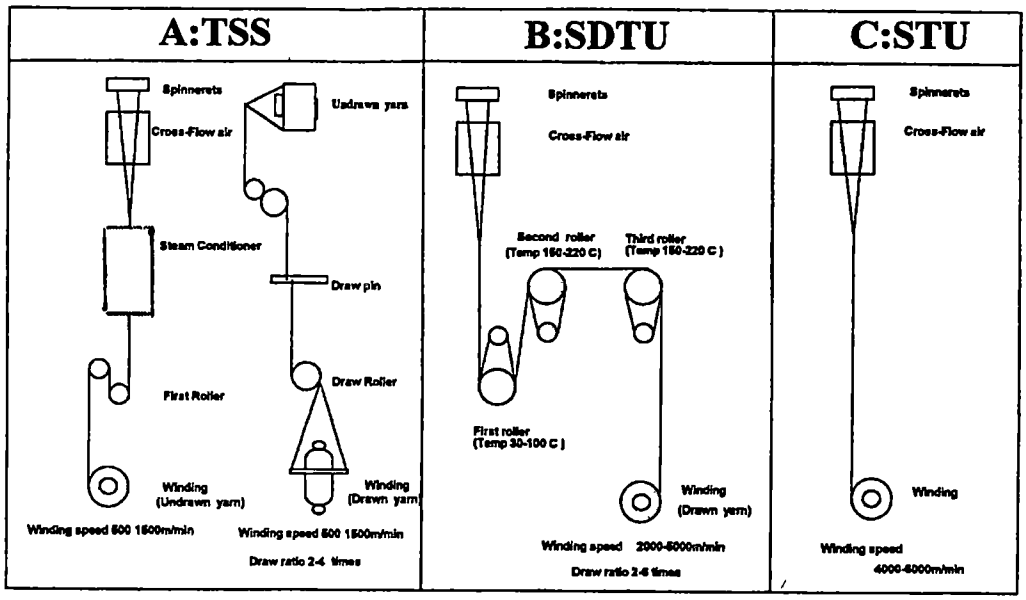


Figure 2.4. Melt spinning and drawing techniques [38].

schematic of this process is shown in **Figure 2.5**. There are many problems associated with these types of systems. One is understanding the rheology of two-phase systems. Another problem involves understanding the hydrodynamics of two-phase flow. Some of the available theoretical solutions include annular flow of Newtonian fluids [15], flow of emulsions of Newtonian suspensions, and two-phase flow of viscoelastic fluids [39].

Several types of two-component fibers can be spun from fiber-forming polymers [39-41]. Generally, they are divided into two categories – bicomponent and biconstiuent fibers. Biconstituent fibers are blends of small, distinct fibrils embedded in a relatively continuous polymer matrix [40]. In contrast, bicomponent fibers are composed of two polymers occupying distinct regions. Typically, bicomponent fibers contain at least one crystalline polymer [41]. Examples include the side-by-side configuration and the

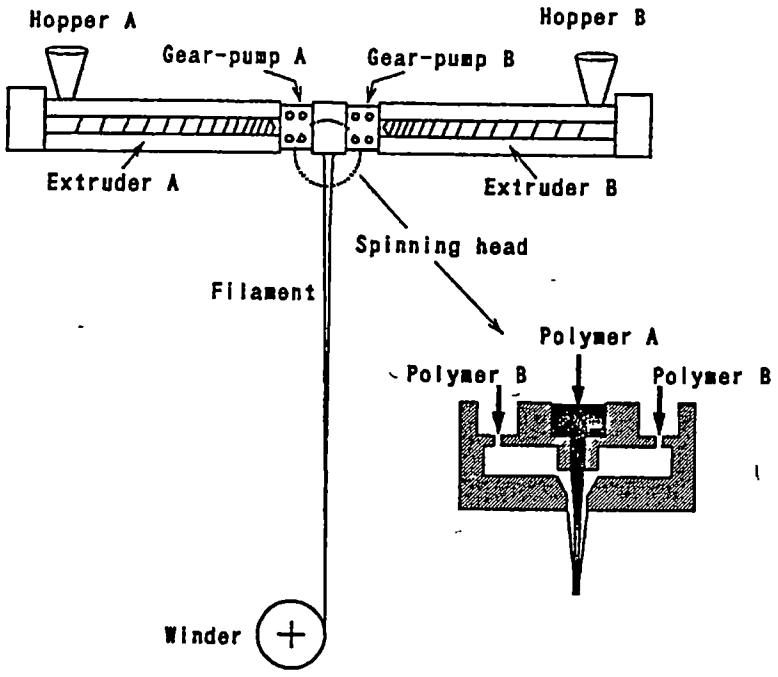


Figure 2.5. Schematic illustration of Bicomponent Spinning setup [41].

sheath-core configuration (**Fig. 2.6**) [40].

A variety of interface shapes can be obtained depending on the types of polymers used and the extrusion conditions. In general, surface tension, viscosity, and elastic normal stresses are the major factors affecting the resulting structure [39]. Two phase flow can be affected by the differences in surface tension between the components. However in bicomponent spinning, the effect is minimal. Interface tension has a greater effect on the shape of the cross-section [39]. In these types of systems, viscosity has the greatest effect on the extrudate. There is a tendency for the component with the lowest viscosity to migrate to the periphery. At high viscosity differences, the cross-section assumes a sheath-core structure [39].

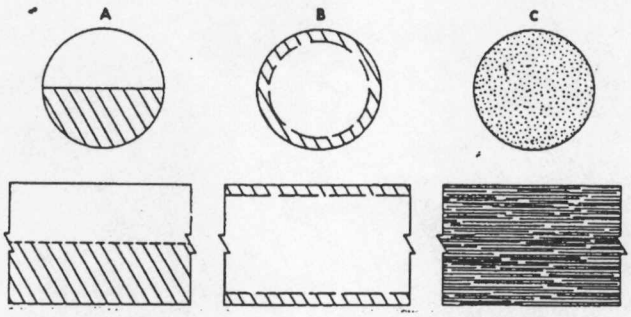


Figure 2.6. The three major types of fibers formed by co-extrusion of two polymers: (a) side-by-side, (b) sheath-core, and (c) matrix-fibril [40].

Bicomponent fiber spinning has been studied by several researchers. Its popularity is growing in the polymer processing industry as a way to produce fibers with noncircular cross sections, various specialty fibers, ultra-fine fibers, electrically conductive fibers, and fibers for thermal bonding [42-44]. The structure development experienced in bicomponent spinning is expected to differ from the properties obtained in single component spinning due to the mutual interaction of the two components in the spinline [18]. Significant differences in their inherent properties (such as activation energy of elongation, viscosity, and solidification temperature) are believed to be the main factors influencing these interactions [13,42]. These interactions can enhance orientation development of the components of the system [13]. Kikutani et al. [43] studied the structural characteristics of PET/PP bicomponent systems. They found through birefringence measurements that the molecular orientation of the PET component increased through bicomponent spinning while the molecular orientation of PP decreased. In addition, they looked at the influence of bicomponent spinning on the density. The results suggest that enhancement of molecular orientation in PET promotes orientation-

induced crystallization [43]. In another study on spinning of high and low molecular weight PET, observations indicate that the sheath/core ratio affects the amount of orientation developed. The birefringence of HMPET in the 1·1 configuration was higher than in the 4:1 system where the ratios are HMPET:LMPET [42].

CHAPTER 3

Experimental Methods: Processing Techniques

3.1 Bicomponent Fiber Spinning

Initial melt spinning experiments were conducted at Randcastle Extruder Systems using two 5/8 – inch single screw extruders with a length to diameter ratio of 20 1. Both extruders had four heating zones. The residence time in this extruder was three minutes The spinning conditions are in **Table 3.1**

The extruder system at the University of Tennessee contained two 3/4 – inch single screw extruders connected by a bicomponent block (see **Fig. 3.1**) Each extruder contained three heating zones; and the bicomponent block contained two zones - the spin block zone and the die block zone (see **Fig. 3.2**). Two metering pumps were connected to the extruders at the spin block to maintain a constant mass thruput (see **Fig. 3.3**) The spin pumps contain solid state AC motor control with variable frequency AC drive The max speed of the pumps is 1720 RPM. The screw speeds

Table 3.1. Bicomponent spinning conditions used at Randcastle Extruder Systems, Inc

	4·1 Core Sheath Ratio		2 1 Core:Sheath Ratio	
	Core	Sheath	Core	Sheath
Screw Speed (RPM)	8 5	2.1	6.7	3 1
Zone 1 Temperature (°C)	340	340	340	340
Zone 2 Temperature (°C)	403	330	403	330
Zone 3 Temperature (°C)	390	250	390	250
Zone 4 Temperature (°C)	364	370	364	370
Temperature of melt (°C)	381	364	381	364
Back Pressure (psi)	710		630	
Mass throughput (g/min)	6 66		14 60	
Take-up speed (FPM)	200-500		200-500	

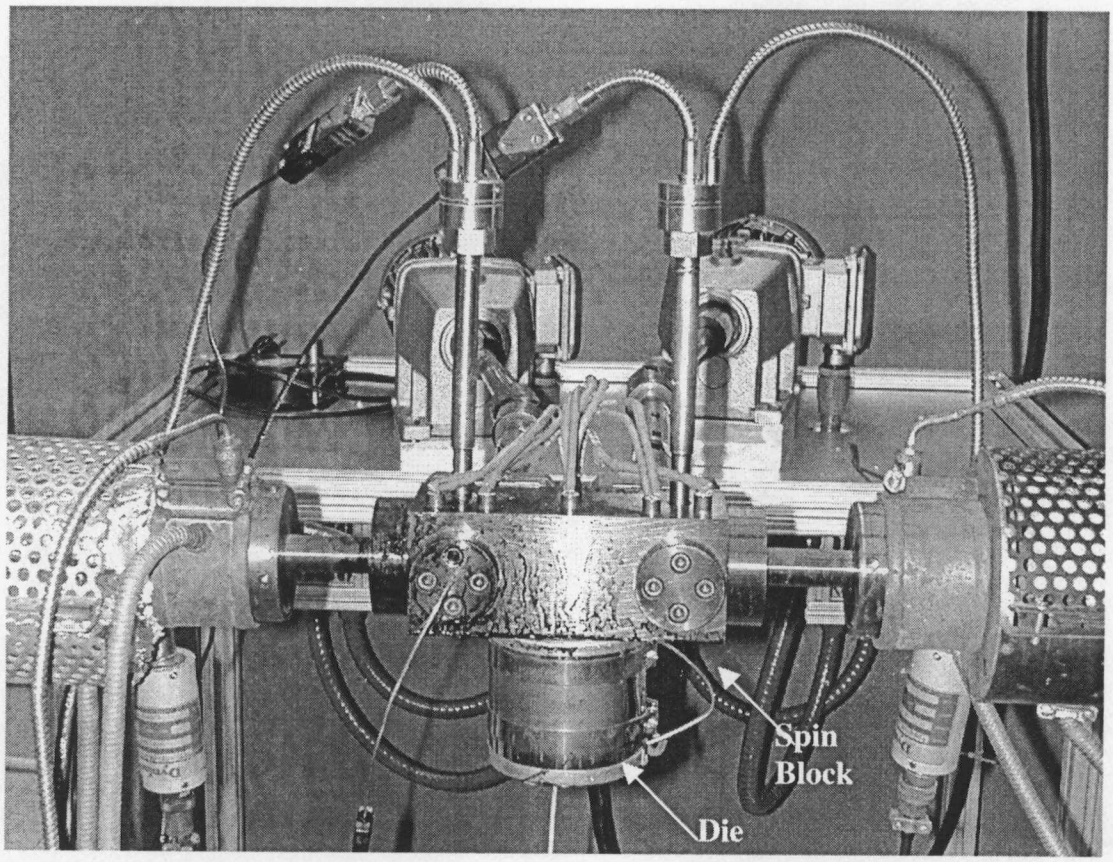


Figure 3.1. Bicomponent spinning equipment. Bicomponent die block connecting two single extruders.

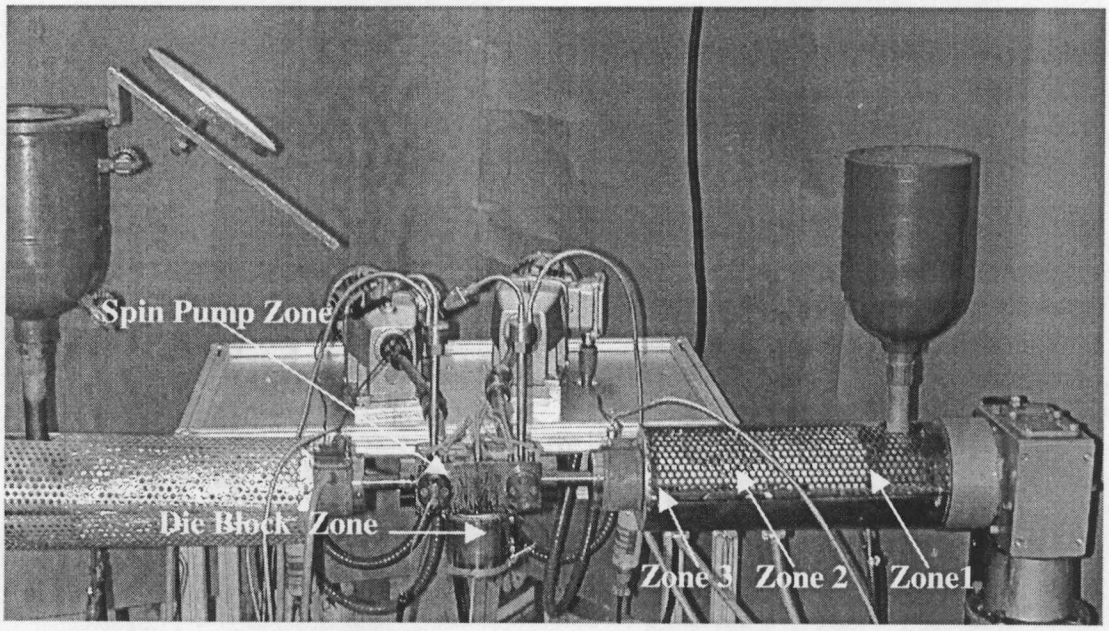


Figure 3.2. Bicomponent spinning equipment. Heating zones of extruder system.

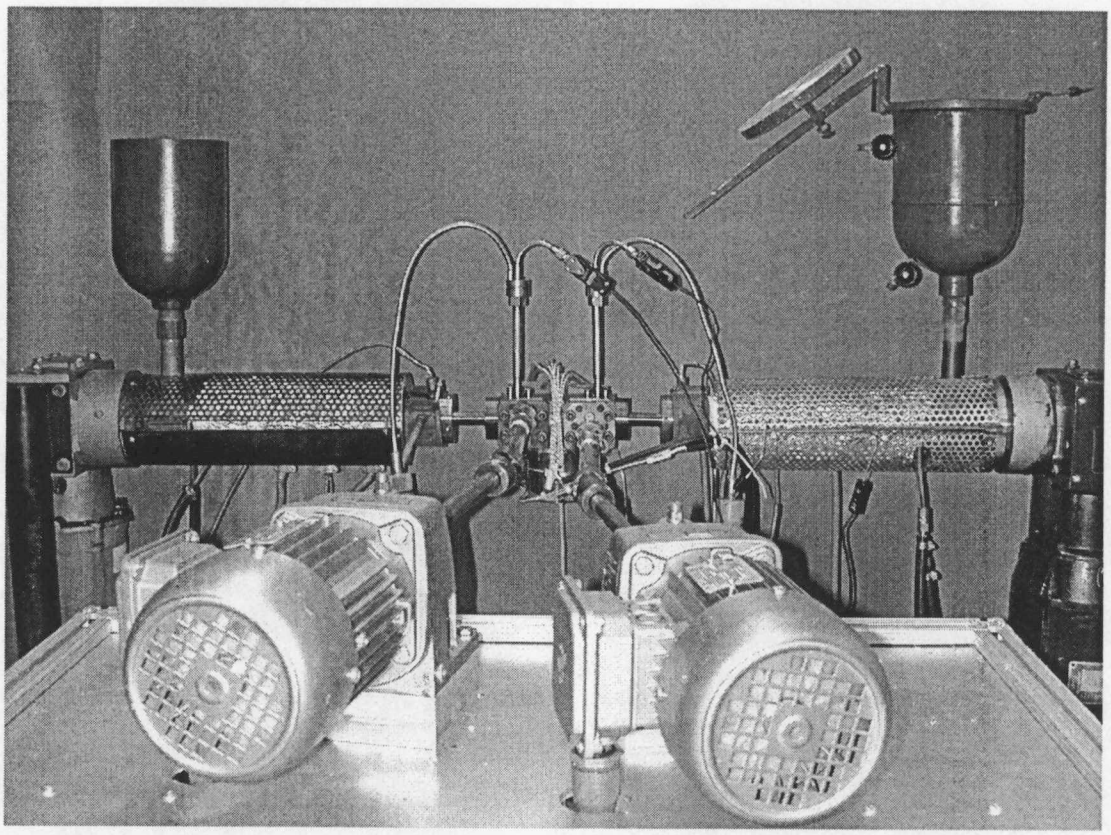


Figure 3.3. Bicomponent spinning equipment. Metering Pumps.

for each extruder were calibrated with a tachometer.

The speed of the spin pumps was adjusted to give the desired core-sheath ratio while maintaining a mass throughput of approximately 8.5 g/min at each ratio The combined spin pump speed was about 18 RPM. The pressure at the spin block was kept between 1000 to 2500 psi. As the fiber exited the die, it was air-cooled by a fan sitting about 4 inches below the die exit. The fiber was guided through a trough and wound onto 4 inch bobbins at a take-up velocity ranging from 95 to 125 MPM (see **Fig. 3.4**). The actual spinning conditions used with this system are in **Table 3.2.**

Because poly(lactic acid) is hygroscopic, the materials were dried in an oven under a vacuum for at least five hours at a temperature of 110 °C. The materials was then transferred to a dessicator until they were to be used in the spinning experiments.

3.2 Continuous Drawing

Drawing was carried out as a separate processing step from melt spinning. The bicomponent filaments were drawn using a heated trough and a temperature controlled continuous drawing machine equipped with two heated godet rolls per stage (see **Fig. 3.5**). Filaments from an undrawn spool of fiber were fed though the trough and then wound onto the first set of rollers The second and third rollers were not used The filament was guided across the top of the second and third rollers and wound onto the bobbin using the constant tension winder.

The temperature of the first roller was set at a constant 60 °C. The second and third rollers were maintained at room temperature. For drawing, the first set of rollers

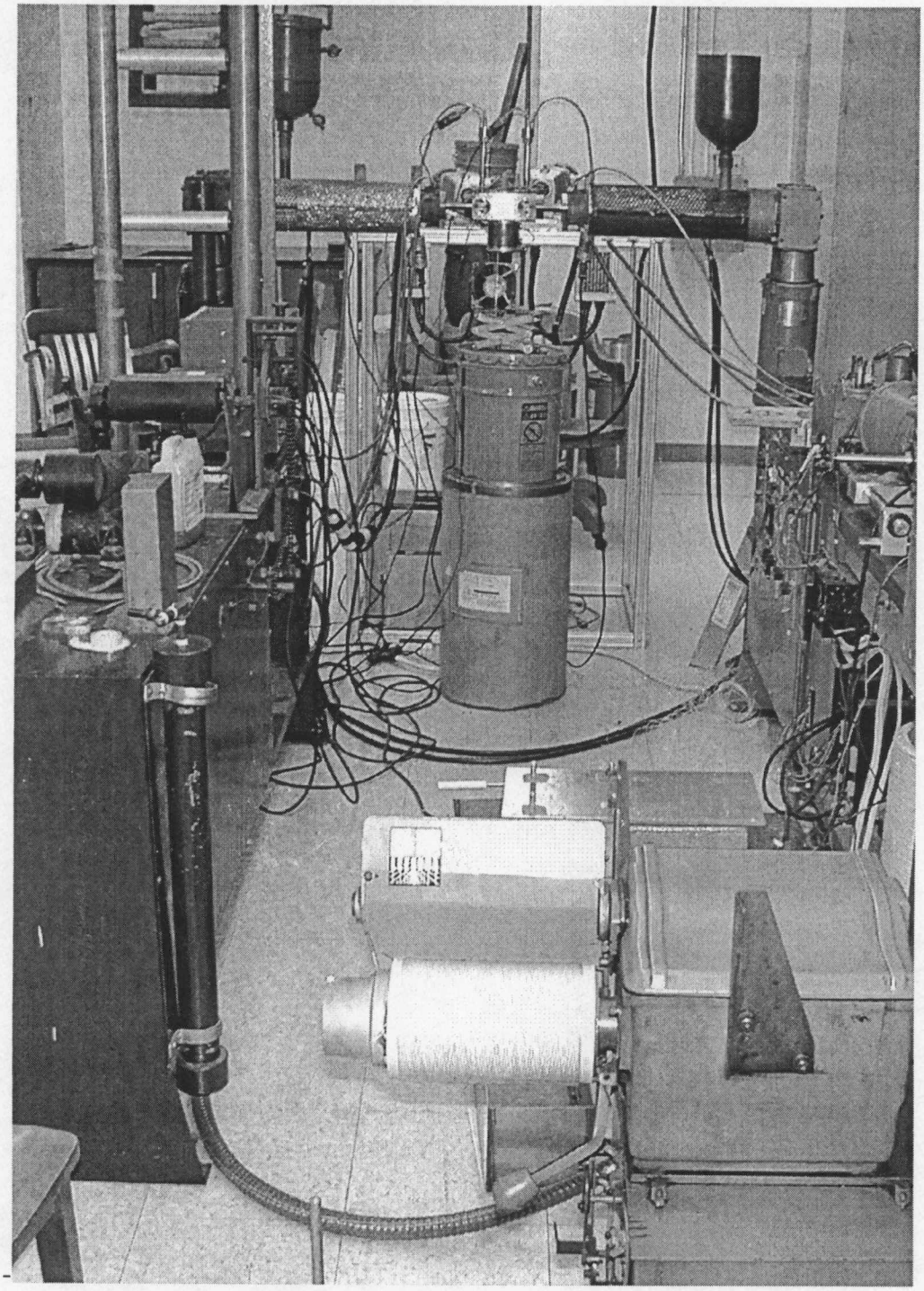


Figure 3.4. Bicomponent spinning system.

Table 3.2. Typical spinning conditions used with the spinning system at the University of Tennessee.

	Industrial-grade Polymers		Medical-grade Polymers	
	Core	Sheath	Core	Sheath
Zone 1 Temperature (°C)	185	193	225	185
Zone 2 Temperature (°C)	220	193	265	185
Zone 3 Temperature (°C)	175	188	240	182
Temperature of melt (°C)	172	176	200	185
Die Block Temperature (°C)	170		187	
Spin Block Temperture (°C)	170		185	
Back Pressure (psi)	1000-2000		1000-2000	
Mass throughput (g/min)	8 5		8.5	

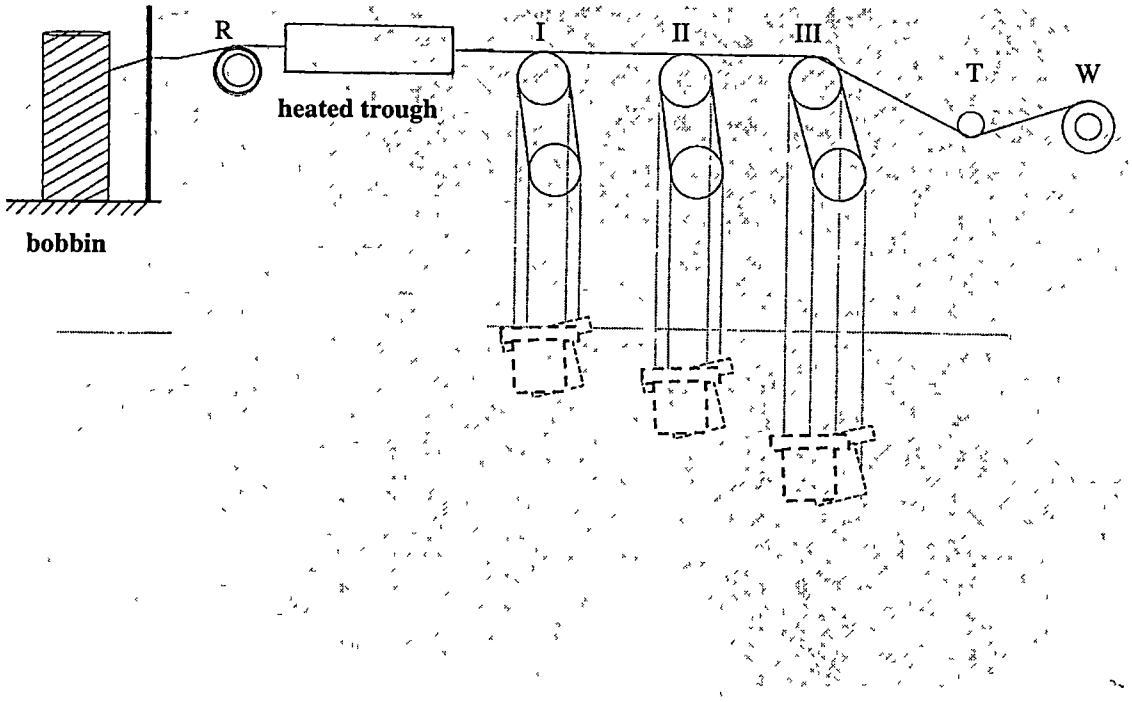


Figure 3.5. Schematic of drawing system R = small feed roller; I, II, III = godet rollers 1,2, and 3, respectively; T = constant tensioner, W = winder.

I, were held constant at 17 RPM. The speed of the leader roller, **R**, (between the spool of fiber and trough) was reduced to slowly cause drawing of the filaments. The filaments were drawn at various temperatures by adjusting the temperature of the trough. The drawn filaments were used to produce 2 0 mm composite rods.

3.3 Composite Rod Fabrication – Pultrusion Die

Two millimeter composite rods were manufactured using the pultrusion die shown in **Figure 3.6**. The system consisted of a conical die with an exit diameter of 2 0 mm The die contained four heaters that were controlled by the temperature control box. A syringe pump motor was used to control the rate at which the filaments were pulled through the die. A metal guide rod with a caster and weight system was used to provide a mechanism for applying tension to the filaments.

The bicomponent filaments were wrapped around a rectangular box a sufficient number of times to provide enough filaments to produce a rod 2.0 mm in diameter. Wire was tied to both ends of the fiber; then the fiber was removed from the box One of the tied ends was threaded through a piece of tubing 2.36 mm in diameter Then the filaments were fed into the die and connected to the syringe pump The back end of the filaments were passed over the caster and tied to a 400 gram weight. The filaments were pulled through the heated die at a constant rate. Different die temperatures and pultrusion rates were used.

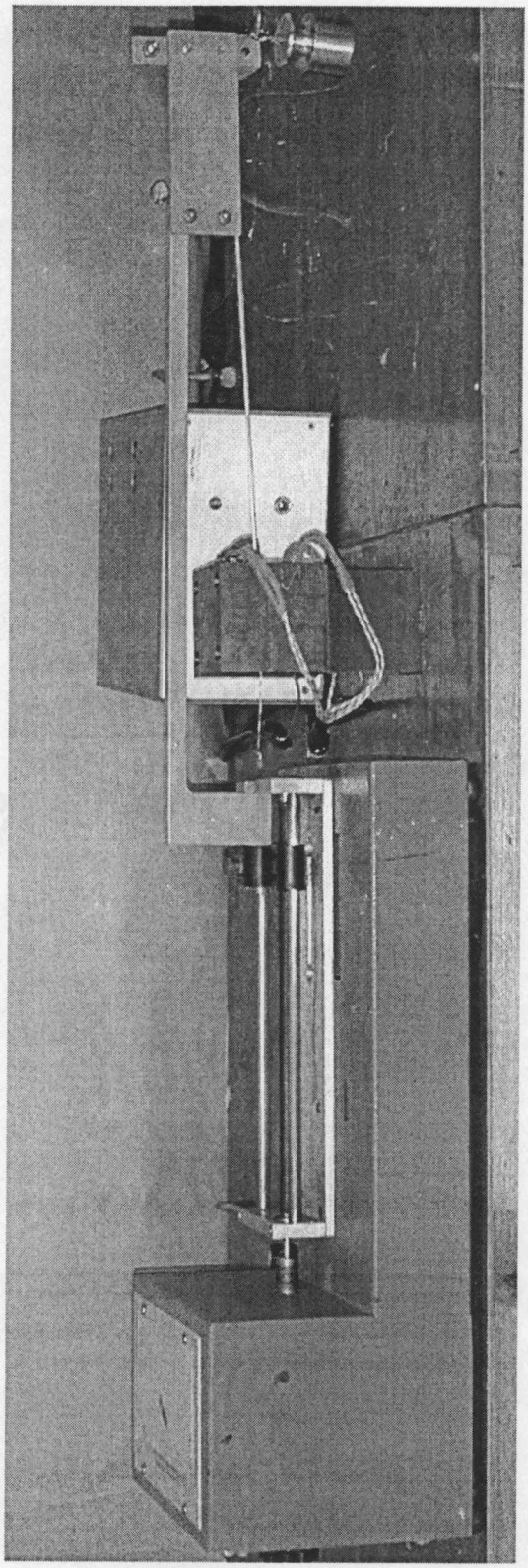


Figure 3.6. Pultrusion Die System.

CHAPTER 4

Experimental Methods: Characterization Techniques

4.1 Materials

The polymers used in this study were obtained from Birmingham Polymers, Inc (BPI), Cargill Inc , and from Purac Biochem b.v. The materials obtained from BPI were used in the polymer selection process and all preliminary fiber studies. The Cargill materials were used to determine the optimum fiber properties and optimum processing conditions for fabricating the composite rods Purac polymers were used in the final fiber spinning and composite rod fabrication processes.

Three amorphous polymers were obtained from Birmingham Polymers, Inc They were poly(trimethylene carbonate) (PTMC), a copolymer of 75 mole percent L-lactide and 25 mole percent dl-lactide (PLDL), and a copolymer of 33% trimethylene carbonate and 67% PLDL (poly(co-TMC, co-PLDL)) The polymers from Cargill, Inc included polylactic acid with ~1% D-lactide and a polylactide with 9.8% D-lactide. Three polymers were custom synthesized by Purac for use in the fiber spinning study. They were poly-L-lactide (PLLA) and two 70/30 poly(L/DL-lactide) copolymers of differing viscosities. The properties of these materials are listed in **Table 4.1**

4.2 Polymer Selection -Peel Test

The purpose of this study was to suggest an optimum temperature and time for the formation of a strong adhesive bond between candidate polymers for processing of sheath-core type bicomponent fibers The T-peel test was used to determine the effects of bonding temperature and contact time on peel strength.

Table 4.1. Properties of polymers.

Sample ID	Mn	Mw	Inherent viscosity (dL/g)	Tm (°C)	Tg (°C)	%D
PTMC			2 77		-20 0	—
75/25 PLDL			1 41		55 0	12 5
33/67P(co-TMC,co-LDL)			0 97		26.2	12 0
PLLA	232 k	387 k	2 63	174 8-191 7	56 0	∠1 0
70/30 PLDL (A)	152 k	237 k	1 62	110 2-116 4	55 0	15
70/30 PLDL (B)			3 98		55 0	
INDPLA 1	105 3 k	212 5 k	1 32	177	55 0	1 0
INDPLA 2	93 1 k	211.9 k	1 65	175	55 0	1 0
INDPLDL	85 6 k	186 k	1 32	180	55 0	9 8

Medical grade poly(L-lactic acid) (PLLA) was adhered to three candidate sheath polymers to form adhesive joints . The sheath materials were PTMC, PLDL, and poly(co-TMC, co-PLDL) produced by BPI

4.2.1 Sample Preparation

For each material, thin films were melt-pressed between two sheets of teflon. PLLA was prepared at 200 °C and the copolymers were prepared at 160 °C. The load applied ranged from 5 to 7000 lbs The polymers were melt-pressed onto fine woven, aluminum wire cloth backed with heavy gauge, heat-tempered foil under loads of approximately 5000 lbs.

PTMC and each copolymer were paired with PLLA; and the polymer surfaces were gently pressed together at low temperature and pressure. Then the sheets were cut into samples 10 cm in length and 1 cm in width. At least 1.5 cm of the length was left unbonded to form arms for the peel test. The sandwich foil samples were then placed

between two aluminum plaques, 0 4572 mm (1/8 –inch) in thickness. Then the plaques were wrapped in foil to prevent the samples from coming into contact with the oil in the oil bath. The samples were heated in a silicone oil bath at various temperatures and contact times (110 °C – 210 °C in 15 °C increments, for 5, 10, 30, and 60 seconds) and quenched in ice water.

4.2.2 Testing

The T-peel test can be used as a qualitative way to compare the strength of various joints. There are three basic types of adhesive joints the Hooking joint, improper joint; and proper joint The hooking joint is formed between grossly porous or fibrous materials [45]. An improper joint contains a weak boundary layer between the adhesive and at least one of the materials to which it is adhered, and the adhesive and adherend together give rise to a weak material [45]. Proper joints are joints that fail cohesively and/or adhesively [45] While adhesive failure involves debonding of the two materials at the interface, cohesive failure takes place within one of the bonded materials [46]. In These experiments, adhesive failure occurs at the interfacial bond between the two polymers; and cohesive failure occurs within the bulk of one the polymeric materials

Peel strength is defined as the average load per unit width of the bondline necessary to continuously separate two flexible materials [47,48] The T-peel strength, n, is calculated as the average force applied to the joint per unit width of the sample The force required for continued peeling of the joint is referred to as the average peel force, P. The equation used for calculating the peel strength is given in Equation 4 1. Some factors which can affect the peel strength include: (1) chemical and physical properties of the

adhesive and the adherends; (2) processing variables such as temperature and time; and (3) testing parameters such as the test temperature and peel rate [47,49].

$$n = \frac{P}{w} \tag{4.1}$$

The T-peel test was performed in accordance with ASTM method D 1876-95 The tests were performed at a constant crosshead speed of 100mm/min. It is assumed that a sharp increase in peel force indicates the conditions required for sufficient bonding.

Adhesion between two materials results from molecular attractions acting across the interface. The diffusion theory of adhesion suggests that creation of a strong bond between two polymers occurs due to interdiffusion of polymer molecules on one surface into the molecular network of the other surface In this case, interfacial bond strength will depend on the degree of entanglement. Diffusion of macromolecules having significantly differing mobility is referred to as adhesion. Conversely, cohesion involves diffusion of molecules with similar mobility [49]. The degree of adhesion is affected by the polymer chain's structure and flexibility, and by the relative viscosities of the adhering materials [49]. Chemical bonding is another mechanism for adhesion. The strength of the adhesive joint depends on the number and type(s) of bond(s). Failure is a consequence of bond breakage. For strong bonds, there exists a high breaking stress for both the adhesive and adherend

4.3 Draw Ratio Determination

Draw ratio is defined as the length of material after drawing divided by its initial length. If the mass is constant, then the draw ratio can be written in the form:

$$DR = l/l_0 = (\rho_0/l_0)/(\rho/l) \quad (4.2)$$

where (ρ/l) is the linear density of the fiber. Then assuming that the volume of a given mass of fiber is constant, the draw ratio can be expressed as the ratio of mass per unit length of as-spun to drawn fiber as shown in **Equation 4.3.**

$$DR = m_0/m \quad (4.3)$$

The mass of one meter of drawn fiber is m and m_0 is the mass of one meter of undrawn fiber. This method was chosen due to variations in the diameter of the as-spun fiber.

4.4 Optical Microscopy

Light optical microscopy was used for quick and easy observations of material morphology. The Olympus BH-2 optical microscope was used to verify that the bicomponent fibers had a sheath/core structure. The fibers were cut perpendicular to the fiber axis into thin sections. The samples were placed on a glass slide and covered with a cover slip. The samples were observed at 100X and 40X magnification.

4.5 Optical Birefringence

Birefringence is defined as the difference between the refractive index in two orthogonal directions [50]. Birefringence techniques can be used to measure the molecular orientation of polymeric materials. The difference in refractive indices

depends on the degree of molecular orientation, the chemical structure of the chains, and deformation effects [51].

4.5.1 Types of Birefringence

Orientation, stress, and form birefringence are the three basic types of birefringence. The total birefringence can be written as the sum of these three types as shown in **Equation 4.4.**

$$\Delta n=\Delta_o+\Delta_s+\Delta_f \qquad (4.4)$$

Orientation birefringence (Δ_o) results from the preferential alignment of polymer chains. It is dependent upon the degree of molecular orientation and the types of bonds present [50,51] Stress birefringence (also called deformation birefringence), Δ_s, occurs due to stretching of bonds. These bond distortions may occur in conjunction with orientation of the polymer Therefore, Δ_s is usually neglected if the orientation birefringence is the principle quantity of concern [51] Form birefringence (Δ_f) may occur when the material contains more than one phase with different refractive indices [50]. It is a result of distortions of the electromagnetic field at the interface For example, form birefringence may occur due to the anisotropy between the fibers and the matrix in a composite system.

4.5.2 Methods

Birefringence measurements were performed using an Olympus BH-2 optical microscope with a 10 order Berek compensator. The retardation was determined using the values given in the Leitz compensator manual. The fiber diameter was determined

with a filar eyepiece. The distances were calibrated with an Olympus graduated slide. A 40X objective and a 100X eyepiece were used for all measurements. The optical birefringence was calculated using the equation:

$$\Delta = \Gamma/d \qquad (4.5)$$

where Δ is the total birefringence of the fiber, Γ is the retardation, and d is the fiber diameter.

4.6 Dilute Solution Viscosity

Measurements of solution viscosity are usually made by comparing the efflux time of the polymer solution to the efflux time of the solvent. The efflux time is the amount of time required for a specific volume of solution to flow through a capillary tube. Using the efflux time of the solvent, t_0, the efflux time of the polymer solution, t, and the concentration, c, the following quantities can be calculated [52]:

Relative viscosity	$\eta_r = t/t_0$	**(4.6)**
Specific viscosity	$\eta_{sp} = \eta_r - 1$	**(4.7)**
Inherent viscosity	$\eta_{inh} = (\ln \eta_r)/c$	**(4.8)**

In this experiment, the inherent viscosity is measured and compared to values given by the manufacturer. The purpose of the experiment is to determine if degradation occurs during fiber spinning.

4.6.1 Sample Preparation

Dilute solutions of poly(lactic acid) in chloroform were prepared to yield a final concentration of about 0 1g/dL. Approximately 100 mg of polymer was dissolved in 100

mL of chloroform. The polymer was placed in a 125 mL volumetric flask, and 100 mL of chloroform was transferred to the flask using a 100 mL pipette. The solution was heated at 50 °C for 20 minutes or until the polymer was completely dissolved. The solution was allowed to cool. The materials used in this experiment are listed in **Table 4.2.**

4.6.2 Testing

The viscosity measurements were performed in accordance with ASTM D 2857-93. The viscometer was rinsed with chloroform. Then, the viscometer was placed in a constant-temperature bath (T=25 °C) securely fastened with the tubes vertical. With a 10.0ml pipette, 10 0 ml of solvent was transferred to the viscometer to bulb C. The temperature was allowed to equilibrate for at least 10 minutes. The liquid level in the viscometer was raised above the upper graduation mark of bulb B. The timer is started as the meniscus passes the upper graduation mark; and is stopped as the meniscus passes the lower mark. This process was repeated $n \geq 5$ times or until the efflux time for chloroform, t_0, was within 0.1% of the mean.

To determine the flow time, t, for each polymer, the following procedure was followed. Ten mL of polymer solution was transferred to bulb C. The flow times were

Table 4.2. Polymers used in inherent viscosity measurements.

Material	*Manufacturer*	*Form*
PLLA	PURAC	Pellet
PLLA	PURAC	Fiber
70/30 PLDL (A)	PURAC	Pellet
INDPLA 1	Cargill	Pellet
INDPLA 1	Cargill	Fiber

determined in the same manner as used for determining t_0 in the steps above. Before each new solution was added, the viscometer was rinsed with chloroform and the efflux time was measured to prevent variations in the readings. The inherent viscosity for each polymer was calculated using these results and reported in dl/g.

4.7 Wide Angle X-Ray Diffraction

Wide-angle X-ray Diffraction (WAXD), flat plate technique was used to compare the relative orientation behavior of the fibers' crystalline phase. WAXD patterns change from circles to distinct, sharp reflections as orientation is increased. Observations of the patterns serve as a qualitative analysis of the effect of take up velocity, draw ratio, and sheath/core ratio on the degree of orientation.

Flat plate film patterns were prepared by developing the film at 35 kV and 15 mA for 5 hours The fibers were aligned such that the transverse axis was perpendicular to the X-ray beam. Flat plate x-ray film patterns were produced using a pin-hole technique which used Cu Kα radiation.

4.8 Static Tensile Testing

Tensile tests were run using a Table Instron Model 1122. The Young's modulus, ultimate tensile strength, tensile yield strength were calculated by the Instron software based on the stress-strain curves. The ultimate tensile strength was calculated using the following equation:

$$S_T = F_{max}/A \qquad (4.9)$$

where F is the maximum Force and A is the initial cross sectional area.

4.8.1 Fiber Sample Preparation and Testing

Single filaments were mounted on paper sample holders with a 20 x 10 mm rectangular window. The fibers were attached to one side of the holder with scotch tape. These samples were also used for birefringence measurements Therefore, the diameters were measured as described in **Section 4.5.2.**

All samples were tested at a rate of 50 mm/min. The gage length was 20 mm. Young's modulus was calculated using a user-defined calculation. Two points on the initial slope were picked and the software calculated the slope of the line between the two points. This method was used to avoid large variations in values that occur due to the slack in the fibers, initially. The sample size was n = 6.

4.8.2 Composite Rod Sample Preparation and Testing

The diameter of the rods was measured using a digital micrometer. Both ends of the rods were adhered to two pieces of sandpaper with epoxy to provide mounting tips.

Young's modulus was calculated using the initial slope of the stress strain curve The ultimate tensile strength and yield strength were calculated using the Instron software standard methods. The sample size was n = 6.

4.9 Static Shear Testing

The double shear method reported by Shikinami [5,22] was used to determine the shear strength of the composite rods. The Instron Model 1122 was used in conjunction with a double shear fixture. The Instron was operated in compression at a rate of 50

mm/min for all samples. The maximum load was recorded; and the shear strength was calculated using the equation:

$$S_S = F_{max}/2A \quad \textbf{(4.10)}$$

F_{max} is the maximum force (N) and A is the cross sectional area (mm^2). The rods had a diameter of approximately 2.0 mm and a length of 55 mm.

4.10 Scanning Election Microscopy

Scanning electron microscopy (SEM) was used in combination with a thin gold coating to produce high resolution images. A Cambridge Instruments Stereoscan 360 scanning electron microscope with a tungsten filament and a resolution capability of 2.5 nm was used. The gold plating was done on a Technics Hummer I gold plater under a 100 millitorr vacuum. A current of 10 mA was set at time of 1 minute for all samples

The fracture surfaces of the fibers and composite rods were obtained during tensile and shear testing were examined using SEM.

4.11 Differential Scanning Calorimetry

Thermal analysis was completed using a Perkin-Elmer series 7 differential scanning calorimeter (DSC) with an Indium calibration standard. Thermal scans were done at a rate of 10 °C/min to determine the melting point and glass transition temperatures, onset of melting, and heat of fusion. The degree of crystallinity was calculated assuming the heat of fusion of the 100% crystalline poly(lactic acid) is equal to 93.1 J/g [53].

CHAPTER 5

Polymer Selection: Results and Discussion

5.1 Peel Test - Sheath/Core Adhesion

PTMC seems to form the best bond with PLLA under the given conditions (see **Table 5.1**). It is believed that PTMC forms a strong adhesive bond with PLLA through transesterification [54]. When comparing the three peeled PTMC surfaces in **Figure 5.1**, the differences in adhesion become clear. At low temperature and contact time, peeling occurred at the interface between the two polymers. In most cases, adhesion between the samples was minimal. Therefore, peeling was inconsistent, resulting in a slip-stick type peel (see **Fig. 5.1 (b)**). Along the length of the sample, there was evidence of some adhesion However, there were also regions where the two polymers did not bond The low bond strength is an indication of weak boundary layers in which there are few or no operative attachment sites Increasing the temperature and/or time serves to increase the effective number of attachments [55]. The increase also facilitates chain interdiffusion in the interfacial region [56]. Thus, peeling is more consistent at higher temperatures and at higher contact times (see **Fig 5.1 (c)**).

Changing from conditions of 110 °C and 30 seconds to 195 °C and 5 seconds caused an increase in peel strength from 0.61 N/mm to 5.272 N/mm. This result indicates that increasing the temperature had a significant effect on adhesion. At 110 °C, chain mobility is minimal; therefore within the range studied, increasing the contact time does not greatly increase degree of bonding (see **Table 5.1**). The same is true at 195 °C. The

Table 5.1. Peel strength in N/mm for joints formed between PLLA and candidate sheath materials.

PLLA-{co-TMC, co-PLDL} joint							
	Temperature (°C)						
Time(s)	**110**	**125**	**140**	**155**	**170**	**195**	**210**
5	0.473	1.005	1.117	1.027	1.273	1.453	1 987
10	0 826	1.508	1.143	1.204	1.887	3.447	4.322
30	1.384	1.648	1.868	1.555	2.609	4.547	4 716
60		1.216		1 478		3 640	
PLLA-75/25PLDL joint							
	Temperature (°C)						
Time(s)	**110**	**125**	**140**	**155**	**170**	**195**	**210**
5	0.068	0.038		0.047	0.127	0.092	
10	0 042	0 085	0.143	0.889	2.376	1.522	2 186
30	0.113	0.574	0.751	0.760	3.153	5.299	4.524
60		0.517	1.018	1.013	3.612	4.028	5.144
PLLA-PTMC joint							
	Temperature (°C)						
Time(s)	**110**	**125**	**140**	**155**	**170**	**195**	**210**
5	0.174	0.200	1.247	0.949	0.535	5.272	
10	0.176	3.556	3.150	3.919	3.834	5.241	4.595
30	0.612	2.848	2.739	3.905	3.147	4.977	
60	0 573	2.232		3.251		4.410	

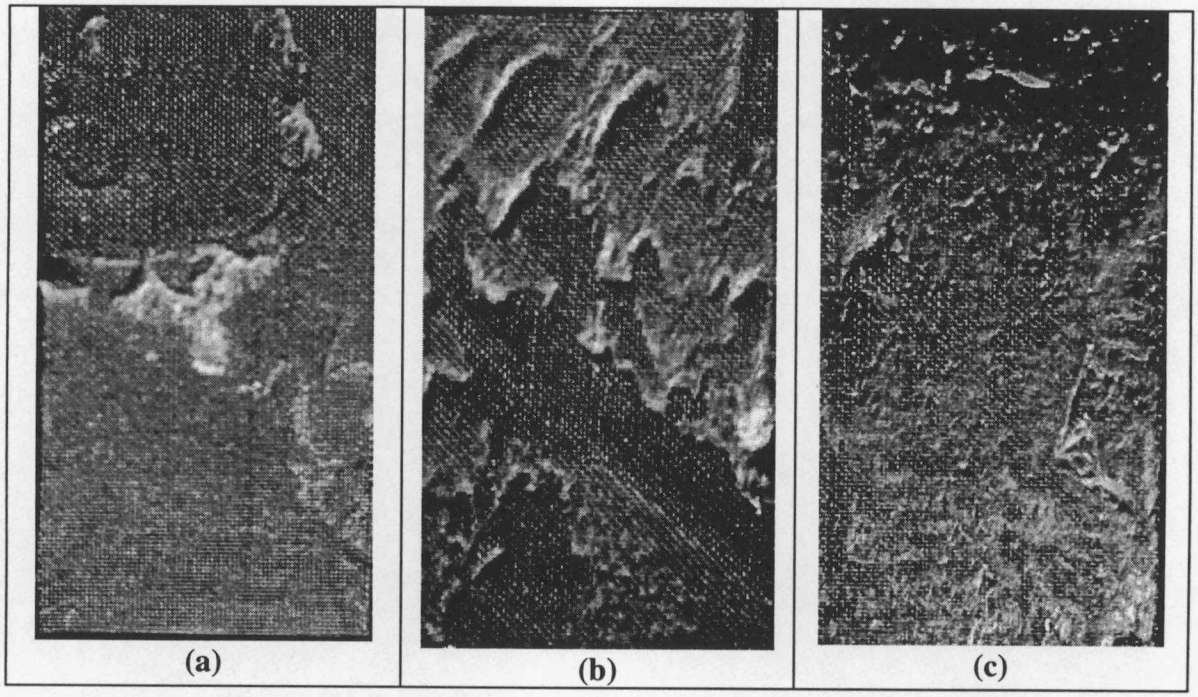


Figure 5.1. Optical micrographs of PTMC peeled surfaces at 25X. (Peel rate = 100mm/min; (a) contact temperature = 110 °C, contact time = 30 sec; (b) contact temperature = 195 °C, contact time = 5 sec; (c) contact temp. = 195 °C, contact time = 30 sec).

peel strength is much higher at this higher temperature, but the effects of increasing the contact time are minimal.

The failure mode changed from one that involved little drawing of polymer and fracture close to the interface (**Fig. 5.2 (a)**) to failure in which there is a significant amount of plastic deformation (**Fig.5.2 (b)**). This transition from adhesive to mixed to cohesive failure has been reported previously [57-61]. **Figure 5.2(b)** shows an increase in cavitation and drawing of polymer over most of the surface with the increase in temperature.

The two other candidate materials also bonded well to PLLA at elevated temperatures. When cohesive failure was observed, peeling occurred in the bulk of the sheath candidate material. This suggests that the bond between the sheath and core materials is stronger than the intrafacial bonds in the sheath. When failure is predominately adhesive, the maximum load required to initiate peeling is low and so was the peel strength [58].

Although the effects of contact time on peel strength for the PLLA-PTMC joint were minimal, this was not the case for the other types of joints (see **Fig. 5.3**). For the PLLA-75/25PLDL and PLLA-(co-TMC,co-PLDL) joints, the peel strength increased with contact time due to an increase in the strength of the adhesive layer, indicating an increase in bond strength. Peel strength increased drastically at times of 30 seconds for all joints.

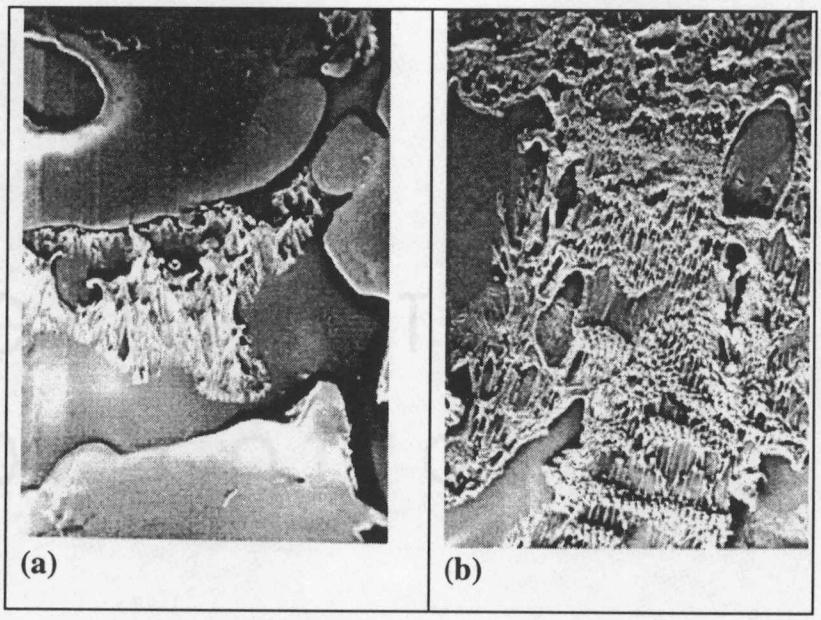


Figure 5.2. SEM micrographs of PTMC peeled surface at a magnification of 10X. (Peel rate = 100mm/min; (a) contact temperature = 110 °C, contact time = 30 sec; (b) contact temperature = 195 °C, contact time = 5 sec).

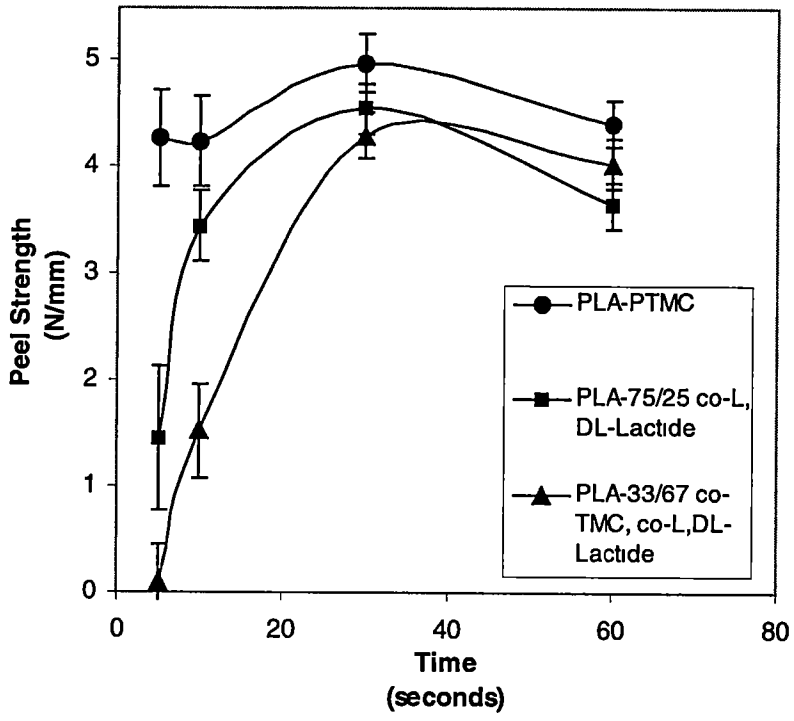


Figure 5.3. Maximum Peel Strength for different polymer joints as a function of contact time. Peel Rate: 100 mm/min. Contact temperature: 195 °C.

Figure 5.4 shows the relationship between temperature and peel strength for the different joints For all samples, minimal bonding occurred at 110 °C. For joints of PLLA and the copolymers, there was a significant increase in peel strength above 150 °C The increase in temperature gave the polymer chains sufficient mobility within the given time frame for adhesion to occur. In all cases, there is an increase in peel strength with temperature and time.

There exists some optimum condition where the maximum peel strength is achieved. Above this optimum, the peel strength will decrease [61]. For these systems, it appears that the optimum contact time lies between 30 and 60 seconds. There also exists some optimum contact temperature. The peel strength increased with contact temperature; then leveled off at approximately 195 °C (see **Fig. 5.4**). Further increases in temperature did not increase the peel strength by a significant amount. It is assumed that maximum bonding has occurred at contact time and temperature of 30 seconds and 195 °C, respectively. Data for the other contact times and temperatures are in **Table 5.1**. Photomicrographs of the peeled surfaces are displayed in **Figure 5.5**. The pictures show the peeled surfaces at the optimum temperature and time.

Although the PTMC-PLLA joint appears to give the best adhesion, it was decided that PLDL would be used in subsequent studies. Body temperature is approximately 37 °C, and the glass transition temperatures of both PTMC and the PTMC copolymer are about 26 °C Since Tg is below body temperature, it is believed that that the mechanical properties will not be sufficiently retained *in vivo* [54]. However, PLDL has a Tg of 55

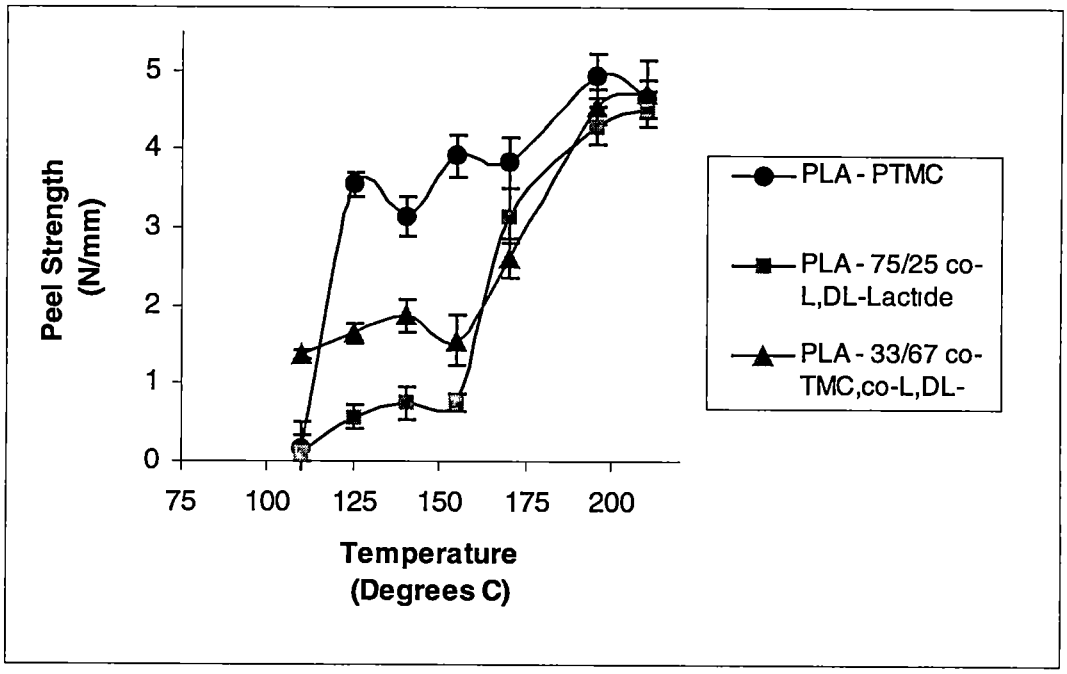


Figure 5.4. Peel Strength as a function of temperature for different polymer joints. Peel Rate 100 mm/min. Contact Time 30 s.

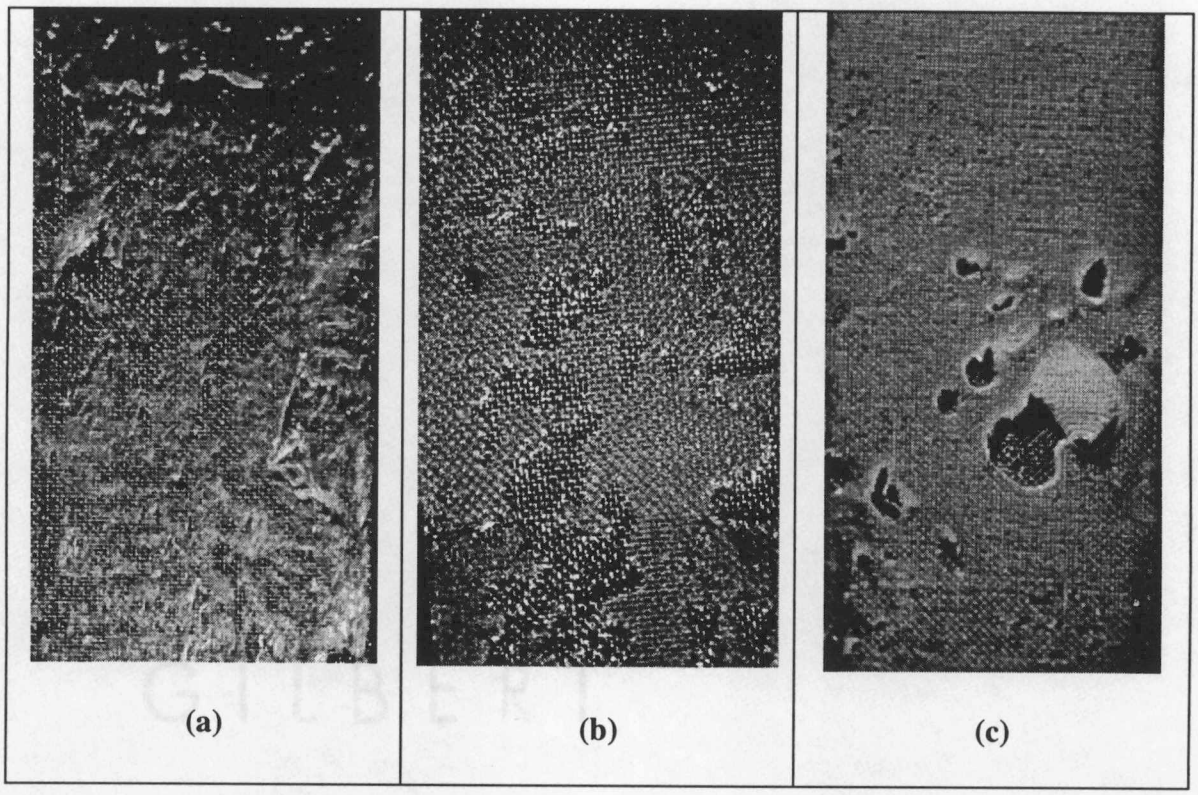


Figure 5.5. Optical micrographs of peeled surfaces of candidate sheath materials: (a) PTMC; (b) poly(co-PTMC, co-PLDL); (c) PLDL. (Peel rate = 100 mm/min; contact temp. = 195 °C; contact time 30 s).

°C. Based on the results of the peel test, we believe that some type of heat treatment may be necessary after the fibers have been extruded to ensure good adhesion between the sheath-core materials. In the study by Bhattacharya et al. [61], they found that secondary heat treatments may increase the strength of the adhesive bond when contact times are relatively low.

The copolymer of PTMC and PLDL was synthesized by Birmingham Polymers, Inc. as another alternative. This polymer is predominately polylactide; but has PTMC in it to increase the possibility of bonding at relatively low temperatures.

5.2 Peel Test - Sheath Cohesion.

After selecting the sheath polymer, peel tests were conducted using PLDL-PLDL joints. The purpose of this experiment was to determine the processing parameters necessary to make the composite rods. Based on some preliminary extrusion studies, the sheath polymer was changed from 75/25PLDL to 70/30PLDL to facilitate processing. Two candidate materials of different molecular weights were obtained from Purac Biochem for this study. The objective was to determine at what temperature did the mode of failure change from cohesive to adhesive. In this case, cohesive failure occurs when there is peeling in the bulk of the polymer material Adhesive failure is described by either brittle failure of the polymer joint and delamination from the foil backing or by peeling at the interface between the foil and polymer sample while the bond between the thin films is maintained. The samples were prepared at different temperatures (85 °C-125 °C) and a constant contact time of 30 seconds. **Table 5.2** lists the failure modes for the two sheath materials studied.

The polymer of lower molecular weight experienced changes in failure mode with temperature. At 115 °C, mode of failure changed from cohesive to mixed mode. Initially peeling occurred, followed by breakage of the polymer joint at the peeling front. This result indicates that the self-bond has become stronger than the bond between the polymer and the foil The polymer of higher molecular weight experienced peeling at all temperatures. It is assumed that higher temperatures would be required to ensure that a strong bond would develop. Therefore, the sheath material chosen was the polymer of lower molecular weight.

Table 5.2. Peel Strength for PLDL-PLDL joints. Contact time 30 seconds, Peel rate· 100 mm/min.

η_{inh}	Contact Temperature (°C)			
(dl/g)	85	105	115	125
		Peel Strength (N/mm)		
3 98	0.183	0 941	1 914	1 880
1.62	1 111	2 210	2 556**	0.288*

*** Adhesive Failure.**
**** Mixed Mode.**

CHAPTER 6

Preliminary Analysis: Results and Discussion

6.1 Rationale for Preliminary Test

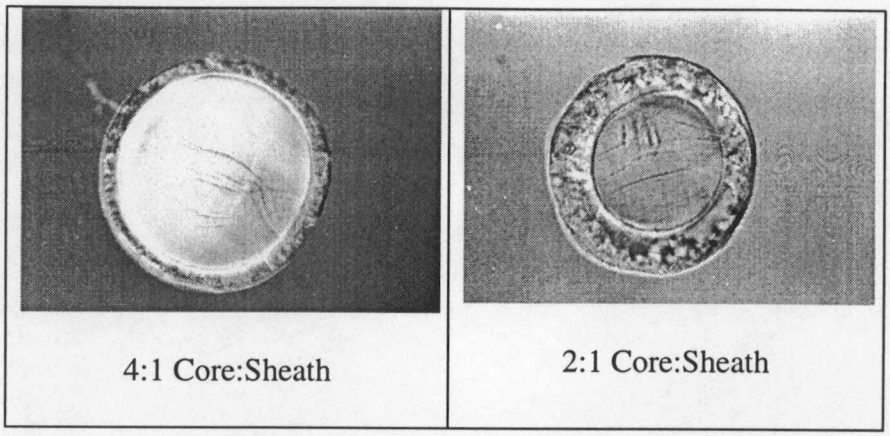
A series of short studies were completed to approximate the processing variables that could be used for the final analysis of the medical grade polymers. Because of the cost of the medical grade polymers, industrial grade polymers were used in the preliminary analyses. It is assumed that the correlations and trends will be the same for the medical grade and industrial grade polymers. However, the actual properties may differ. The results of these tests served as guidelines for processing the medical grade polymers. Only a summary of the findings is reported

6.2 Initial Bicomponent Spinning Experiments: Medical Grade Polylactides

Initial bicomponent spinning was experiments were done at Randcastle Extruder Systems, Inc. in Cedar Grove, New Jersey. The fibers were spun from medical grade poly(lactic acids). The core material was PLLA from Purac, and the sheath material was 75/25 PLDL from BPI (see **Section 4.1**). The purpose of the experiments was to determine if bicomponent fibers with the core sheath morphology could be spun from the chosen materials, and to determine if fibers of different core sheath ratios could be produced.

6.2.1 Determination of Bicomponent Structure

Bicomponent fibers with core:sheath ratios of 2:1 and 4:1 were produced by adjusting the velocity of the two screws to change the ratio of mass throughput. The core:sheath ratio for each type of fiber is shown in **Figure 6.1**. The actual core.sheath



4:1 Core:Sheath

2:1 Core:Sheath

Figure 6.1. Photo micrographs (25X magnification) of bicomponent fiber cross-sections from spinning experiments at Randcastle Extruder Systems, Inc.

ratios were determined by comparing the ratios of the cross-sectional areas occupied by the core and the sheath. It was determined that the actual core:sheath ratios were 1.7:1 (2:1, expected) and 4.3:1 (4:1, expected).

During the spinning of the fibers, it was determined that the quality of the 75/25 PLDL pellets was poor. The shape and size of the pellets varied widely; and the larger pellets migrated to the top of the hopper. These variations would affect the consistency of throughputs, thus contributing to variations in fiber diameter and core:sheath ratio. It was advised by Randcastle personnel that more uniform pellets be used for future processing. Since the core material obtained from Purac was in powder form, it was easier to extrude. Therefore, it was decided that the medical grade sheath material to be used in the final experiments would be obtained from Purac. This would ensure uniformity of the materials and uniformity when spinning.

Based on the recommendations, additional spinning experiments were completed using the bicomponent spinning equipment at The University of Tennessee. Bicomponent fibers with core:sheath ratios of 1:1 and 3:1 PLLA:70/30 PLDL were produced from the polymers obtained from Purac.

6.2.2 Amorphous and Crystalline Orientation

From the X-ray patterns of **Figure 6.2**, it is evident that the as-spun filaments develop some crystalline orientation and this orientation is dependent upon take-up velocity. However, the effect of drawing on the crystalline orientation is not clear from the X-ray patterns. The fact that filaments were drawn to relatively low draw ratios (maximum draw of 2.9) may contribute to this uncertainty. At higher draw ratios, there may be distinct differences due to the higher orientation produced by drawing. At the time, drawing of the filaments to high draw ratios was not achieved.

The overall orientation of the filaments was determined using birefringence. The orientation appears to increase upon drawing (see **Figs. 6.3** and **6.4**) for all types of filaments. Orientation of the as-spun filaments developed faster when the amount of semi-crystalline polymer (PLLA) was increased. At the lowest take up velocities, the filaments with a 4·1 core.sheath ratio had considerably more orientation than the 1·1 core·sheath filaments. This is also true for the drawn samples. The 1:1 core:sheath filaments developed an appreciable amount of orientation above a draw ratio of 4; where as, the other filaments had developed some orientation at a draw ratio of approximately 1.5.

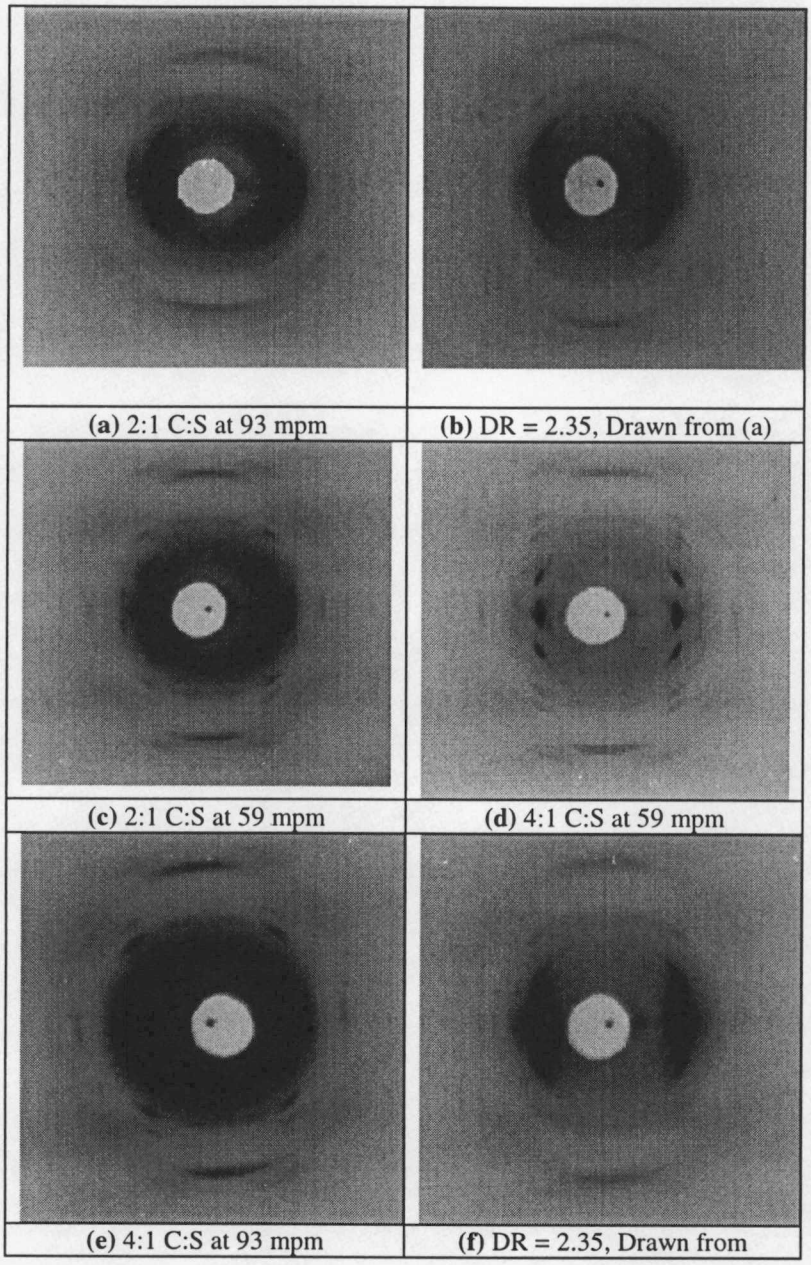


Figure 6.2. WAXD patterns for bicomponent filaments spun at Randcastle Extruder Systems, Inc.

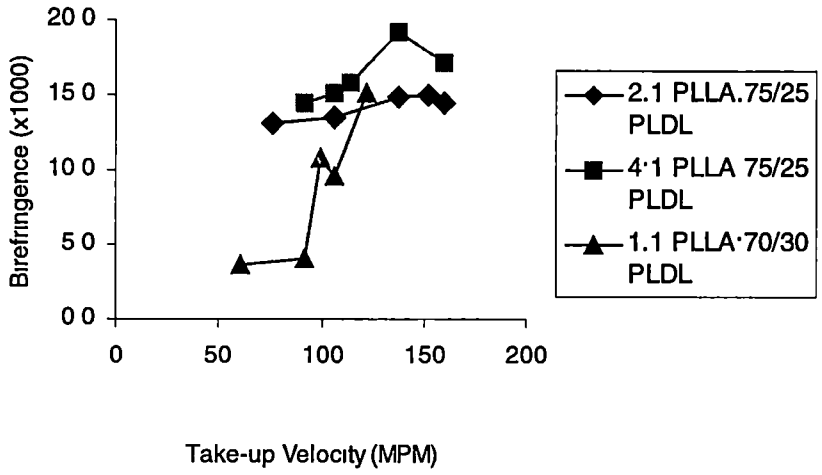


Figure 6.3. Overall orientation of as-spun PLLA:PLDL filaments.

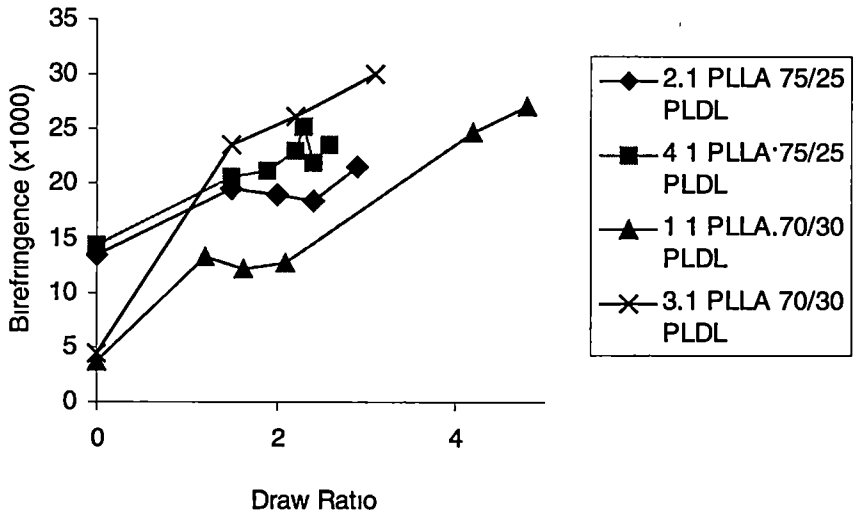


Figure 6.4. Effect of drawing on the overall orientation of PLLA:PLDL filaments.

In this case, birefringence is used as a qualitative analysis of the molecular orientation. The degree to which each component contributes to the overall orientation is not known. The refractive indices of the sheath and core parts could not be obtained using the method described in **Section 4.5**.

6.2.3 Tensile Properties

The tensile strength of these filaments increased with take-up velocity and draw ratio (see **Figs. 6.5** and **6.6**). The data indicates that as-spun filaments have relatively low strength regardless of take-up speed in the range studied. The tensile strength increases substantially upon drawing. The resulting filaments have reasonable strength that agrees with the strength values typically seen for melt-spun poly(lactic acid) at low draw ratios [1-5].

6.3 Production of Composite Rods from Bicomponent Filaments

Before the design of the pultrusion die that would be used to make the composite rods was complete, it was necessary to determine if two millimeter rods could be made from the bicomponent filaments. Therefore, rods were made using shrink wrap tubing. The tubing shrinks compressing the filaments. Because the sheath is molten at 130 °C, auto adhesion of the sheath material occurs. This produces a composite with sheath material as the matrix and PLLA as the reinforcing core fibers The fibers were packed tightly in the tubing and heated in an oven at approximately 130 °C for 20 minutes. The results of this short experiment are discussed in this section.

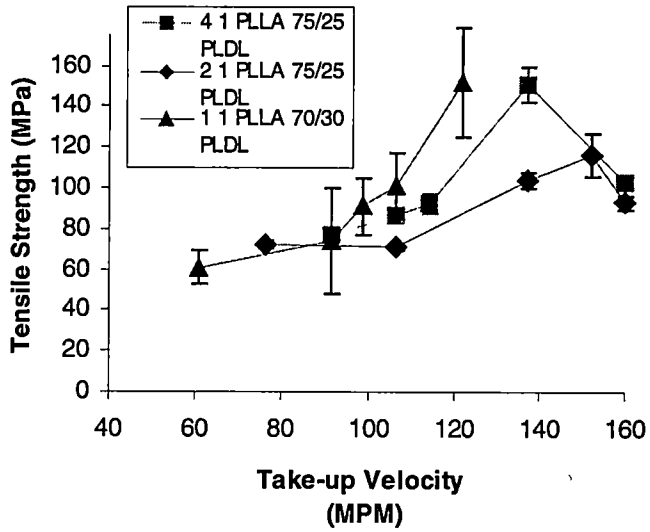


Figure 6.5. Tensile strength of as-spun PLLA:PLDL filaments.

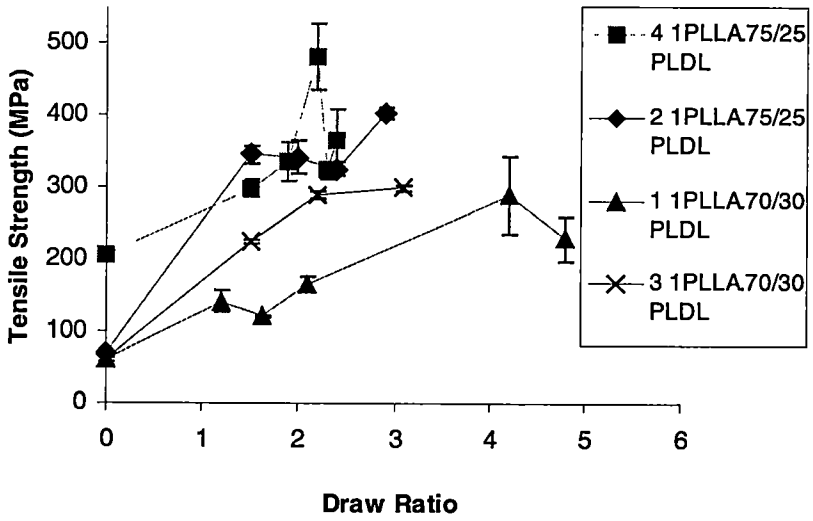


Figure 6.6. Effect of drawing on the tensile strength of PLLA:PLDL filaments.

6.3.1 Mechanical Properties of Rods Prepared via Shrink Wrap Tubing

The mechanical properties of the rods were relatively low in comparison to bicomponent fibers. **Table 6.1** contains the properties of the composite rods. Fiber strength typically ranged from 200 to 400 MPa. However, the strength of the rods only reached a maximum of 111 MPa.

Due to the fact that a crude processing technique was used to make the rods, it was not surprising that the rods were relatively weak. When making the rods, it was difficult to keep the fibers taut. The fibers tended to coil during heating. Also, there were air bubbles in the rods. The presence of voids acts to decrease the overall strength of the composite. With improved processing methods, it is anticipated that more efficient fiber packing will be achieved, and the properties of the composite should improve.

Under these processing conditions, the properties of the fibers had not been transferred to the composite rods. It was concluded that the fibers needed to be drawn to higher draw ratios to yield fibers with higher strength and modulus, which in turn would yield rods with higher strength. Consequently, the rods would have higher strength.

6.3.2 Composite Morphology

The fracture surface of the composite rods was studied using SEM (see **Fig. 6.7, 6.8**). From the micrographs, it is evident that the PLLA fibers are embedded in a matrix of PLDL as expected. Under shear loading, the integrity of the sheath/core

Table 6.1. The effects of core:sheath ratio on the mechanical properties of the composite rods prepared via shrink wrap tubing (temperature = 130° C; time = 20 min.) Ss = Shear Strength; St = Tensile Strength; Et = Tensile Modulus; TensileYield Strength

Materials (Core:Sheath)	Core:Sheath Ratio	Draw Ratio	S_s MPa	S_t MPa	E_t GPa	Y_t MPa
PLLA:75/25 PLDL	1:4	1.30	62.6	94	2.3	74
PLLA 75/25 PLDL	1·4	1 43	80 6	96	1.9	73
PLLA 75/25 PLDL	1:4	1.70	61 5	68	1.2	55
PLLA·75/25 PLDL	1·4	2 60	64 5	95	1.5	82
PLLA.75/25 PLDL	2:1	1.43	72 9	73	1.6	68
PLLA:75/25 PLDL	2:1	2.00	63.5	71	1.5	64
PLLA:75/25 PLDL	1:2	2 20	61.2	68	1.9	64
PLLA.75/25 PLDL	1 2	2.90	74.7	111	1.9	86
PLLA:70/30 PLDL	1·1	0	21.6	—	—	—
PLLA·70/30 PLDL	1·1	1.21	32.1	—	—	—
PLLA 70/30 PLDL	1 1	1.62	42.4	—	—	—

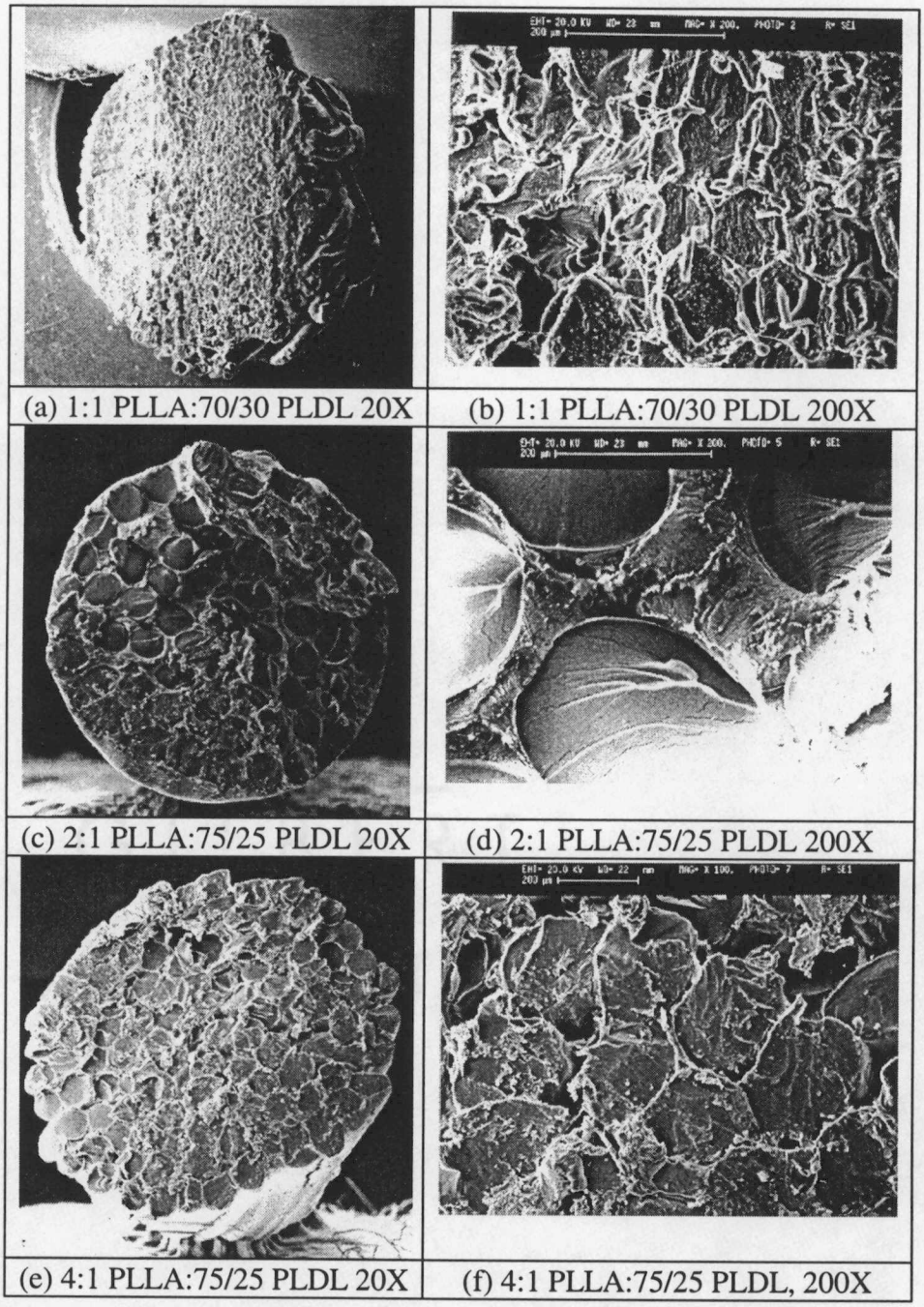
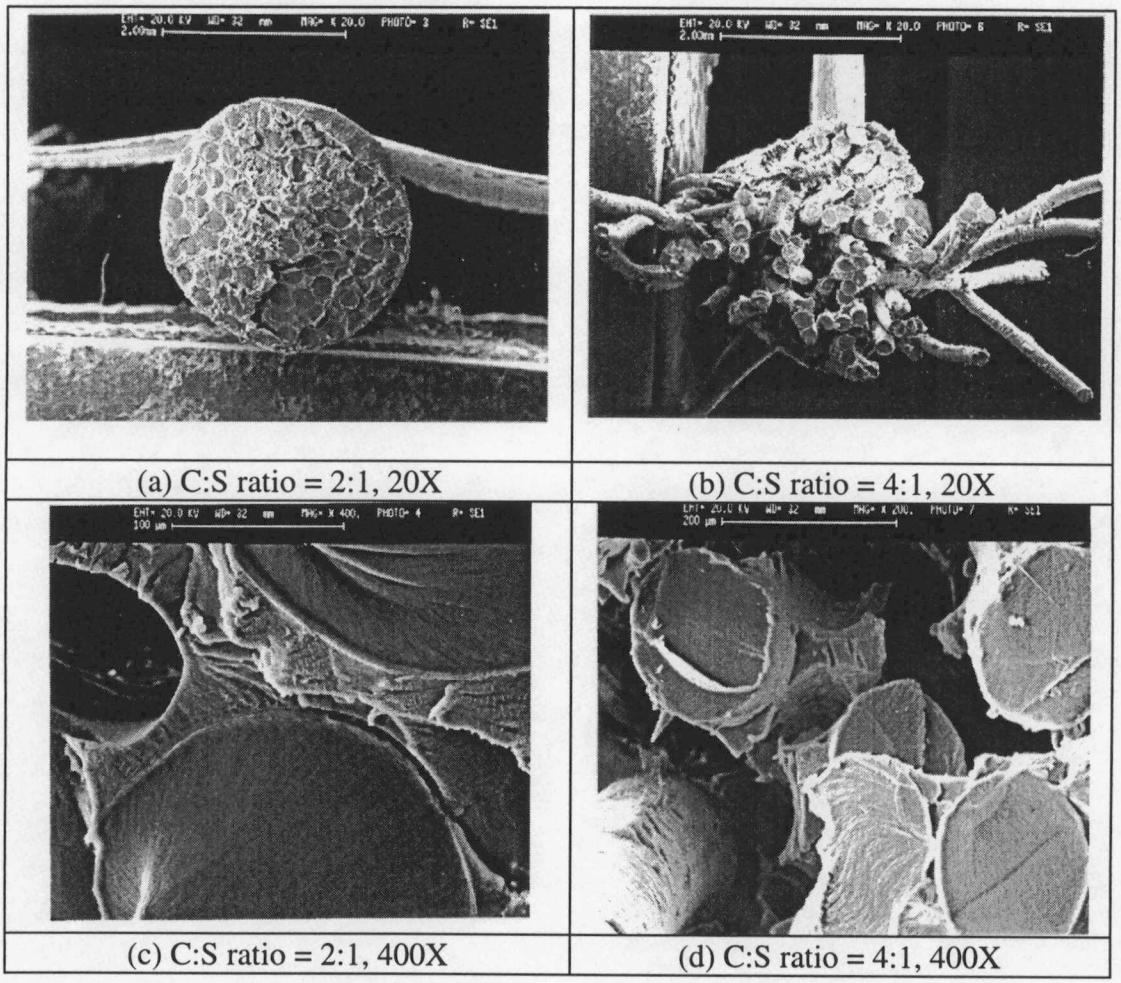


Figure 6.7. SEM micrographs of fracture surfaces of composite rods tested under shear loads. Magnifications of 20 X and 200X. Shrink wrap tubing experiments.



(a) C:S ratio = 2:1, 20X

(b) C:S ratio = 4:1, 20X

(c) C:S ratio = 2:1, 400X

(d) C:S ratio = 4:1, 400X

Figure 6.8. SEM micrographs of fracture surfaces of composite rods (made from PLLA:25/75 PLDL filaments) tested under tensile loads. Shrink wrap tubing experiment.

interface is maintained. There is some evidence of cracks in the matrix (see **Fig. 6.7 (a), (f)**); but it is minimal.

Under tensile loading, failure is relatively brittle for the 2.1 PLLA:75/25 PLDL rods. **Figure 6.8 (a)** shows very little deformation of the rod. The circular cross-section is maintained. Even at higher magnifications, evidence of voids or delamination are rarely seen. The rods made from 4:1 PLLA:75/25 PLDL fibers exhibit catastrophic failure under tensile loads (see **Fig. 6.8 (b)**). Massive fiber delamination occurred proving that the initial rods did not have a sufficient amount of sheath material to produce a tough composite. The flaws at the interface are magnified due to the low amount of matrix material. Therefore delamination and fiber pull-out proceed uninhibitedly. For this reason, the 4:1 core:sheath fibers were eliminated as candidate materials in the production of the composite rods.

6.4 Bicomponent Spinning of Industrial-Grade Polylactides

Based on the findings from the series of experiments on the medical-grade materials used in the previous sections, a directed study was done using industrial-grade polylactides manufactured by Cargill, Inc. Due to the costs of the medical grade polymers, it was decided that the remaining preliminary tests would employ industrial grade polylactides that are chemically similar to the medical grade polymers to be used in the final analyses.

The sole purpose of the study was to provide information regarding which core:sheath ratio should be used to produce bioabsorbable bicomponent fibers that will give sufficient strength to be used in the composite rod production. Analysis of

the industrial-grade fibers and composite rods will provide qualitative information about the conditions under which the medical grade polylactides can be processed. Although the value of properties such as tensile strength and modulus may differ from that of the medical grade polylactides, it is anticipated that the overall behavior will be the same. For example, if the strength of industrial-grade composite rods made from 2:1 core:sheath fibers is 500 MPa and the strength of 1:1 core·sheath fibers is 300 MPa, then is can be assumed that medical-grade rods made from the 2:1 core.sheath materials will have higher strength than the rod made from the 1:1 core:sheath material. Neither the fibers nor the composite rods are expected to provide information about the exact value of the mechanical properties.

The polylactides used as the core material were INDPLA 1 and INDPLA 2 (PLA). Both polymers contained about 1% D-lactide and had molecular weights of approximately 212,000 daltons. The sheath material INDPLDL (PLDL), had a lower molecular weight of 186,000 daltons and contained 9.8% D-lactide. (see **Section 4.1** for specifications). Bicomponent filaments of 1:1, 2:1, and 3:1 core:sheath ratios were made using the bicomponent extrusion system at The University of Tennessee as described in **Chapter 3**. These filaments were drawn and then processed into composite rods.

First, the effect of temperature on drawing was determined for these filaments. In all cases, the maximum draw attainable increased with temperature. The maximum draw was achieved with 1:1 PLA:PLDL filaments (see **Fig 6.9**). The overall orientation of the filaments generally increased with drawing to a draw ratio of about

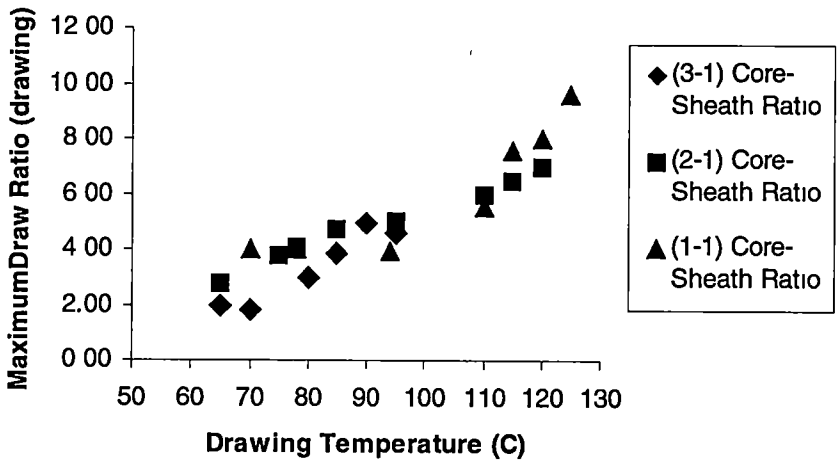


Figure 6.9. Maximum draw attained at various temperatures for PLA.PLDL filaments.

four. After which, the orientation begins to decrease (see **Fig 6.10**). At a draw ratio of four, the filaments also have reasonable strength. The average tensile strength is between 300 and 400 MPa (see **Fig 6.11**). These results are consistent with the results reported for the medical grade polylactides in **Section 6.3**. **Figure 6.12** shows that there is some correlation between birefringence and tensile strength. As the filaments were drawn, there was an increase in orientation of the crystalline and amorphous regions which led to an increase in strength.

The SEM micrographs show that core:sheath interface is intact after fracture. There is a noticeable difference in core:sheath ratio which proves that ratios can be controlled and varied using this system (see **Fig 6.13**).

6.5 Composite Rod Fabrication from Industrial-Grade Polylactides

Bundles of the bicomponent fiber were processed into 2 0 mm diameter rods using the pultrusion technique described in **Section 3.3**. Several attempts were made to make rods at different temperatures. Rods that were aesthetically pleasing were made at 155 °C. This temperature was kept constant; and the fibers were pultruded at three different rates.

Figure 6.14 shows the relationship between shear strength and pultrusion rate. The shear strength of these rods was highest at the slower pultrusion rates. The greatest strength was achieved for rods made from the 1:1 core:sheath filaments. The shear strength was 83 MPa at a pultrusion rate of 0.15 in/min. The shear strength of rods made at the highest pultrusion rate (0.27 in/min) had the lowest strength. The

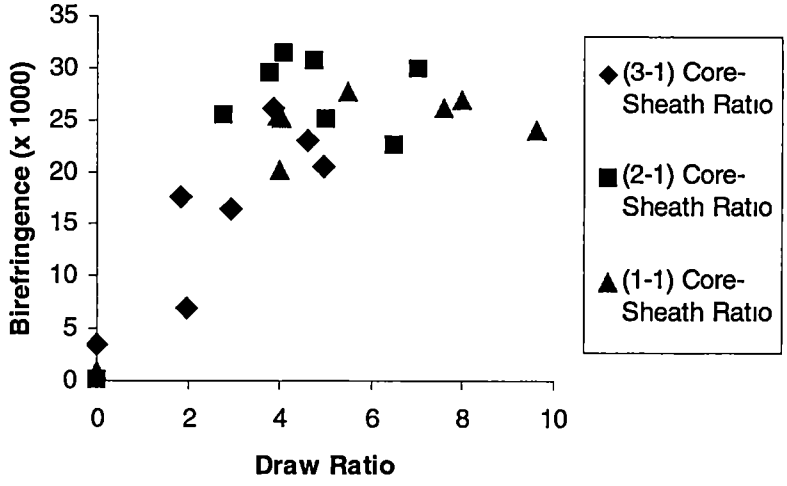


Figure 6.10. Overall orientation of PLA.PLDL filaments.

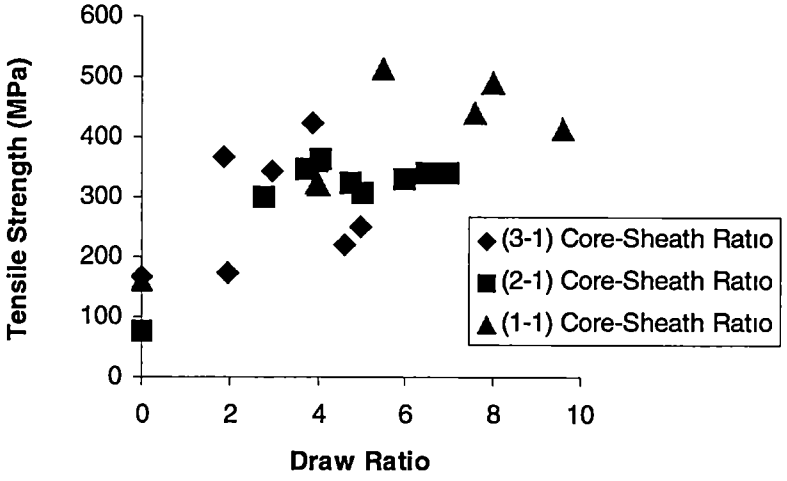


Figure 6.11. Tensile strength of PLA:PLDL filaments.

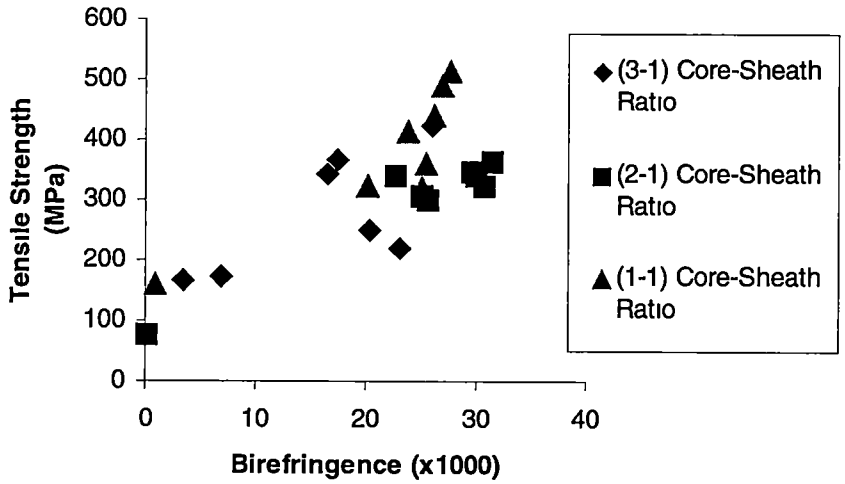
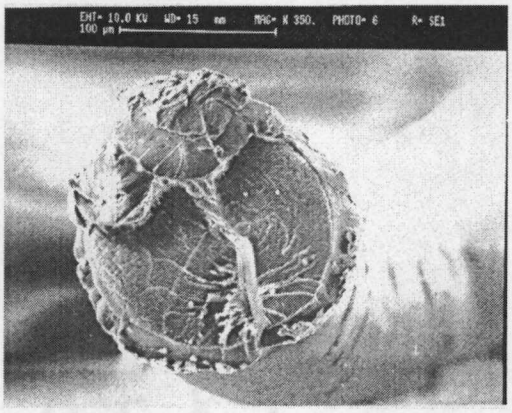


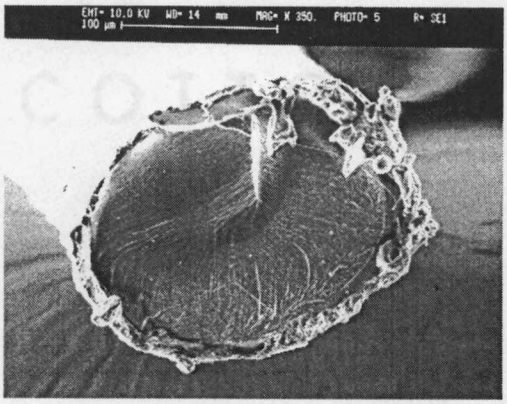
Figure 6.12. Relationship between tensile strength and birefringence for the PLA.PLDL filaments



1:1 core:sheath ratio



2:1 core:sheath ratio



3:1 core:sheath ratio

Figure 6.13. SEM micrographs of the tensile fracture surfaces of PLA:PLDL filaments. 350X Magnification.

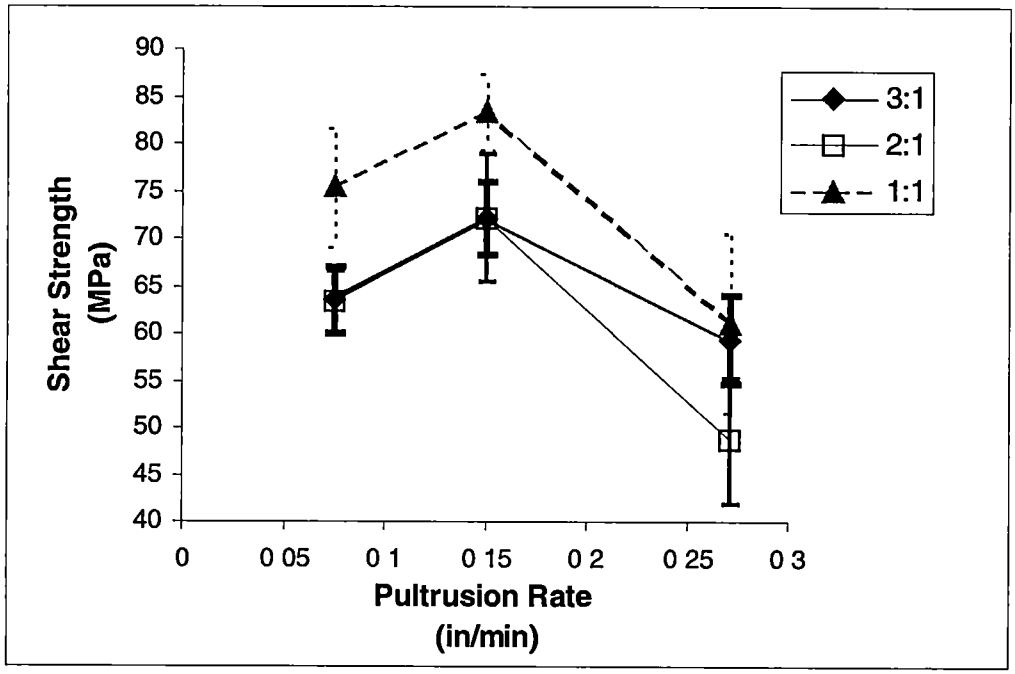


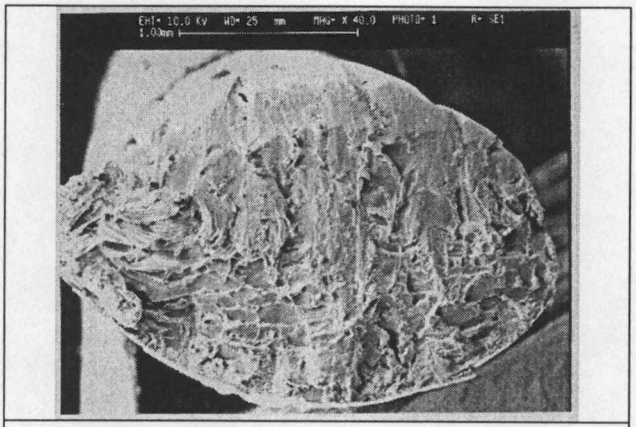
Figure 6.14. Shear strength of PLA·PLDL composite rods. Die temperature = 155 °C.

surfaces of these rods were visibly rough. Also, the individual fibers could be seen within the matrix. This was not the case for the other rods. The surfaces were relatively smooth; and the individual fibers could not be seen.

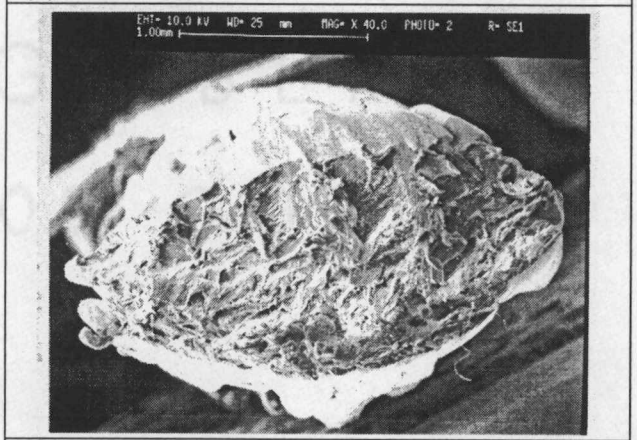
SEM micrographs of the sheared surfaces give very little information about the integrity of the core:sheath interface. The sheath appears to be smeared during shearing for all three core:sheath ratios. The circular rod is deformed giving an oblong cross-section (see **Fig. 6.15**). In some portions of **(a)**, core fibers are still visible. Here, it can be seen that the individual fibers are deformed; but they are still bonded to the matrix.

The tensile strength of these rods was also low (see **Fig. 6.16**). The tensile strength only reached as high as 82.8 MPa with a modulus of 2766 MPa. These values were obtained for the rods made from 1:1 core:sheath filaments. The elongation to break was also higher for this rod (see **Fig 6.17**). The modulus and elongation to break of the other two types of rods were similar in value.

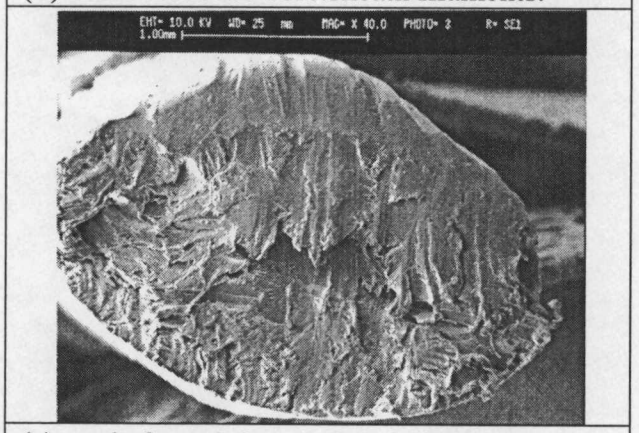
SEM micrographs of these rods are in **Figure 6.18**. The rods made from the 3:1 core:sheath filaments in **(a)** show that fiber necking occurred under the tensile load. This indicates that the fibers may not have been drawn to give the maximum orientation and strength before the composites were made. There is high level of debonding and deformation of the composite cross-section. The rods made from the 2:1 core:sheath filaments in **(b)** have a mixture of fracture surfaces. In some sections, it appears that fiber-pull out may have occurred leaving holes in the rod. Smearing of the matrix is prevelant for this type or rod. The interface between the sheath and core



(a) made from 1:1 core:sheath filamens.



(b) made from 2:1 core:sheath filaments.



(c) made from 3:1 core:sheath filaments

Figure 6.15. SEM micrographs of sheared surface of PLA:PLDL composite rods.

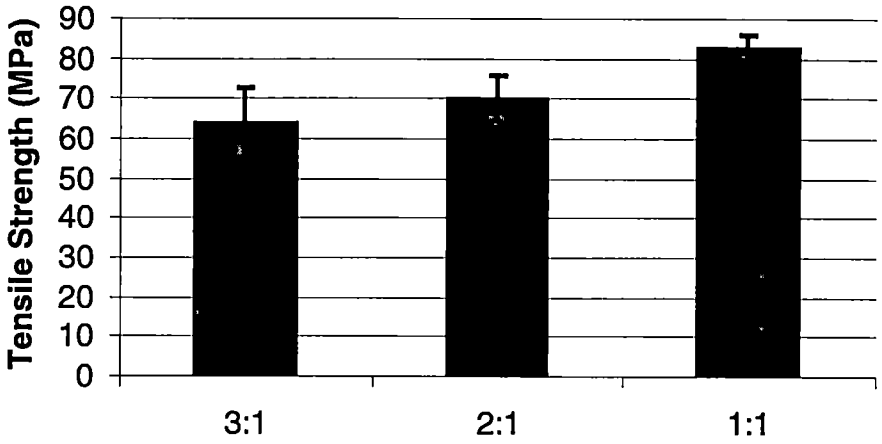


Figure 6.16. Tensile strength of PLA:PLDL composite rods from 3:1, 2 1, and 1:1 core:sheath filaments. Pultrusion die temperature = 155 °C. Pultrusion rate = 0.15 in/min.

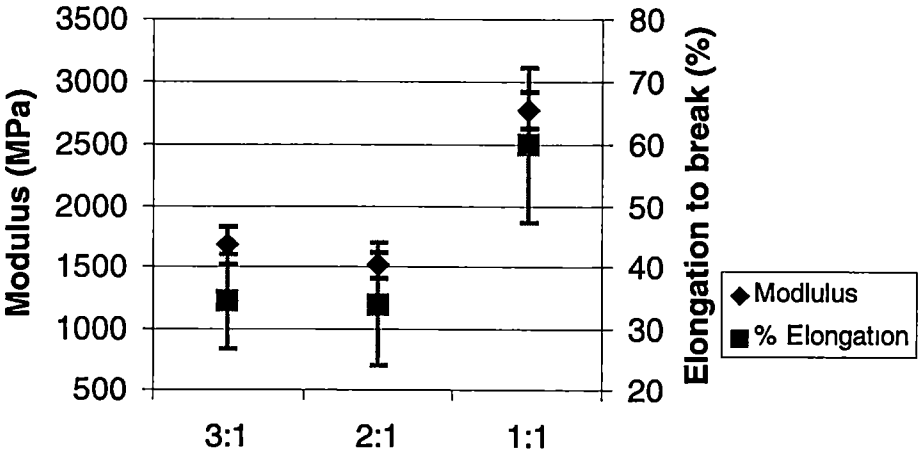
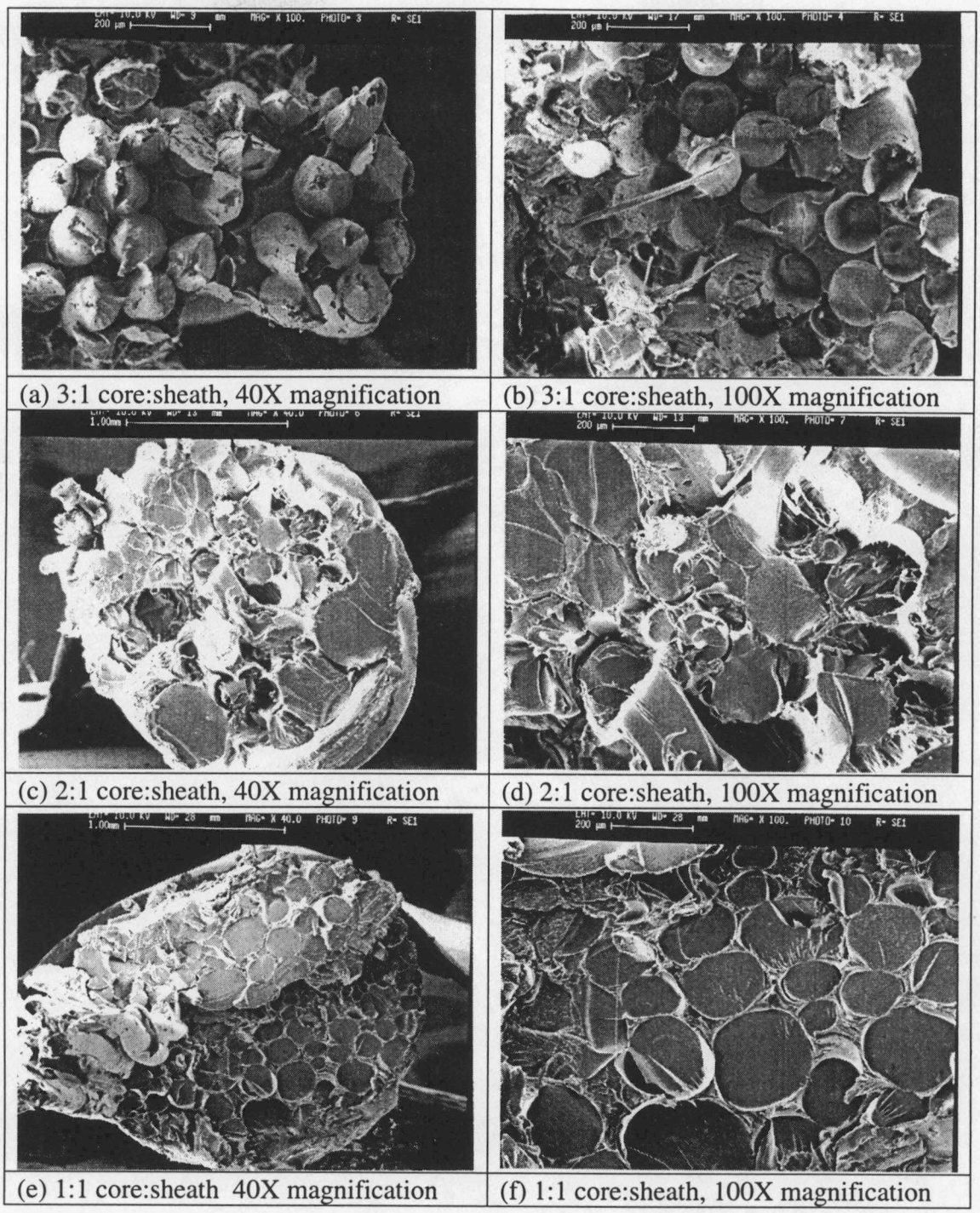


Figure 6.17. Modulus and strain of PLA:PLDL composites from 3:1, 2:1, and 1:1 core.sheath filaments. Pultrusion die temperature = 155 °C. Pultrusion rate = 0.15 in/min.



(a) 3:1 core:sheath, 40X magnification

(b) 3:1 core:sheath, 100X magnification

(c) 2:1 core:sheath, 40X magnification

(d) 2:1 core:sheath, 100X magnification

(e) 1:1 core:sheath 40X magnification

(f) 1:1 core:sheath, 100X magnification

Figure 6.18. SEM micrographs of tensile fracture surfaces of PLA:PLDL composite rods.

is not clearly defined except in places where debonding has occurred. The rods made from the 1:1 core:sheath filaments have the most defined core:sheath interface (see **Fig 6.18 (f)**). In most instances, the fibers have a clean fracture surface with no evidence of fiber necking or fiber pull-out. There is evidence of matrix cracking and delamination at the interface.

The strength of these rods were still relatively low in comparison the strength of the fibers from which the rods were made. The fiber strength ranged from 300 to 400 MPa; whereas the composite strength was below 100 MPa. The WAXD pattern in **Figure 6.19** shows that the rods have some orientation after going through the pultrusion process. The reason for the low strength still remains unclear.

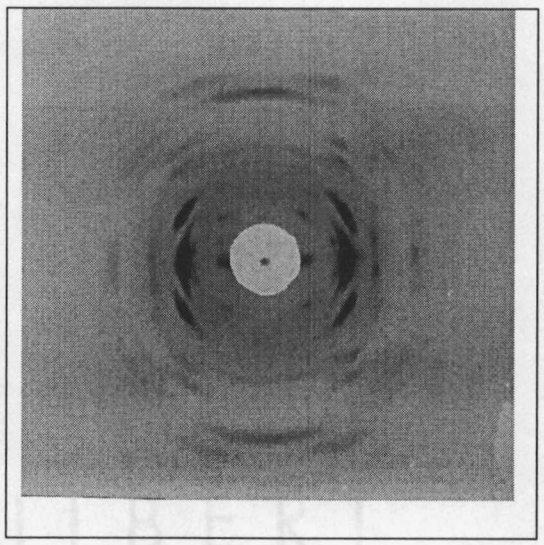


Figure 6.19. WAXD pattern of composite rod made from 1:1 PLA:PLDL filaments. Die temperature = 155 °C; pultrusion rate = 0.15 in/min.

6.6 Conclusions

The results of this study showed that composite rods made from bicomponent filaments of 4:1 core:sheath ratios did not have enough matrix material to hold composite together when subjected to tensile loads. The mechanical properties of all the rods were relatively low in comparision to the properties of the fibers.

The study using the industrial grade polylactides showed that the core fibers packed together better when there is more sheath polymer present. During processing, the excess polymer accumulated in the die indicating that the fibers were being squeezed together during processing. The 1:1 PLA:PLDL fibers had reasonable strength under these processing conditions. And the corresponding rods maintained a relatively stable structure during testing because of good adhesion between the sheath and core components. Therefore, the core:sheath ratio of 1:1 was selected for use in the final analyses using the medical-grade polylactides.

From a manufacturing standpoint, it is easier to extrude the filaments of 1:1 core:sheath ratio using the bicomponent system at The University of Tennessee. The extruder motors expend the least amount of energy; and the resulting fibers have the most consistent diameters.

CHAPTER 7

Analysis using Purac, Medical-Grade Polymers: Results and Discussion

7.1 Analysis of Bicomponent Fibers

The results of the preliminary analysis were used to determine which core:sheath ratio would be used to fabricate the fibers and composite rods for final analysis of the medical grade polymers. The sheath material is 70/30 PLDL, and the core material is PLLA. Both materials were manufactured by Purac (see Section **4.2**). The filaments were made in a 1:1 sheath:core ratio The purpose of the analysis was to determine the conditions for optimum fiber properties that would result in composite rods with favorable properties.

7.2 Degradation Due to Melt Extrusion

Because poly(lactic acid) is very sensitive to temperature it has a narrow processing window. At elevated temperatures, the polymer can undergo thermal-oxidative and/or hydrolytic degradation. The result is a material with lower molecular weight and viscosity. The reduction in viscosity experienced by the polymers during melt extrusion is listed in **Table 7.1**. The viscosity of PLLA decreased by 24 3%, while the viscosity of 70/30 PLDL decreased by 12.8%. The final viscosities were 1.71 dL/g and 1.23 dL/g, respectively. One possible cause of the degradation may be ester group cleavage by hydrolysis due to presence of moisture. The viscosity of the as-spun bicomponent filaments lies between these values and is 1.54 dL/g.

Table 7.1. Thermal characteristics of polylactides before and after melt spinning.

	Form	Viscosity (dL/g)	Die Temp. (°C)	Decrease %
1 1 PLLA 70/30 PLDL	Fiber	1.54	176	
PLLA	Pellet	2 26		
PLLA	Fiber	1 71	185	24.3
70/30 PLDL	Pellet	1 41		
70/30 PLDL	Fiber	1.23	180	12.8

The reduction in viscosity is consistent with the findings by other groups [16,17,63,64]]. The extent of the decrease in viscosity was dependent on the temperature of the die Eling et al. produced fibers that degraded by 40% at a low extrusion temperature of 185 °C [17] At a higher extrusion temperature (210 °C), the reduction was 60% [64]. Fambri et al reported a reduction in viscosity average molecular weight due to melt spinning The reduction in molecular weight reached as high as 64% at an extrusion temperature of 240 °C [16].

Yuan et al also studied the effects of hot-drawing on reduction in molecular weight. They found that the effects of hot-drawing the filaments on molecular weight were minimal in comparison to the effects of melt-extrusion [63]

7.3 Crystallinity and Molecular Orientation

It is well known that polylactide filaments reach their maximum orientation and strength when drawn at temperatures between 75°C and 100°C. Therefore, the filaments were drawn at temperatures of 75°C, 85°C, 95°C and 105°C The properties were determined at the maximum draw ratio for each temperature As

expected, the draw ratio increased with drawing temperature (see **Fig. 7.1**). The maximum draw ratio was 10 at a temperature of 105°C.

7.3.1 Thermal Analysis - DSC

The structural state of the as-spun and drawn bicomponent filaments were analyzed using DSC. **Figure 7.2** exhibits a crystallization exotherm at about 90 °C for the as-spun fibers. The presence of this peak indicates that a high degree of crystallinity was not developed prior to drawing. The DSC thermograms for the drawn fibers do not show this crystallization peak (see **Figs. 7.3 – 7.6**). Drawing produces orientation in the filaments. As a consequence, the molecular orientation is enhanced; and crystallization occurs via a stress-induced crystallization mechanism.

Melting of these crystals occurs between 170 °C – 180 °C. **Table 7.2** compares the degree of crystallinity of the as-spun and drawn filaments As expected, the crystallinity increases with increases in draw ratio and draw temperature. The as-spun fibers are 21.58% crystalline. The highest degree of crystallinity is 44 09% at a draw ratio of 10 and a draw temperature of 105 °C.

7.3.2 Crystalline Orientation - WAXD

The increase in crystallinity upon drawing is confirmed by the X-ray diffraction patterns shown in **Figure 7.7**. This method was used qualitatively to judge the amount of orientation and crystallinity in the filaments. The lack of distinct reflections in **Figure 7.7 (a)** indicates that the as-spun filaments were highly disordered Because the fibers were spun at relatively slow speeds, the spinline

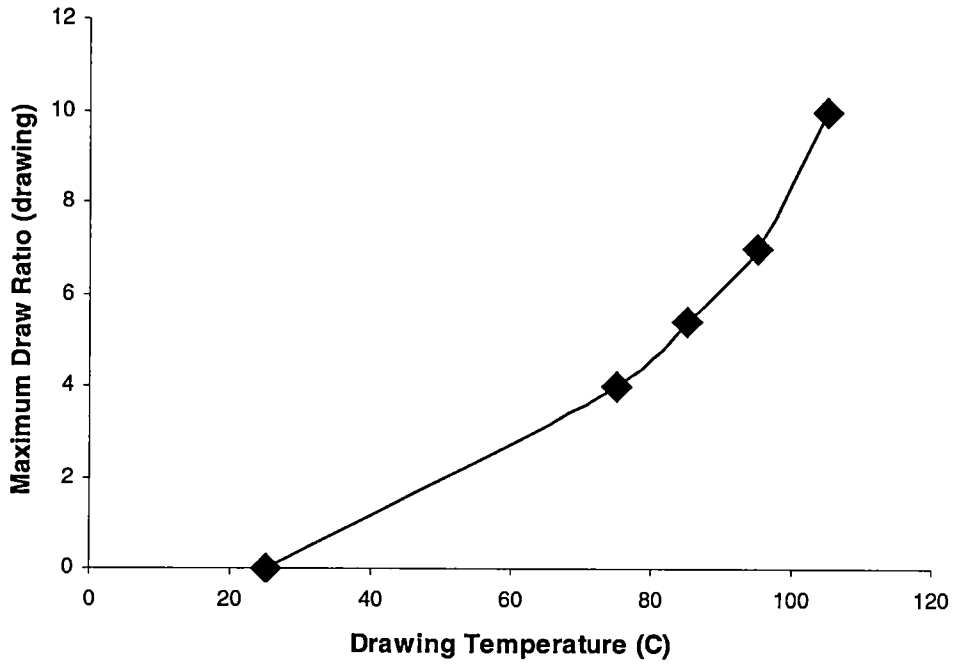


Figure 7.1. Maximum draw ratio attained at different drawing temperatures. 1:1 PLLA:70/30 filaments As-spun fiber take-up velocity ~93 MPM. Spinning experiments at The University of Tennessee.

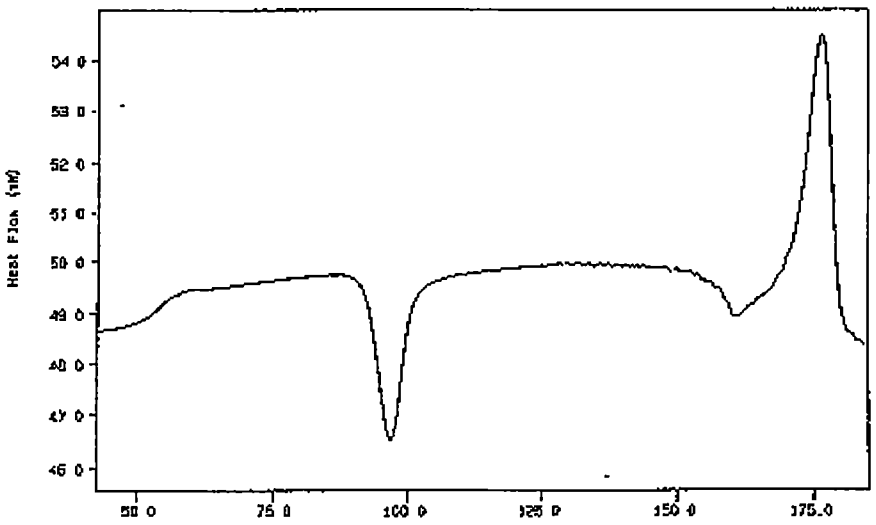


Figure 7.2. DSC scan of 1.1 PLA:PLDL as-spun fiber.

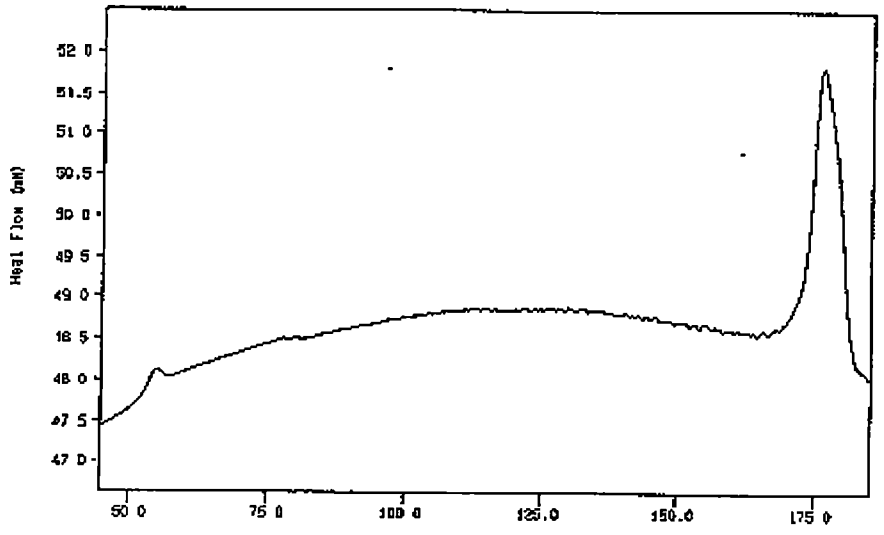


Figure 7.3. DSC scan of 1:1 PLA PLDL fiber. Draw Temperature 75 °C, DR = 4

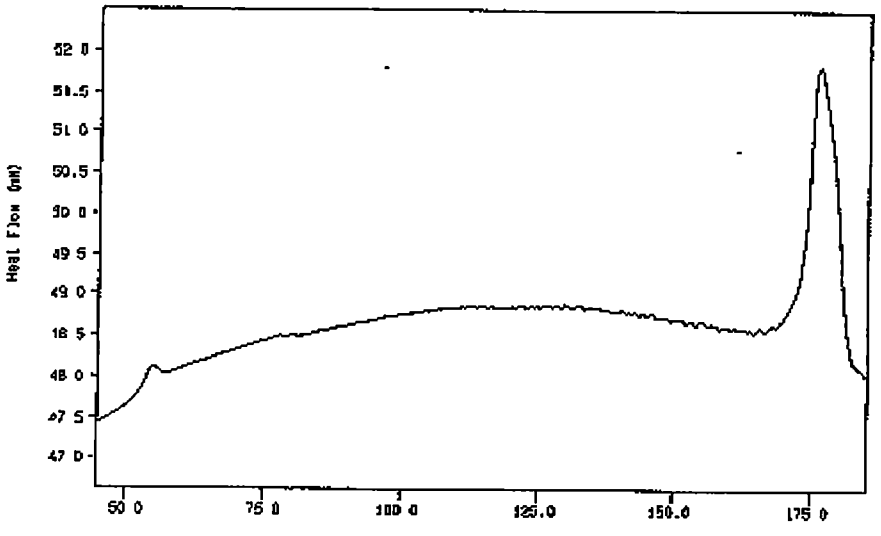


Figure 7.4. DSC scan of 1:1 PLA:PLDL fiber. Draw Temperature 85 °C, DR = 5.4

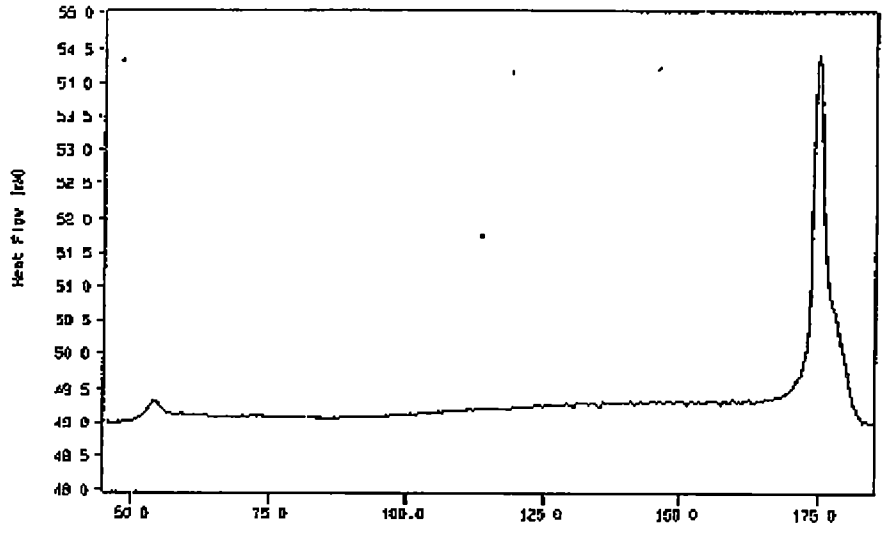


Figure 7.5. DSC scan of 1·1 PLA.PLDL fiber. Draw Temperature 95 °C, DR = 7.

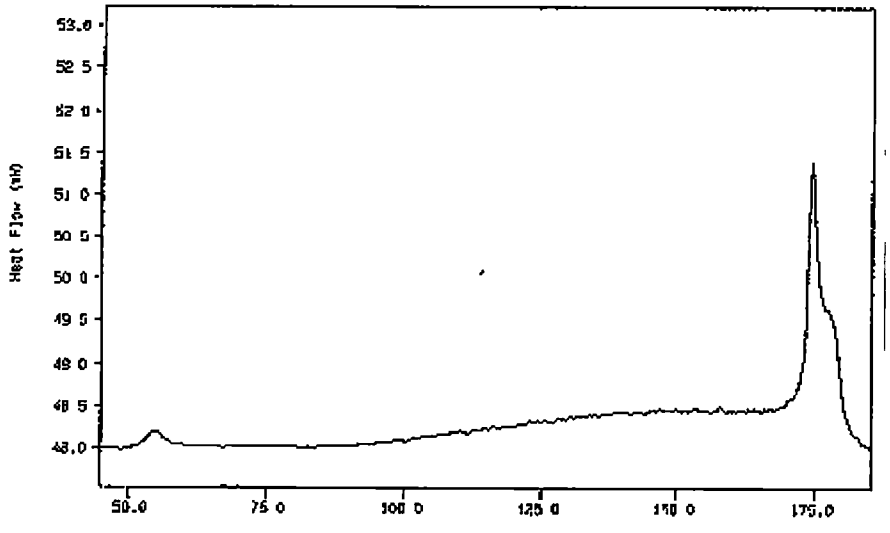


Figure 7.6. DSC scan of 1.1 PLA:PLDL fiber. Draw Temperature 105 °C, DR = 10.

Table 7.2. Effect of drawing on degree of crystallization as determined by DSC analysis.

Draw Ratio	Draw Temp. (°C)	Tm (°C)	Crystallinity (%)
0	—	176.65	21.58
4	75	176.45	24.46
5.4	85	176.24	32.13
7	95	174.84	34.64
10	105	174.29	44.09

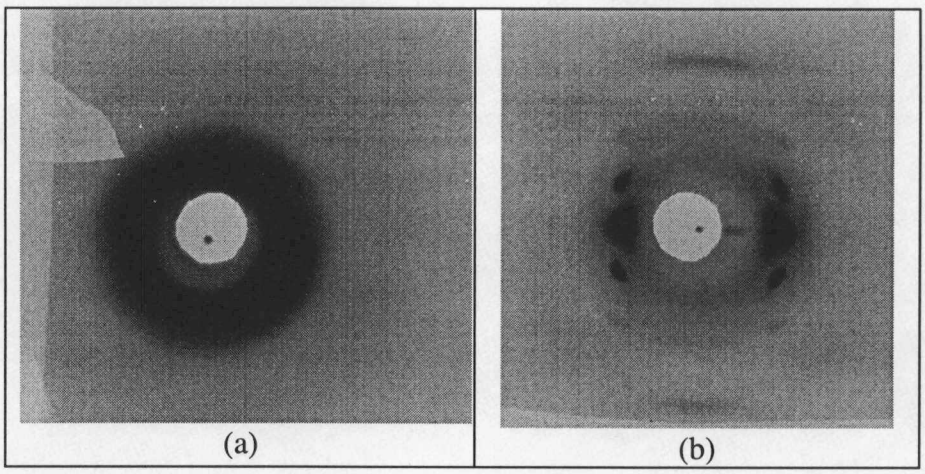


Figure 7.7. WAXD patterns of 1:1 PLLA:70/30 PLDL bicomponent filaments: (a) as-spun at 93 mpm; (b) draw ratio = 7.

stresses were not sufficient to promote molecular orientation along the fiber axis. However, orientation increases considerably after drawing as shown in **Figure 7.7 (b)** During drawing, the filaments are stretched along the fiber direction causing the molecules to align in that direction. The increase in orientation is depicted by the differences in the flat plate patterns for the as-spun and drawn filaments. The blurred halos due to the amorphous phase in the pattern of the as-spun filaments become short arcs and spots in the pattern of the drawn filaments, indicating that substantial crystallinity and crystalline orientation have occurred.

7.3.3 Molecular Orientation -Birefringence

While the WAXD patterns give a good indication of the crystalline orientation (which is high in **Figure 7.7 (b)**), the overall molecular orientation can be evaluated using birefringence. The overall orientation of the as-spun and drawn filaments is shown in **Figure 7.8**. Birefringence increases consistently with draw ratio up to a draw ratio of seven. Then the filaments undergo a slight decrease in birefringence after further increases in draw ratio. At a draw ratio of seven, the birefringence is about 0.25. At a draw ratio of 10, the birefringence is approximately 0.24. At the higher temperature, the increase in draw ratio occurs as a consequence of flow drawing in which polymer chains slide passed each other. This type of drawing occurs with minimal chain orientation [17]. Therefore, the birefringence decreases slightly.

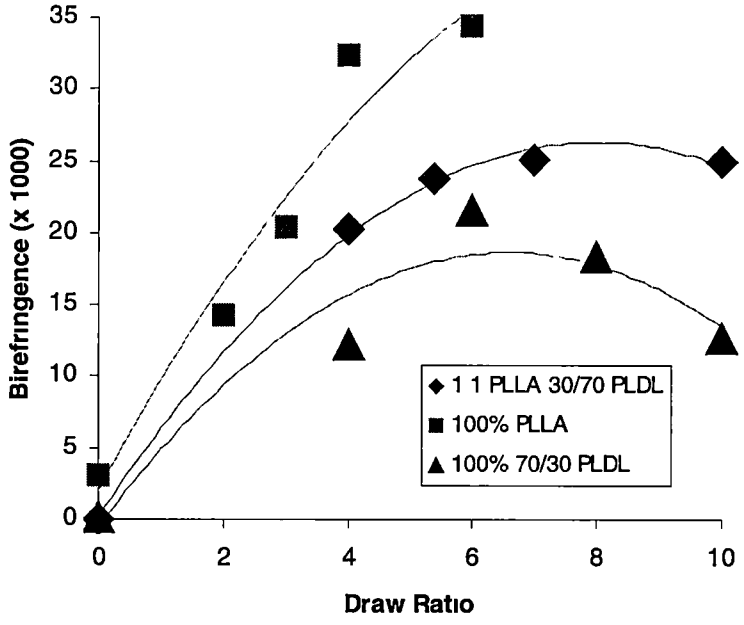


Figure 7.8. Effect of drawing on the overall orientation of 1:1 PLLA: 70/30 PLDL, 100% PLLA [8], and 100% 70/30 PLDL filaments.

7.4 Mechanical Properties of 1:1 Core:Sheath Fibers

The increases in orientation are accompanied by increases in tensile strength (see **Fig. 7.9**). This result indicates that there is some correlation between orientation and tensile strength. The tensile strength of drawn filaments ranged from 240 to 325MPa. The tensile strength increased with increasing draw ratio, reaching a maximum at a draw ratio of seven and temperature of 95°C due to molecular orientation development. Then the tensile strength decreased at the higher draw ratio of 10 and temperature of 105°C (see **Fig. 7.10**), which is consistent with the decrease in birefringence shown in **Figure 7.8**.

Figure 7.11 shows the relationship between modulus and elongation to break The stiffness of the filaments increases with drawing and the percent strain to break decreases. The modulus shows a maximum at a draw ratio of about 7, which is consistent with the maximum birefringence observed (see **Fig. 7.8**). Since modulus is a function of molecular orientation and crystallinity, this result is not surprising As the filaments became stronger, a higher degree of orientation was developed in the direction of drawing. Tensile testing was done in the fiber direction which is the direction of crystalline orientation; so the filaments developed the most strength in this direction. As the filaments became stronger, the modulus increased. Likewise, the filaments become more resistant to deformation with increases in tensile strength and crystalline orientation. Therefore, the elongation to break decreased.

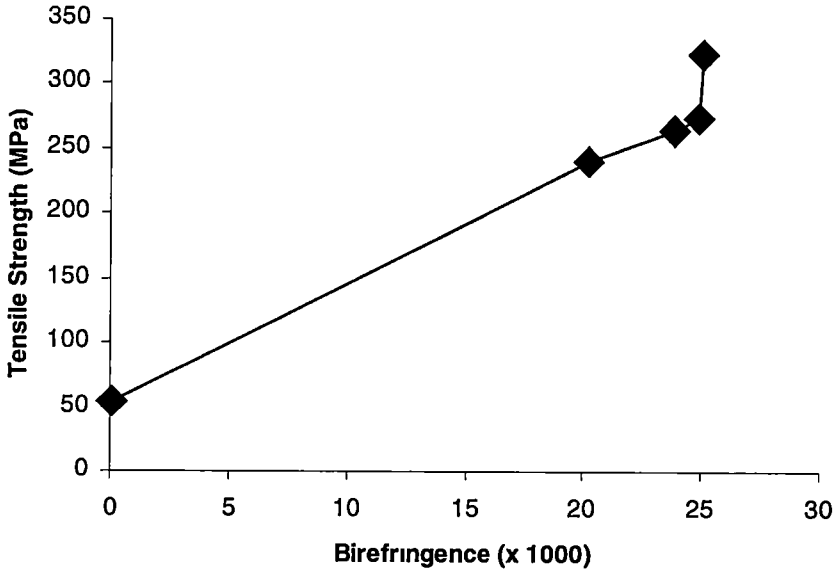


Figure 7.9. Correlation between tensile strength and orientation of 1 1 PLLA.70/30 PLDL filaments

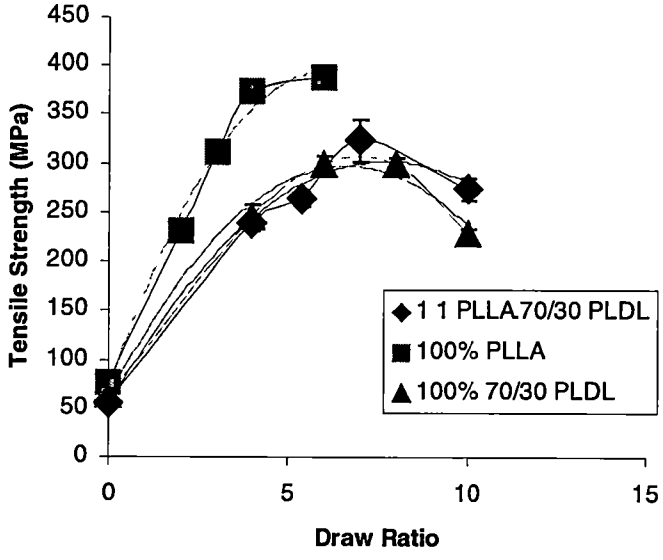


Figure 7.10. Effect of drawing on tensile strength of 1·1 PLLA.70/30 PLDL, 100% PLLA [8], and 100% 70/30 PLDL filaments

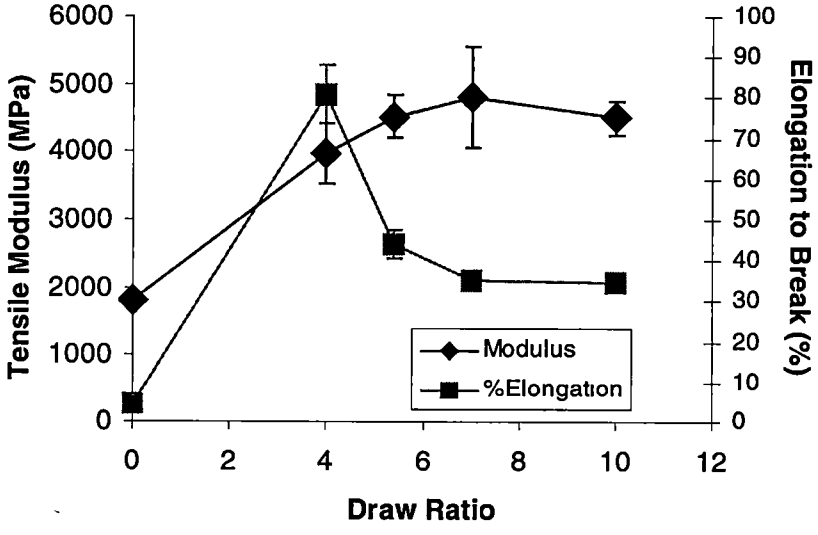


Figure 7.11. Modulus and elongation to break for drawn 1:1 PLLA:70/30 PLDL filaments

The tensile strength of single component PLLA and 70/30 PLDL filaments were compared to the tensile strength of the bicomponent fibers. The single component filaments have higher strength than the bicomponent fibers. Single component filaments of polylactic acid produced by melt spinning and drawing have shown a maximum tensile strength at break of 500 MPa [17]. Filaments with similar draw ratios have been obtained tensile strengths at break ranging from 200 to about 450 MPa [17] As-spun filments produced by a high speed melt spinning process have shown a tensile strength and modulus of 385 MPa and 6 GPa, respectively [35].

The addition of 70/30 PLDL causes a reduction in the overall strength of the filaments. This result agreed with the observed molecular orientation of each component in the bicomponent fibers as shown in **Figure 7.8**. The single-component PLLA filaments developed a relatively high degree of orientation in comparison to the 70/30 PLDL filaments. The 70/30 PLDL filaments do not crystallize; so they cannot add orientation via an oriented nucleation and growth crystallization process.

Similar studies have been done on poly(ethylene terephthalate) (PET) systems [18,43,] Kikutani *et al.* produced core-sheath bicomponent fibers of PET and polypropylene (PP) with various core-sheath ratios. Structure development was significantly different for the single-component and bicomponent systems due to the mutual interactions of the polymers during bicomponent spinning. Molecular orientation of the core (PET) was enhanced while the molecular orientation of the sheath (PP) was suppressed [43]. Kikutani *et al* suggested that the core solidifies

faster than the sheath, causing stress-relaxation in the sheath. Thus, the sheath experiences a reduction in orientation [43].

7.5 SEM Analysis for Fracture Surfaces

Scanning electron micrographs were taken of the tensile fracture surfaces of the bicomponent filaments (see **Fig. 7.12**). The differences in fracture mode between the two components of the bicomponent system allow a distinction to be made between the regions occupied by sheath and core. Thus, the interface between the sheath and core could be seen. The micrographs show that the interface between the sheath and core was maintained. Examination of the filaments showed little evidence of delamination at the interface.

There are substantial differences between the fracture surface of the as-spun filament shown in **Figure 7.12 (a)** and the fracture surfaces of the drawn filaments in **Figure 7.12 (b) – (e)** The interface of the as-spun fiber was deformed while the interface of the drawn fibers was not. This indicates that the as-spun fiber was more ductile, as expected.

Also from these SEM micrographs, the actual core:sheath ratios could be determined by measuring the area of the filament occupied by each component of the system. From the calculations, it was determined that the core occupied 45% of the area and the sheath occupied 55% of the area. So, the actual core:sheath ratio was 1:1 2 PLLA:70/30PLDL. The discrepancy between actual and expected core:sheath ratio may have occurred due to inaccurate rate calibration of the metering pumps.

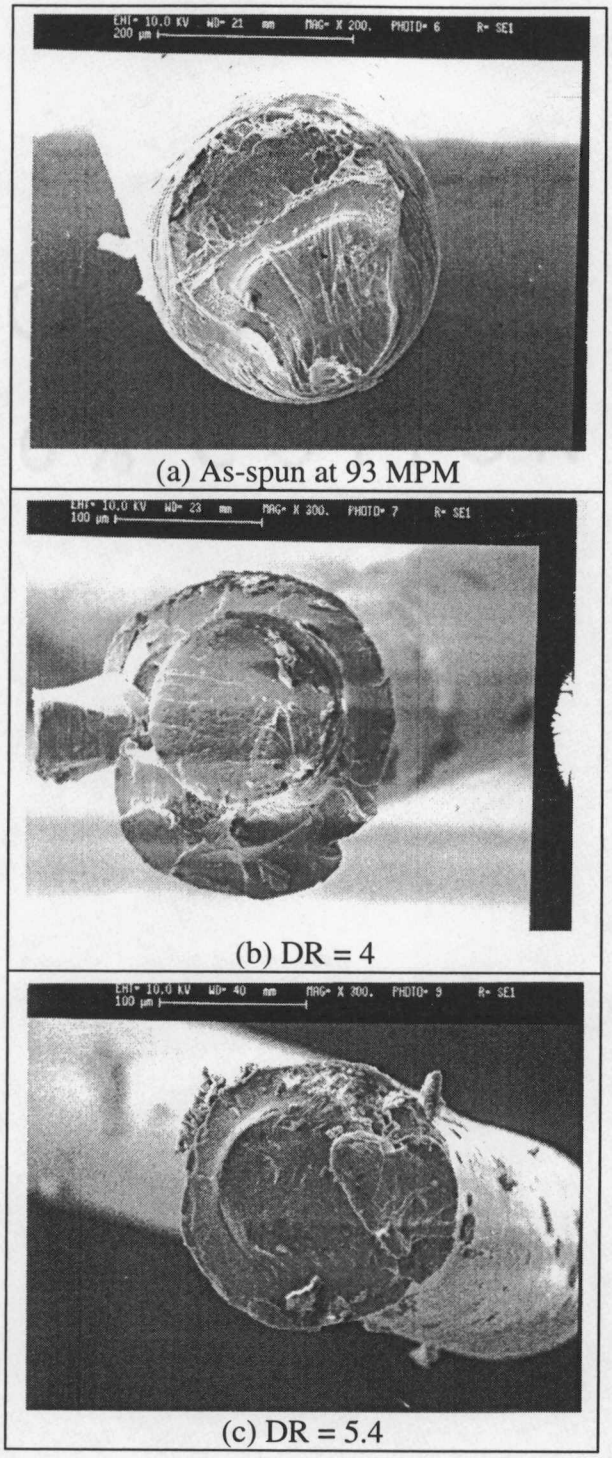
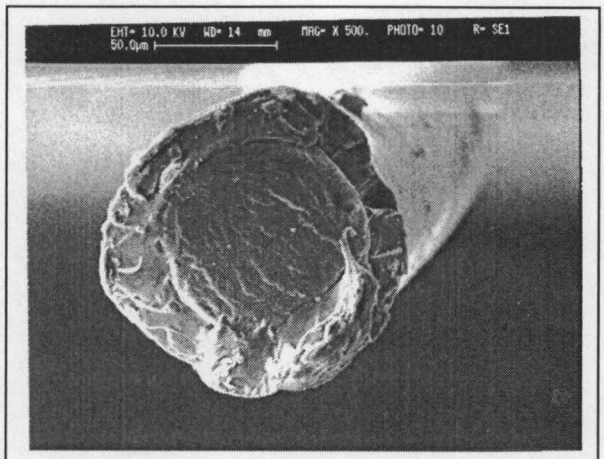
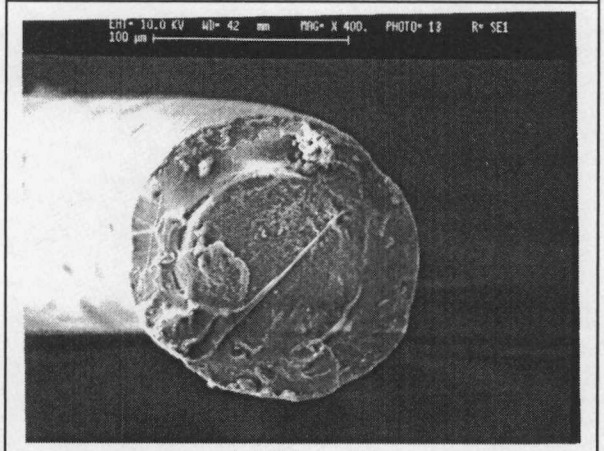


Figure 7.12. SEM micrographs of tensile fracture surfaces of 1:1 PLLA:70/30 PLDL as-spun and drawn filaments (continued on next page).



(d) DR = 7



(e) DR = 10

Figure 7.12. (continued)
SEM micrographs of tensile fracture surfaces of 1:1 PLLA:70/30 PLDL as-spun and drawn filaments.

CHAPTER 8

Final Analysis of Composite Rods

8.1 Composite Rod Fabrication

Based on the results of the preliminary tests described in **Chapter 6**, the composite rods were made from 1:1 PLLA:70/30 PLDL bicomponent filaments by pulling the filaments through the pultrusion die at a rate of 0.15 in/min. Properties of the resulting 2.0 mm diameter rods are reported in the following sections.

8.2 Orientation of Composite Rods

Pulling the bicomponent filaments through the pultrusion die produces rods which have a higher degree of crystalline orientation than the bicomponent filaments (WAXD patterns for the filaments were shown in **Figure 7.6**) Crystalline orientation of the rods tends to increase with temperature as shown in **Figure 8.1** It can be concluded from the patterns that the rods have very high molecular orientation and crystallinity.

Other authors have seen this high degree of orientation in melt-spun and solution-spun poly(lactide) fibers [17,65] The sharp reflections are characteristic of the α-crystalline modification in which the polymer chains form a helical conformation [17]. The smeared layer lines that are most visible in **(a) – (c)** are caused by the presence of the β-modification [17] According to Eling, the presence of β indicates a high level of disorder in the planes perpendicular to the fiber axis. As the draw ratio is increased, the amount of β-form also increases [17]. At lower draw ratios, the α-form is seen exclusively [17]. At 175 °C, the diffuse reflections caused by the β- phase are no longer

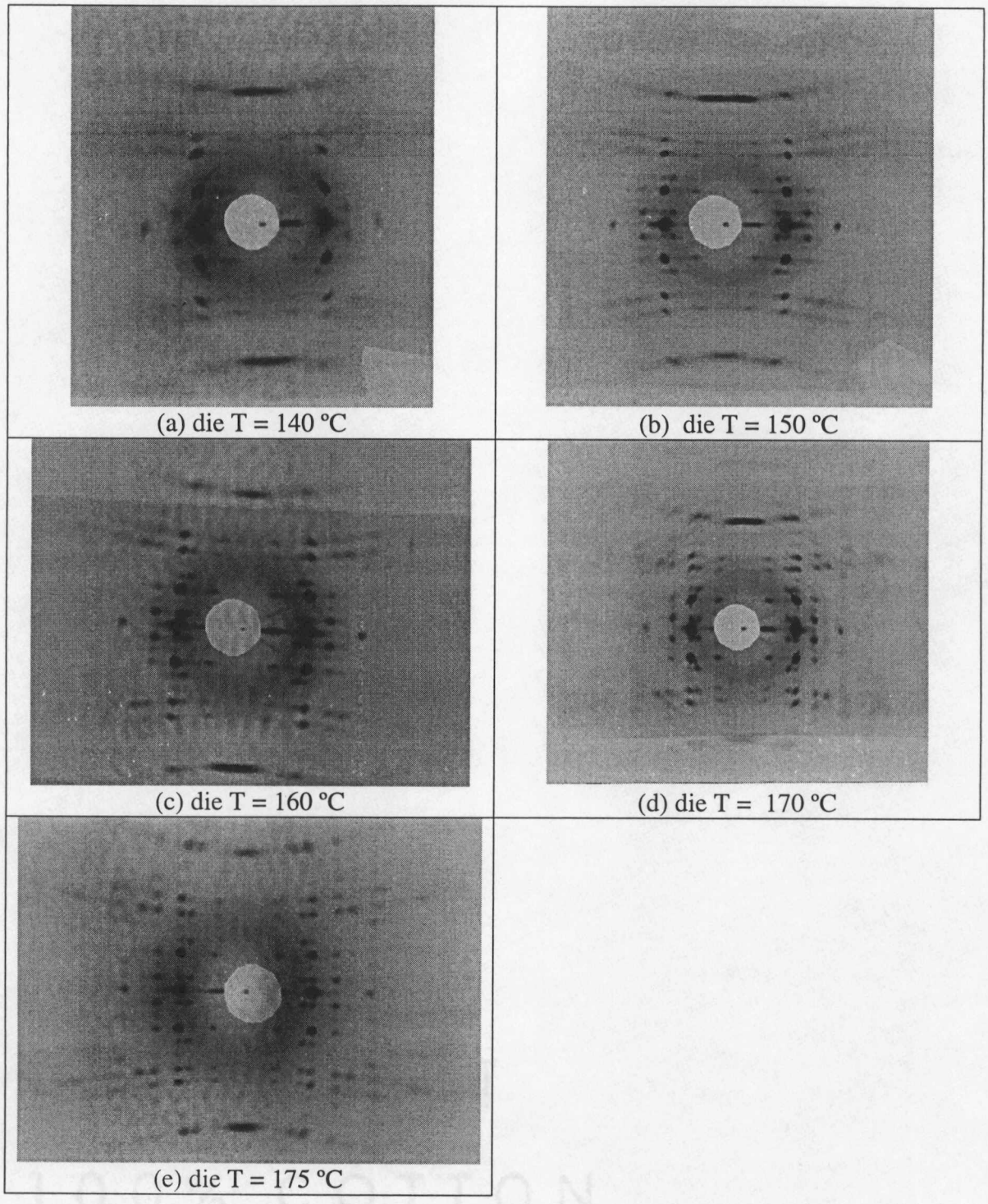


Figure 8.1. WAXD patterns for composite rods fabricated at different temperatures.

present. This observation suggests that some reordering occurred that allowed crystallinity and orientation of the core fibers to increase. However, this may also have reduced the number of tie molecules connecting the crystals. Further, at high temperatures the sheath is molten and amorphous orientation may be reduced by the molecular relaxation process [17].

8.3 Mechanical Properties of Composite Rods

The stress-strain behavior of the composite rods produced at different temperatures is shown in **Figure 8.2.** The maximum stresses occurred for rods pultruded at a die temperature of 150 °C. The behavior of the rods was similar up to about 160 °C. Above this temperature there is a significant reduction in strength (see **Fig. 8.3**) which is accompanied by a large reduction in strain. This decrease in strain indicates that the rods become more brittle when processed at elevated temperatures. Similarly, the stiffness of these rods is affected by processing temperature. At the lower die temperatures, the modulus ranges between 2000 to 2500 MPa (see **Fig. 8.4**) And above 160 °C, there is a substantial reduction in modulus.

The SEM micrographs of the tensile fracture surfaces support the idea of the composites becoming more brittle at higher processing temperatures (see **Fig. 8.5**) At processing temperatures of 140 °C **(a) – (c)** and 150 °C **(d), (e)**, the composite undergoes a mixture of failure modes, indicating sufficient fiber-matrix interface strength [32]. The fibers blunted crack growth, causing fiber breakage in several places

At the higher processing temperatures of 160 °C shown in **(f)** and **(g)**, there was a greater occurrence of individual fiber pull-out due to the presence of a relatively weak

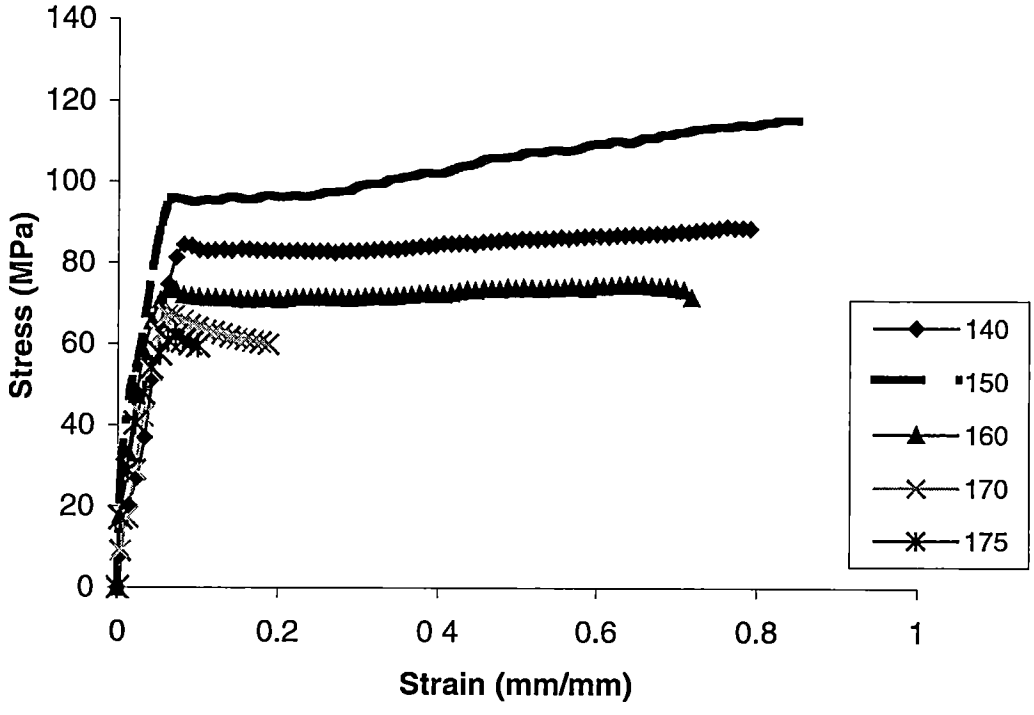


Figure 8.2. Stress versus strain for composite rods produced at different pultrusion die tempertures Pultrusion rate = 0.15 in/min.

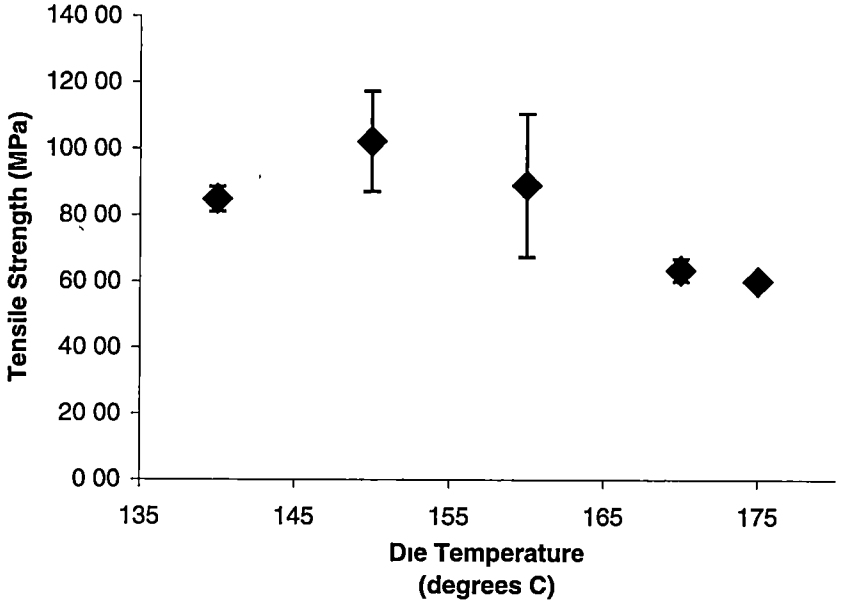


Figure 8.3. Effect of fabrication temperature on the tensile stength of the composite rods Pultrusion rate = 0 15 in/min

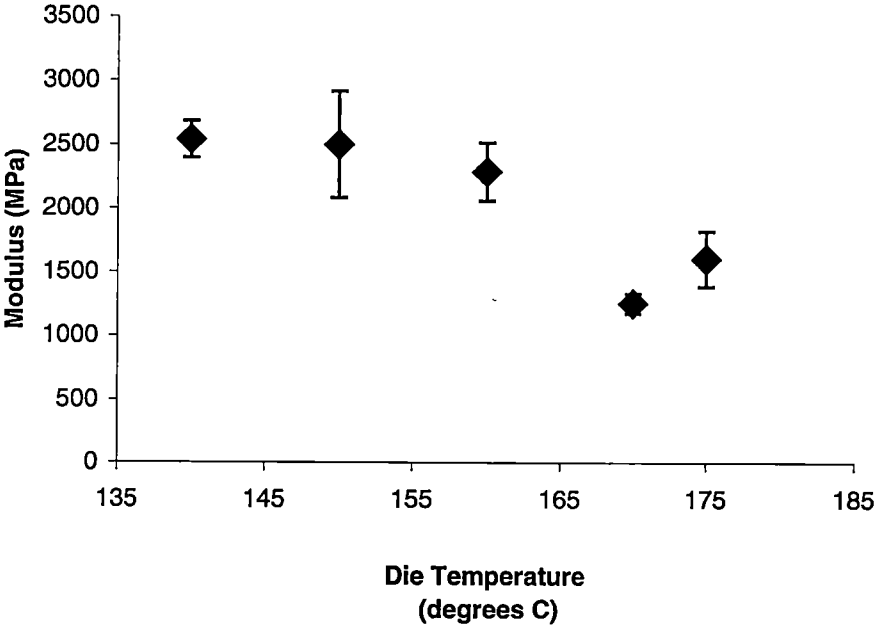
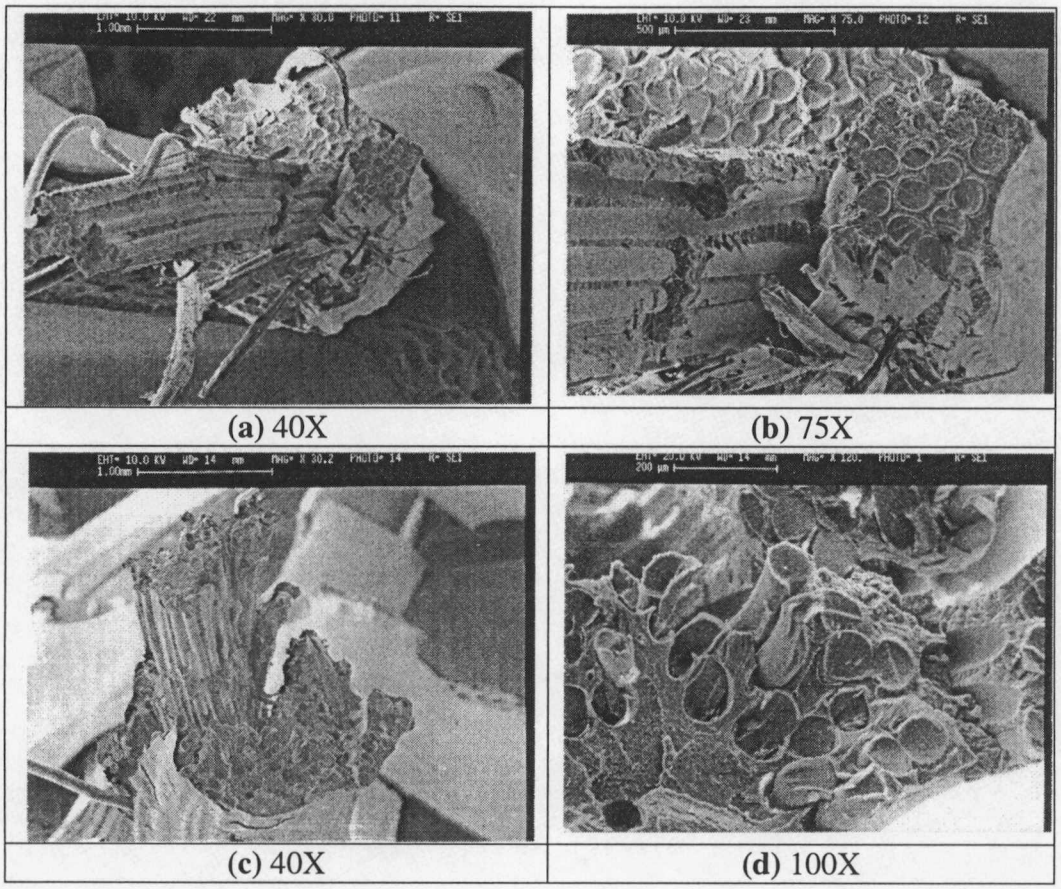


Figure 8.4. Effect of fabrication temperature on the tensile modulus of the composite rods. Pultrusion rate = 0.15 in/min

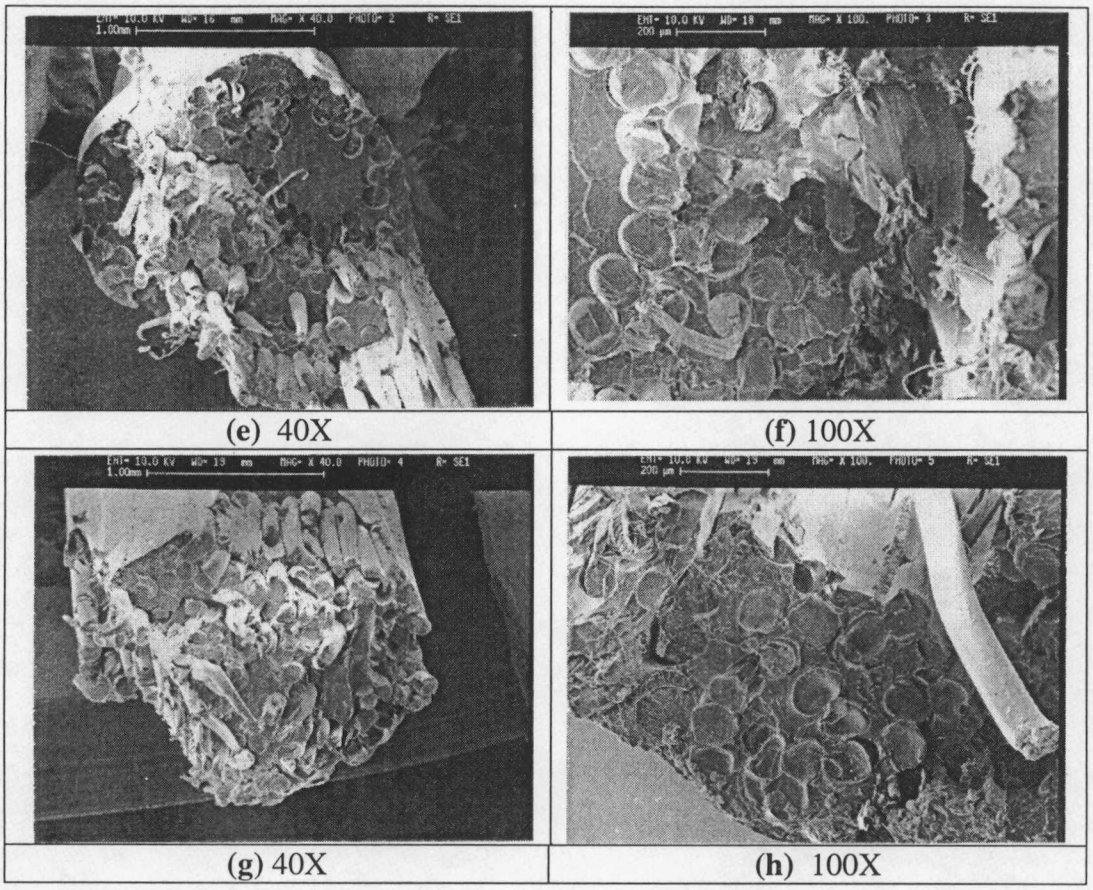


(a) 40X (b) 75X

(c) 40X (d) 100X

Figure 8.5. SEM micrographs of tensile fracture surfaces of PLLA:70/30 PLDL composite rods made at different die temperatures (a) –(b) Die temperature = 140 °C; (c) – (d) Die temperature = 150 °C; Pultrusion rate = 0.15 in/min (continued on next page).

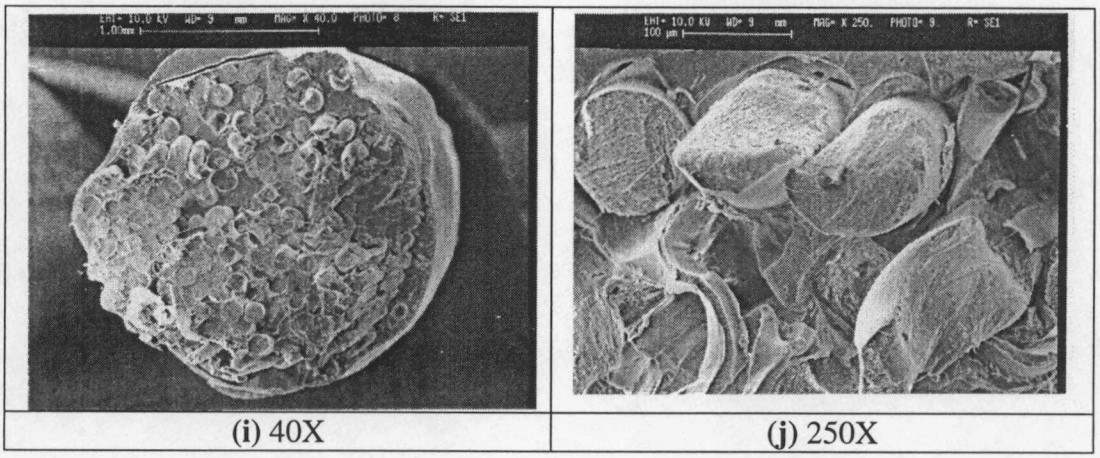
GILBERT
100% COTTON



(e) 40X | (f) 100X

(g) 40X | (h) 100X

Figure 8.5. (continued)
SEM micrographs of tensile fracture surfaces of PLLA:70/30 PLDL composite rods made at different die temperatures (e) –(f) Die temperature = 160 °C; (g) – (h) Die temperature = 170 °C; Pultrusion rate = 0.15 in/min (continued on next page).



(i) 40X (j) 250X

Figure 8.5. (continued)
SEM micrographs of tensile fracture surfaces of PLLA:70/30 PLDL composite rods made at different die temperatures (i) –(j) Die temperature = 175 °C; Pultrusion rate = 0.15 in/min.

interface. At 170 °C and 175 °C, fracture became brittle in nature. The crack propagated uniformly across the surface There are relatively few raised surfaces indicating the absence of plastic deformation (see **Fig. 8.5 (h) – (l)**). It appears that some fiber drawing occurred before fracture. This may be an indication that the fibers were getting weaker as the processing temperature was increased (see **Fig. 8.5 (l)**). The X-ray diffraction patterns shown in **Figure 8.1** indicate that major changes in the structure of the core fibers occurred at the higher pultrusion temperatures.

Shear strength behavior showed a steady decline as the pultrusion die temperature was increased (see **Fig 8.6**). The shear strength was the highest at 140 °C with a value of 75 MPa. At 175 °C, the shear strength was 48 MPa The SEM photomicrographs in **Figure 8.7** show that the interface between the core fibers and the matrix become less visible at higher temperatures. During the failure, the matrix appears to become smeared at the sheared surface. This effect may result from the corresponding loss of strength, causing deformation to occur more readily. This smearing is not as prevalent at the lower processing temperatures The matrix material became more deformable as the temperature increased. The fibers also tend to deform more readily at elevated temperatures. This result agrees with the fracture behavior of the composites in tension (see **Fig. 8.5 (l)**).

Continuous fiber-reinforced composites of PLLA embedded in a 70:30 PLDL matix have been produced previously by compression molding various ratios of PLLA and 70/30 PLDL melt-spun filaments [67]. A decrease in strength also occurred during fabrication of this composite. Using PLLA fibers with an initial strength of 800 MPa the

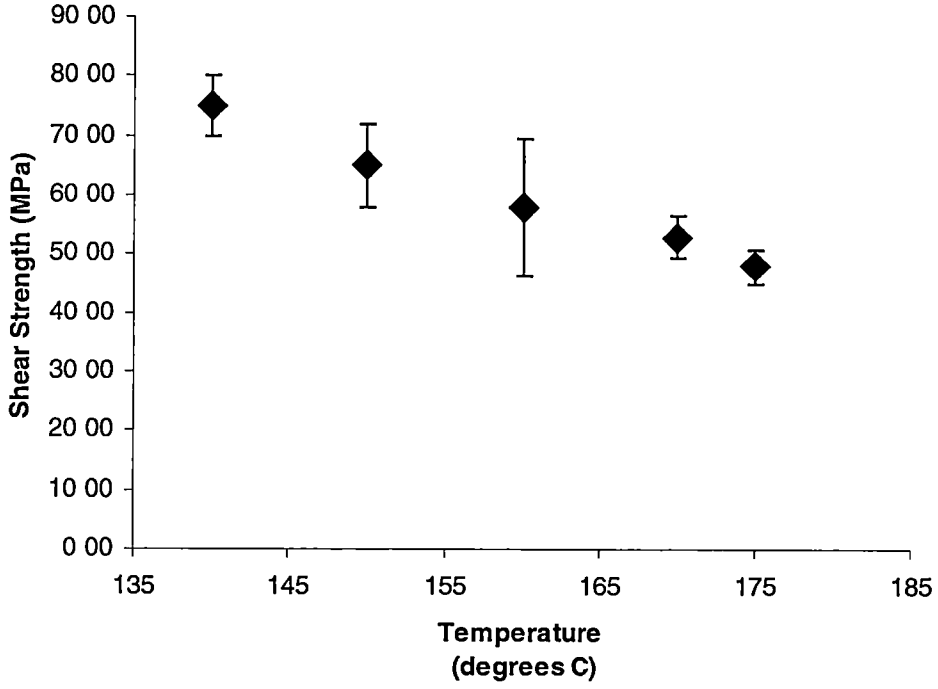
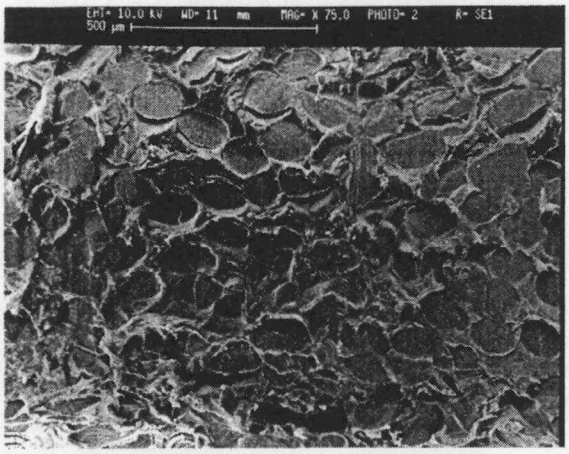
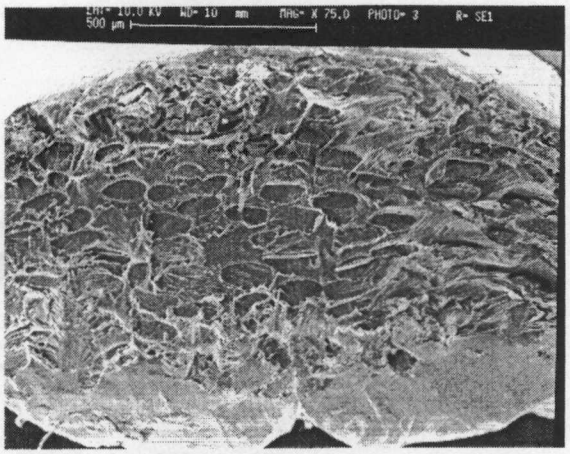


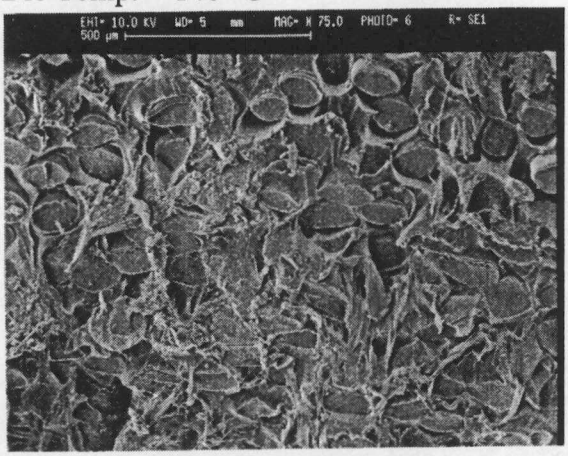
Figure 8.6. Effect of fabrication temperature on the shear strength of the composite rods Pultrusion rate = 0.15 in/min.



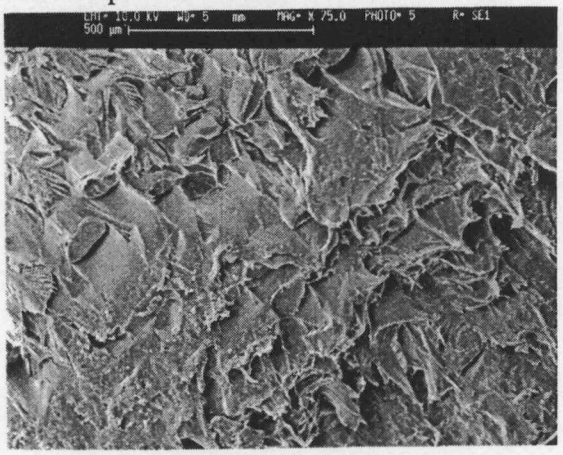
Die Temp. = 140 °C



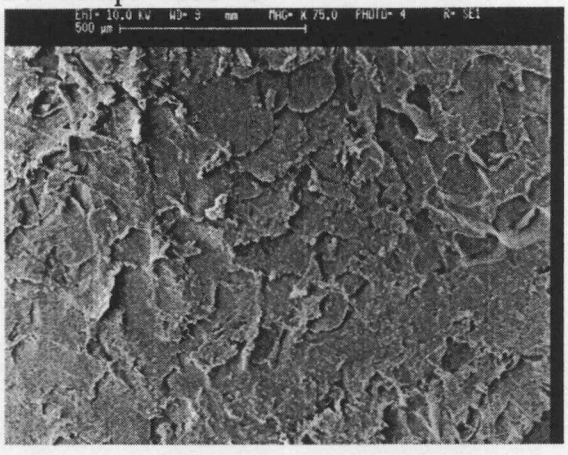
Die Temp. = 150 °C



Die Temp. = 160 °C



Die Temp. = 170 °C



Die Temp. = 175 °C

Figure 8.7. SEM micrographs of shear fracture surfaces of PLLA:70/30 PLDL composite rods at different processing temperatures. 75X magnification.

researchers produced 3.0 mm diameter pins with a shear strength of 104 MPa [67]. However, this processing technique yielded a composite with satisfactory strength for its application The causes of the loss in strength are not reported.

The flexural strength and bending modulus of the 2.0 mm composite rods pultruded at 145 °C and 150 °C were determined by persons in the Orthopedic Bioengineering Lab at Georgia Institute of technology [66]. The results are reported in **Table 8.1**

In **Table 8.2**, the mechanical properties of the 2 0 mm 1:1 PLLA.70/30 PLDL composite rods are compared to the 2 0 mm Bionx Smart Pin™ which is commercially available. The Bionx pin is self-reinforced poly(L-lactide) (PLLA) which is processed by die drawing molded PLLA rods For all measured properties, the present composite rods have lower strength than the Bionx pins. The greatest disparity in strength arises for the shear and flexural properties. In both cases, the strength of the Bionx Smart Pin™ is two times the values for the proposed composite rod.

In shear, the Bionx pin experienced some fibrillation (see **Fig. 8.8**) Pins consisting of only PLLA have been known to release acidic degradation products which cause foreign body reactions when released in high concentrations [11,30]. Fibrillation increases the surface area that can be attacked by enzymatic fluid in the body This result

Table 8.1. Flexural properties of composite rods made from 1:1 PLLA 70/30 PLDL filaments.

Pultrusion Die Temperature	Bending Strength MPa	Flexural Modulus Gpa
145 °C	101.6 ± 9.1	4.61 ± 0 29
150 °C	117 9 ± 8.1	5.47 ± 0 31

Table 8.2. Mechanical properties of 1:1 PLLA:70:30 PLDL rod and commercial control.

	Tensile Strength MPa	Tensile Modulus GPa	Shear Strength MPa	Bending Strength MPa*	Flexural Modulus GPa*
1:1 PLLA:70/30 PLDL rod	102.3	2.50	75.0	117.9	5.47
Bionx Smart Pin ™	126.6	2.71	169.7	250.8	7.69

*Courtesy of [66].

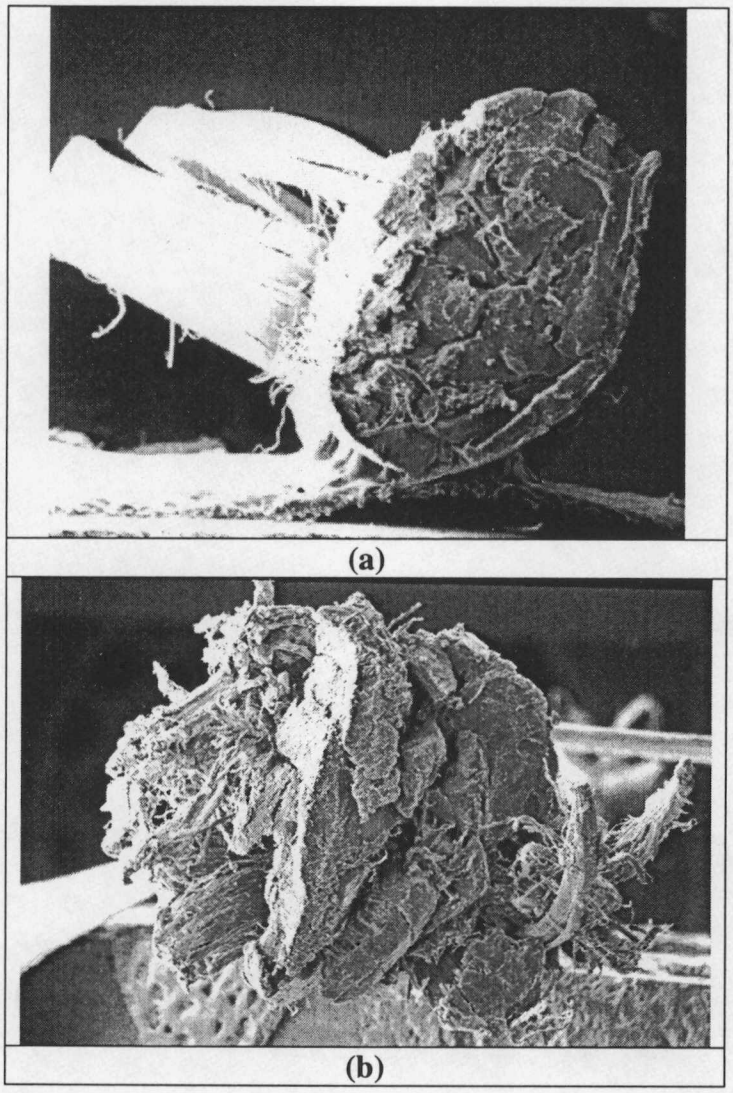


Figure 8.8. SEM micrographs of Bionx Smart Pin ™ fracture surfaces: (a) Shear failure; (b) Tensile failure. 20X Magnification.

could possibly lead to faster degradation of PLLA. The 1:1 PLLA:70/30 PLDL rods do not fibrillate under shear or tensile loads (see **Figure 8.5**). Therefore, it is conceivable that complications may be reduced if this alternative processing method is used.

8.4 Comparison of Fiber and Composite Properties

The results of the analysis of the composite rods indicate that the fiber strength is not transferred to the composite rods. The fibers used to make the rods had a tensile strength and modulus in the range of 300 MPa and 4000 MPa, respectively. The maximum tensile strength of the composite rod was 101 MPa; and the modulus was 2500 MPa Interestingly, the crystalline orientation is enhanced despite the loss in strength (see **Fig. 8.1** and **Fig. 7.6 (b)**).

To determine the cause of this reduction in properties, a short study was conducted. Fibers that were used to produce the composite rods were subjected to heat treatment. The fibers were held in tension and heated in an over at 140 °C and 160 °C for twenty minutes. The tensile properties and crystalline orientation were determined and compared to the properties of the fibers prior to the heat treatment. The results are reported in **Table 8.3**.

The data show that heating the drawn fibers results in a reduction in strength and stiffness; and the effect of annealing increases with temperature. Annealing has a greater

Table 8.3. Comparision of tensile properties of 1:1 PLLA:70/30 PLDL filaments before and after annealing.

Heat Treatment	Strength MPa	Reduction	Modulus MPa	Reduction	% Elongation	% Increase
None	323	—	4825	—	34.91	—
140 °C	219	32 %	4407	8.7 %	79.87	128.8 %
160 °C	161	50 %	3909	19 %	97.34	178.8 %

effect on fiber strength than stiffness The fibers experienced a 50 % reduction in strength at 160 °C. However, the modulus is only reduced by 19 %. The increase in percent elongation that occurs indicates that the fibers become more deformable after annealing. This behavior also occurred for the composite rods. As the processing temperature was increased, the matrix and core materials deformed more readily (see **Fig 8.5, 8.7**).

The crystalline orientation of the fibers before and after annealing is shown in **Figure 8.9** The behavior is consistent with that of the composite rods. Although, the mechanical properties of the annealed fibers have decreased, they show an increase of crystalline orientation

The results of this study help to explain the reduction in strength that occurred for the composite rods It appears that heating the fibers after the drawing process causes a reduction in the strength of the fibers. The crystals remain aligned, and crystalline orientation is not reduced. During the pultrusion process, the sheath material is molten. It is plausible that any amorphous orientation that developed during the fiber-drawing process was destroyed, and the strength of the fiber was reduced for this reason. Also, the amorphous fraction of the core fibers may have relaxed; and the number of taut tie molecules may have decreased. This process would reduce the strength and modulus of the core fibers.

The decrease in strength of the core PLLA fibers was addressed previously in a study by C M Agrawal *et al.* Drawn PLLA monofilaments were annealed at 140 °C and constrained in tension for 15 minutes. Annealing resulted in a reduction in tensile strength and an increase in the percent elongation to break [24]. They proposed that the

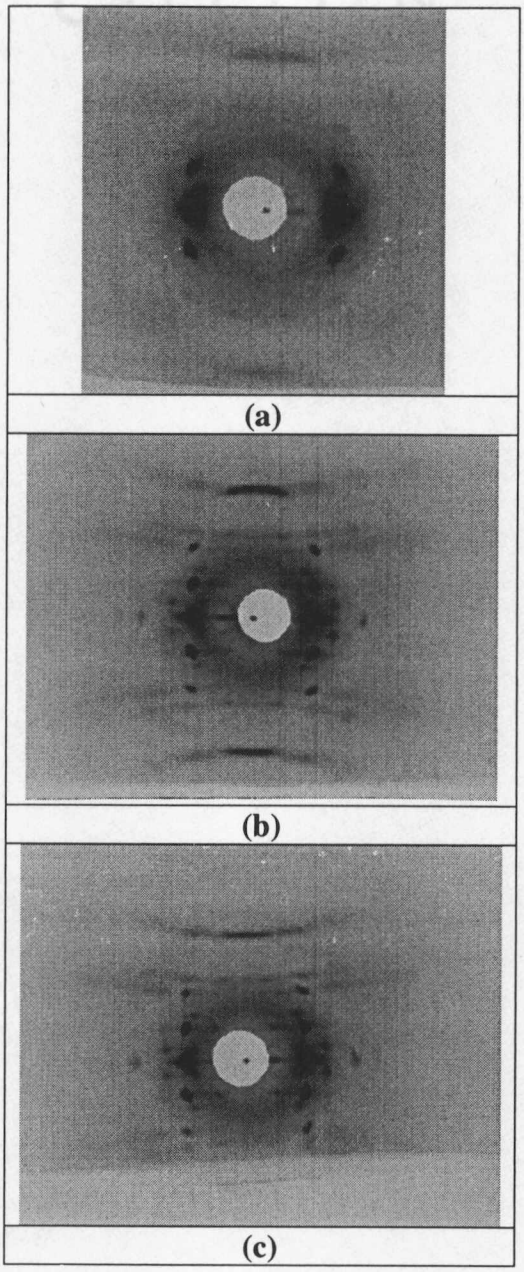


Figure 8.9. WAXD patterns of 1:1 PLLA:70/30 PLDL filaments before and after annealing. (a) fiber at DR =7, not annealed; (b) fiber annealed at 140 °C; (c) fiber annealed at 160 °C.

reason for this reversal of the effects of drawing is that heating the filaments increases molecular movement. Therefore, the molecular chains gained enough thermal energy to facilitate reorganization of the molecular chains to a lower energy state. Thus, they became more crystalline and less oriented [24].

Although the crystalline orientation remains high, the orientation of the chains between the crystals relative to the fiber axis may have decreased due to a more helical conformation of the molecules. This may also result in fewer tie molecules connecting the crystals. As a result, the strength and modulus of the fibers and rods could also be reduced

In addition, polymer degradation may have contributed to the loss in strength. The fibers were consolidated at temperatures near the melting temperature of PLLA. At these high temperatures, it is likely that cleavage of the ester groups occurred through a hydrolytic process due to the presence of water in the processing environment [16]. The effect of degradation is a reduction in molecular weight; thus, reducing the overall strength of the composite.

CHAPTER 9

Conclusions and Recommendations

9.1 Conclusions

Poly(L-lactic acid) (PLLA) and poly(L/DL-lactide) copolymers were used to produce core:sheath bicomponent fibers with 1:2, 1:1, 2:1, 3:1, and 4:1 core sheath ratios by melt-spinning and drawing processes. Molecular orientation developed during the drawing process yielding filaments with reseasonable strength and modulus.

These fibers were pulled through a heated pultrusion die to produce 2 0 mm composite rods of PLLA core fibers embedded in a 70/30 PLDL matrix. There exists some critical core:sheath ratio above which the resulting composite does not contain a sufficient amount of sheath material to prevent catastrophic failure during loading. If the level of core material is too high, massive delamination occurs Below this critical core:sheath ratio, the integrity of the interface between the core and sheath is maintained. In the present experiments, massive delamination occurred at a core:sheath ratio of 4:1. Below this value, the interface remained intact. The best mechanical properties were obtained when the composite rods were made with 1:1 core:sheath bicomponent filaments.

Comparison of the mechanical properties and crystalline orientation of the bicomponent fibers and the composite rods showed that heat treating the bicomponent filaments after the drawing process weakens the filaments. The bicomponent filaments had an initial tensile strength and modulus of 300 MPa and 4000 MPa, respectively. After heat treatment, the composite strength and modulus were 101 MPa and 2500 MPa.

Despite the loss in strength, the composite rods developed a high degree of crystalline orientation and crystallinity characteristic of the α-crystalline modification.

The loss in strength was caused by the annealing process which reversed some of the effects of fiber drawing. Consolidation of the fibers into rods was not a factor Other possible reasons for the decrease in mechanical properties were degradation of the fibers due to the presence of moisture, loss of amorphous orientation, changes in the crystalline modification of the fibers upon heating, and changes in the fiber morphology – including a reduction in the number of taut tie molecules connecting the crystals.

The mechanical properties of the composite rods were also compared to the properties of the 2 0 mm diameter Bionx Smart Pin™ The tensile, shear, and bending strengths of the Bionx pin were higher than the composite rods. For the proposed composite to become a viable material for use in the medical device industry, improvements in the properties of the proposed composites are desirable

9.2 Recommendations

Although the composite rods produced from bicomponent filaments lacked sufficient mechanical properties, it is likely that the bicomponent filaments can be used to produce composites with high strength and modulus under different processing conditions To address this issue, the following action items are recommended

9.2.1 Processing Modifications

1 Consolidate the as-spun bicomponent filaments by pulling them through the pultrusion die. Subject the resulting composite to a drawing processs to increase the strength and modulus

2. Use a swagging process to produce orientation. After the bicomponent filaments have been consolidated using the pultrusion die or shrink wrap tubing, the swagging process can be applied to draw the rods. This may potentially produce rod with better quality, increased uniformity and increased strength
3. There is a possibility that the decrease in strength from fiber to rod is due to degradation of the polymer. If so, the following actions can be taken to keep the fibers or rods as dry as possible.
    a During the spinning process, purge the hoppers with nitrogen gas to prevent moisture sorption
    b. After spinning, dry filaments in a vacuum oven at low temperature.
    c. Devise a method to maintain the fibers in the dry state while they are being consolidated into the composite rods.
4 Explore possibility of preparing composites in a control room environment, at low temperature and relative humidity By controlling the amount of moisture in the processing environment, it may be possible to decrease the amount of degradation due to moisture
5 Change the orientation of the fibers in the matrix by twisting, or braiding the filaments Then heat the filaments to a temperature at which autoadhesion of the sheath material will occur.
6 Use lower temperatures and longer dwell times (in the pultrusion die) to consolidate the core:sheath fibers.

9.2.2 Additional Testing

1 More extensive investigation of the effects of annealing on the mechanical properties of the fibers and the composites should be conducted.

2 Measure the molecular weight of the fibers and the rods to see if there is a reduction in molecular weight.

3 Further drawing experiments are needed to determine the effects of drawing rate, drawing temperature, and multiple stage drawing on the mechanical properties

4. Investigate the possibility of using a semi-crystalline polylactide for the sheath component of the bicomponent system. Lowering the amount of DL-lactide will allow some crystalline orientation to develop in the sheath This may greatly affect the deterioration of properties on heating.

5. Bicomponent filaments should be melt-spun using PLLA and PLDL of various molecular weights to determine the effect of molecular weight on the processability and resulting mechanical properties of the bicomponent filaments.

6 Birefringence measurements should be carried out to determine the refractive indices of the sheath and core parts separately. As a result, the molecular orientation of each component can be evaluated and the contributions of each component to the overall strength of the filament can be determined

7. The fiber-matrix proportions in the composite should be determined by numerical analysis And the effects of varying fiber-matrix proportions on the mechanical properties should be further investigated

REFERENCES

REFERENCES

1 S. Ferguson, D. Wahl, and S. Gogolewski, "Enhancement of the mechanical properties of polylactides by solid-state extrusion: Poly(L-lacitde), poly(L/D-lactide), and poly(L/DL-lactide)." *Fifth World Biomaterials Congress,* Toronto, Canada (1996).

2 W. Weiler and S. Gogolewski, "Enhancement of the mechanical properties of polylactides by solid-state extrusion." *Biomaterials,* **17,** 529-35 (1996).

3 M. Slivka and C. Chu, "Fiber-matrix interface studies on bioabsorbable composite materials for internal fixation of bone fractures. II A new method using laser scanning confocal microscopy." *J. Biomed Mater Res.*, **37(3),** 353-362 (1997).

4 P. Tormälä, J. Vasenius, S. Vainionpaa, J. Laiho, T. Pohjonen, and P. Rokkanen, "Ultra-high-strength absorbable self-reinforced polyglycolide (SR-PGA) composite rods for internal fixation of bone fractures In vitro and in vivo study." *J. Biomed. Mater. Res.*, **25,** 1-22 (1991).

5 Y. Shikinami and M. Okuno, "Bioresorbable devices made of forged composites of hydroxyapaptite (HA) particles and poly-L-lactide (PLLA): Part 1 Basic characteristics." *Biomaterials*, **20,** 859-77 (1999).

6 D. H. Kohn, E. M Richmond, E. R. Dootz, S E Feinberg, and W. S. Pietrzak, "In vitro comparison of parameters affecting the fixation strength of sagittal split osteotomies." *J Oral Maxillofac. Surg* , **53,** 1374-1383 (1995).

7 M. Deguchi, B. Cheng, K Sato, Y. Matsuyama, and T. A. Zdeblick, "Biomechanical evaluation of translaminar facet joint fixation· A comparative study of poly-L-lactide pins, screws, and pedicle fixation." *Spine*, **23(12),** 1307-13 (1998).

8 A. Weiler, H. J Windhagen, M J Raschke, A. Laumeyer, and R. Hoffman, "Biodegradable interference screw fixation exhibits pull-out force and stiffness similar to titanium screws " *Am. J Sports Med*, **26,** 119-28 (1998).

9 K. D. Nelson, A. R Phansalkar, A. A Romero, Y. Ye, R. Eberhart, C. Landau, and R S Meidell, "Degradation of poly(L-lactic acid) monofilaments for experimental intravascular stent designs." *Adv Bioeng.*, **36,** 333-334, (1997)

10 M. Slivka, C. Chu, and I Adisaputro, "Fiber-matrix interface studies on bioabsorbable composite materials for internal fixation of bone fractures. I Raw material evaluation and measurement of fiber-matrix interfacial adhesion " *J. Biomed. Mater. Res* , **36,** 469-477 (1997)

11. A. Tegnander, L. Engebretsen, K Bergh, E Eide, K. Holen, and O Iversen, "Activation of the complement system and adverse effects of biodegradable pins of poly-lactic acid (Biofix®) in osteochondritis dissecans " *Acta Orthop Scand.* **65,** 472-475 (1994).

12 J. A Ray, N. Doddi, D. Regula, J. A. Williams, and A. Melveger, "Polydioxanone (PDS), a novel monofilament synthetic absorbable suture." *Surg. Gynec. Obstet*, **153,** 497-507 (1981)

13 J. Radhakrishnan, T. Kikutani, and N. Okui, "Thinning behavior of the spinline in high-speed bicomponent spinning of high molecular weight and low molecular weight poly(ethylene terephthalate)." *Sen'I Gakkaishi,* **52,** 618-22 (1996).

14 S. Hyon, K. Jamshidi, and Y. Ikada, "Melt spinning of poly-L-lactide and hydrolysis of the fiber *in vitro,*" in *Polymers as Biomaterials,* S. Shalasky, A. Hoffman, B. Ratner, and T. Horbett, (eds.), Plenum Press, New York, 1984, p.51.

15 J. C. Slattery, "Two-Phase, annular, laminar flow of simple fluids through cylindrical tubes." *AICHE J.,* **10,** 817-19, (1964).

16 L. Fambri, A. Pegoretti, R. Fenner, S D. Incardona, and C. Migliaresi, "Biodegradable fibers of poly(L-lactic acid) produced by melt spinning." *Polymer,* **38,** 79-85 (1997).

17 B. Eling, S. Gogolewski, and A Pennings, "Biodegradable materials of poly(L-lactic acid) 1 Melt-spun and solution-spun fibers." *Polymer,* **23,** 1587-92 (1982).

18 J. Radhakrishnan, H. Ito, T. Kikutani, and N. Okui, "Enhancement of fiber structure formation of liquid crystalline copolyester via ultra-high speed bicomponent spinning with poly(ethylene terephthalate) " *J. Polym. Eng Sci.,* **39,** 89-98 (1999)

19 P K. Gita, "Bioabsorbable antimicrobial polymers based on polyglycolic and polylactic acid " Ph.D Dissertation, Center of Biomedical Engineering, Indian Institute of Technology-Delhi, New Delhi (1992).

20 J. Kohm and R Langer, "Bioresorbable and Bioerodible Materials," in *Biomaterials Science· An Introduction to Materials in Medicine,* Buddy D. Ratner, A. S. Hoffman, F. J. Schoen, and J E Lemons (eds.), Academic Press, San Diego, 1996, Chapter 2

21 Y. Kimura, "Biocompatible Polymers," in *Biomedical Applications of Polymeric Materials,* Teiji Tsuruta (ed.), CRC Press, Boca Raton, FL 1993, Chapter 3.

22 P J Atkinson, R. L. Lancaster, T. S. Atkinson, S P Amoczky, R. C. Haut, S. E Weisbrode, "Breaking strength retention and histologic effects around 1 3-mm ORTHOSORB® polydiocanone absorbable pins at various sited in the rabbit." *J. Foot & Ankle Surg.*, **37(1),** 42-47 (1998).

23 M. Vert, P. Christel, H Garreau, M. Audion, M. Chanavez, and F. Chabot, "Totally Bioresorbable Composites Systems for Internal Fixation of Bone Fractures," in "Polymers in Medicine II Biomedical and Pharmaceutical Applications", E Chiellini, et al. (eds), Plenum Press, New York (1986)

24 C. M.. Agrawal, K. F Haas, D A. Lepold, and H. G. Clark, "Evaluation of poly(L-lactic acid) as a material for intravascular polymeric stents." *Biomaterials*, 13, 176-82 (1992)

25 D H. Lewis in "Biodegradable Polymers as Drug Delivery Systems," M Chasin and R. Langer, (eds), Marcel Dekker, New York, 1990, p.1.

26 P Tormala, "Biodegradable self-reinforced composite materials; manufacturing structure and mechanical properties." *Clin. Mater.*, **10,** 29-34 (1992)

27 J Merendion, G. Sertl, and J Skondia, "Use of biocompatible orthopedic polymer for fracture treatment and reconstructive orthopedic procedures." *Journal of Internal Medicine Research,* **12,** 351-55 (1984).

28 M. S. Madhukar, Fundamental Principles of Composite Materials, Fall 1999, The University of Tennessee, Knoxvilee, TN. Class notes.

29 Derek Hull, "Fibers and matrices," in *An Introduction to Composite Materials,* Cambridge University Press, London, 1981, Chapter 2.

30 L. E. Claes, A.A. Ignatius, K.E. Rehm and C. Scholz, "New bioresorbable pin for the reduction of small bony fragments: Design, mechanical properties and in vitro degradation." *Biomaterials*, **17,** 1621-26 (1996).

31 C. C. Chamis, "Mechanics of load transfer at the interface," in *Composite Materials: Interfaces in Polymer Matrix Composites,* E.P Plueddeman (ed.), Academic Press, New York, 1974, Chapter 2.

32 M R. Piggott, "Reinforced polymers," in *Load-Bearing Fibre Composites,* Pergamon Press, Oxford, 1980, Chapter 9.

33 S. Ferguson, D. Wahl, and S. Gogolewski, "Enhancement of the mechanical properties of polylactides by solid-state extrusion. II. Poly(L-lactide), poly(L/D-lactide), and poly(L/DL-lactide) " *J. Biomed. Mater. Res* , **30,** 543-551 (1996).

34 J. E. McIntyre and M J. Denton, "Fibers, Manufacture" in *Concise Encyclopedia of Polymer Science and Engineering,* J. Kroschwitz (ed), John Wiley and Sons, New York, 1990, p.389.

35 K. Mezghani and J. Spruiell, "High speed melt spinning of poly(L-lactic acid) filaments." *Journal of Polymer Science. Part B. Polymer Physics,* **36,** 1005-12 (1998).

36 S. Gogolewski and A. Pennings, "Resorbable materials of poly(L-lactide). II. Fibers spun from solutions of poly(L-lactide) in good solvents." *Journal of Applied Polymer Science,* **28,** 1045-61 (1983).

37 G. Kruder, "Fibers, Manufacture" in *Encyclopedia of Polymer Science and Engineering,* John Wiley and Sons, New York, 1986, Volume 6.

38 K Okajima, C. Yamane, F. Ise, "Polyamide fibers, aliphatice (nylon 66 and nylon 6)" in *Polymeric Materials Encyclopedia, Volume 7,* J C. Salamone (ed), CRC Press, New York, 1996, p 5387.

39 A Ziabicki, "Fundamental Aspects of Other Spinning Procedures and Special Fibre Spinning" in *Fundamentals of Fibre Formation,* John Wiley and Sons, New York 1976, Chapter 5.

40 Hersh, "Polyblend Fibers," in *Handbook of Fiber Science and Technology: High Technology Fibers Volume III, Part A,* Lewin, M. and J. Preston (eds.), Marcel Dekker Inc., New York 1985, Chapter 1.

41 J Manson and L Sperling, "Bicomponent and biconstituent fibers" in *Polymer Blends and Composites,* Plenum Press, New York, 1976, Chapter 9.

42 J. Radhakrishnan, T. Kikutani, and N Okui, "High-speed melt spinning of sheath-core bicomponent polyester fibers. High and low molecular weight poly(ethylene terephthalate) systems " *Textile Research Journal,* **67,** 684-94 (1997)

43 T. Kikutani et al., "High-speed melt spinning of bicomponent fibers Mechanism of fiber structure development in poly(ethylene terephthalate)/polypropylene system " *Journal of Applied Polymer Science,* **62,** 1913-24 (1996)

44 C. Han, "A study of bicomponent coextrusion of molten polymers." *Journal of Applied Polymer Science,* **17,** 1289-1303 (1973)

45 J J. Bikerman, "Tests for adhesion of polymers," in *Testing of Polymers Volume 4,* W E Brown, (ed), John Wiley & Sons, New York 1969, Chapter 1.

46 L. H Sperling "Adhesion in composite materials," in *Polymeric Multicomponent Materials· An Introduction,* John Wiley & Sons, New York, 1997, Chapter 6.

47 G W. Kamykowski and S. Goto, "The effect of layer geometry on the layer adhesion of coextruded films " *TAPPI Journal,* **80,** 227-31 (1997).

48 S R. Wu, "Kevlar Fiber-Epoxy Adhesion and Its Effect on composite mechanical and fracture properties by plasma and chemical treatment." *Journal of Applied Polymer Science,* **62,** 1347-60 (1996).

49 S S Voyutskii, "Adhesion of high polymers," in *Autohesion and Adhesion of High Polymers,* John Wiley & Sons, New York, 1963, Chapter 5

50 D Campbell and J R. White, "Light optical techniques," in *Polymer Characterization· Physical Techniques,* Chapman and Hall, New York, 1989, Chapter 11

51 Wilkes, "Rheo-Optical methods and their application to polymeric solids " *J Macromol. Sci – Revs Macromol. Chem.,* **C10,** 149-261 (1974)

52 F. W Billmeyer, *Textbook of Polymer Science, 208-213* (1984)

53 E. W Fischer, H. J Sterzel, and G Wegner, "Investigation of the structure of solution grown crystals of lactide copolymers by means of chemical reaction " *Journal of Polymer Science Chemical Education,* **17,** 2593-99 (1979)

54 T. H Barrows, personal communication.

55 W. L Baun, "The effect of etchıng on TI6AI4V ınterfacial chemıstry and adhesion to evaporated gold and a commercial adhesive." *J Adhesion,* **12,** 81-98 (1981).

56 G. Fourche, "An overvıew of the basic aspects of polymer adhesıon. Part 1: Fundamentals " *Polymer Engineering and Science,* **12,** 957-67 (1995).

57 N. R. Manoj and P. P. De. "Adhesıon of Poly(vınyl chlorıde) to Hydrogenated Nıtrıle Rubber: Partl, Peel Studies." *J. of Elastomers and Plastics,* **26,** 265-76 (1994)

58 D E Packham, J R G Evans, and P. R. Davıes, "The effect of temperature of test on the adhesion of polyethylene coatıngs applıed to metals as a hot melt." *J Adhesıon,* **13,** 29-40 (1981).

59 D.H. Kaelble, "Theory and Analysıs of Peel Adhesion: Rate-Temperature Dependence of Vıscoelastıc Interlayers." *J. Colloıd Science,* **19,** 413-24 (1964).

60 W M Brıght ın *Adhesıon and Adhesives,* J. Clark, J.E Rutzler, and R. L Savage (eds.) John Wıley and Sons, New York, 1954, p. 130.

61 T. Bhattacharya, B K. Dhındaw, and S K. De, "Reusable dry adhesive: Aluminum-Aluminu, Bondıng by self-vulcanısable blend based on carboxylated nıtrıle rubber and chlorobutyl rubber " *J Adhesion,* **34,** 45-63 (1991)

62 M. Wılliams, Thesıs The Unıversity of Tennessee, Knoxvılle, TN (2000).

63 X Yuan, A. Mak, K.W. Kwok, B. Yung, and K. Yao, "Preparatıon and characterization of poly(L-lactıde) fibers with dıfferent molecular weights by melt spinning." In Press

64 J P. Pennings, H. Dijkstra, and A.J. Pennings, "Preparation of absorbable fibres from L-lactide copolymers." *Polymer,* **34,** 942-51 (1993).

65 P De Santis and A. Kovacs, "Molecular conformation of poly(S-lactic acid)" *Biopolymers,* **6,** 299-306 (1968)

66 A Lin, Orthopedic Bioengineering Lab, Georgia Institure of Technology, Atlanta, GA.

67 M Dauner et al, "Resorbable continous-fibre reinforced polymers for osteosynthesis." *Journal of Materials Science: Materials in Medicine,* **9,** 173-79 (1998)

VITA

Regina Natasha Holmes was born on October 1, 1972 in Fort Benning, Georgia to Roderick and Ezera Holmes. She received her primary and secondary education in Muscogee County schools. She received a Bachelor of Science degree in Biomedical Engineering from Mercer University, Macon, GA. Her Master of Science degree is in the field of Polymer Engineering. Her professional and social affiliations include the Society for Plastics Engineers and United Way, respectively.